Dissertation zur Erlangung des Doktorgrades
der Fakultät für Chemie und Pharmazie
der Ludwig-Maximilians-Universität München

Novel insights into the role of microRNAs in chemoresistance, tumor progression and cancer therapy

Florian Kopp
aus
Augsburg, Deutschland
2013

Erklärung

Diese Dissertation wurde im Sinne von § 7 der Promotionsordnung vom 28. November 2011 von Herrn Prof. Dr. Ernst Wagner betreut.

Eidesstattliche Versicherung

Diese Dissertation wurde eigenständig und ohne unerlaubte Hilfe erarbeitet.

München, 17.09.2013

Florian Kopp

Dissertation eingereicht am: 23.09.2013

1. Gutachter: Prof. Dr. Ernst Wagner

2. Gutachter: Prof. Dr. Stefan Zahler

Mündliche Prüfung am: 14.11.2013

TABLE OF CONTENTS

1. INTRODUCTION

1.1 Biogenesis and function of microRNAs

In the early 90s, Ambros and Ruvkun discovered that the gene lin-4 encodes for a small RNA which posttranscriptionally regulates the lin-14 gene and thereby mediates temporal development in *Caenorhabditis elegans.* Henceforward, a vast number of studies have been conducted and much effort has been spent to understand the biogenesis, the physiological effects and the mechanism of these tiny RNA molecules known as microRNAs (miRNAs). miRNAs are small non-coding RNAs of ~22 nucleotides which are broadly conserved and endogenously regulate gene expression in plants and animals. In the nucleus, they are transcribed mostly by RNA polymerase II, resulting in primary transcripts (pri-miRNAs), which can be up to one kilobase in length and contain one or more hairpin structures. These motifs are then recognized by a protein complex which amongst others consists of the RNase III endonuclease Drosha. This microprocessor generates a 60 – 70 nucleotide stem loop called precursor miRNA (pre-miRNA), which is actively transported into the cytosol *via* Ran-GTP and Exportin 5. In the cytoplasm, pre-miRNAs are recognized by another protein complex containing the RNase III endonuclease Dicer, which cleaves the pre-miRNA resulting in a ~22 nucleotide mature miRNA duplex. Only one strand of the miRNA:miRNA* (miR:miR*) duplex is usually incorporated into the RNA-induced silencing complex (RISC) and thus biologically active. The passenger strand (miRNA*) is mainly degraded, whereas the single-stranded mature miRNA enables the RISC, which contains Argonaute proteins (Ago), to recognize and target respective mRNAs due to partial sequence complementarity between the miRNA and the 3'UTR of the mRNA. Thereby, a perfect match of the seed, i.e. nucleotides 2 – 7 at the 5' end of the miRNA, is crucial for the miRNA functioning. Gene expression can be subsequently inhibited by two main mechanisms: deadenylation of the polyA tail of the target mRNA, which in consequence leads to destabilization and degradation of the mRNA; and blockade of translation by hindering either initiation or elongation. Moreover, mRNAs bound to the RISC can be stored in P-bodies, where they are either recycled or degraded. One additional possibility, though unlikely in mammals due to inadequate base pairing, is mRNA cleavage. This mechanism

requires perfect base pairing as it is for instance the case for siRNA and therefore frequently occurs in plants, in which a sufficient complementarity between miRNAs and target mRNAs is commonly given. Apart from the described gene silencing functions, some miRNAs have also been reported to rather activate than inhibit gene expression by binding to the 5'UTR of mRNAs, to have decoy activity by binding to RNA-binding proteins, or to regulate gene transcription by interacting directly with the DNA. Although the exact mechanisms and the actual relevance of these emerging miRNA functions have to be elucidated, these findings illustrate the complexity of miRNA-regulated gene expression (Figure 1). (1-6)

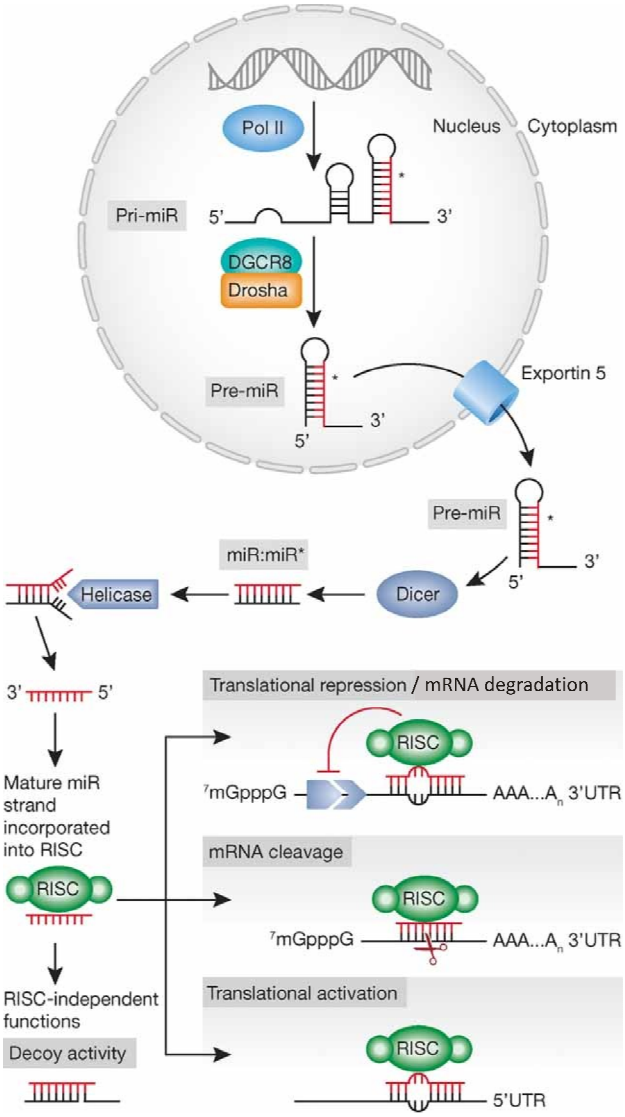

Figure 1. ***Biogenesis and function of microRNAs***

In the nucleus, miRNAs are transcribed as primary transcripts (Pri-miR) and further processed into precursor miRNAs (Pre-miR). Upon transport into the cytoplasm, the precursors are finally converted into mature miRNAs which are then biologically active. (Pol II = RNA polymerase II; DGCR8 = Di George syndrome critical region 8, also knowm as Pasha in *Drosophila melanogaster*; RISC = RNA-induced silencing complex)
(Adapted from Iorio MV, Croce CM. EMBO molecular medicine. 2012 Mar;4(3):143-59. © 2012 by WILEY)

1.2 Role of microRNAs in cancer

miRNAs are often dysregulated in many types of cancer being either up- or down-regulated. Differential miRNA expression patterns between cancerous and normal tissue further implicate that these tiny RNAs play a crucial role in tumorigenesis. Depending on their expression levels and their respective targets, miRNAs can be divided into two groups: tumor suppressor (tumor-suppressor-miRs) and oncogenic (onco-miRs) miRNAs, which target oncogenes and tumor suppressor genes, respectively. Examples of prominent tumor suppressor and oncogenic miRNAs including some selected dysregulations and validated targets are shown in Table 1.

miRNA	Expression level	Function	Validated targets
miR-15a and miR-16-1	low in CLL, multiple myeloma and prostate cancer	tumor suppressor	BCL2, MCL1, WT1
let-7 family	low in lung, colon, breast, ovarian and stomach cancer	tumor suppressor	KRAS, NRAS, CDK6, MYC
miR-29 family	low in CLL, AML, lymphoma, lung, liver and breast cancer	tumor suppressor	MCL1, CDK6, diverse DNMTs
miR-34 family	low in colon, lung, breast, kidney, pancreas, liver and bladder cancer	tumor suppressor	BCL2, MET, MYC, CDK4, CDK6
miR-155	high in CLL, AML, lymphomas, lung, colon and breast cancer	oncogene	SHIP1
miR-17-92 cluster	high in lung, breast, colon, pancreas and stomach cancer	oncogene	BIM, PTEN, E2F1
miR-21	high in CLL, AML, breast, pancreas, lung, prostate and stomach cancer	oncogene	PTEN, PDCD4

Table 1. Selected tumor suppressor and oncogenic miRNAs. Examples of tumor-suppressor-miRs and onco-miRs and their respective mRNA targets are depicted in the table.

In cancer cells, the loss of tumor-suppressor-miRs can be achieved by many different mechanisms, such as mutation, deletion or epigenetic silencing *via* promoter methylation or histone deacetylation. Furthermore, defects in the miRNA processing machinery, e.g. a loss of Drosha or Dicer, can result in a deregulated miRNA expression. On the other hand, onco-miRs can be up-regulated by gene amplification, translocation or transcriptional activation leading to a decreased expression of target tumor suppressors. Finally, these alterations comprise a complex regulatory network of different miRNAs and target genes which facilitates oncogenesis by causing pleiotropic effects, such as enhanced genomic instability, proliferation, invasion and reduced apoptosis. (5-8)

1.3 miR-200c and breast cancer

Breast cancer is the most common malignancy in women with 230,000 estimated new cases and 40,000 estimated deaths in the United States in 2012 (9). Even though early detection methods and treatment options greatly improved due to a better understanding of the underlying molecular mechanisms, resistance to classical chemotherapeutics is still a tremendous challenge for breast cancer therapy. About 30% of all breast cancer patients who are successfully treated at early stages are suffering a relapse accompanied by metastasis and chemoresistance to classical drugs (10, 11). While the response rates for first-line chemotherapy including anthracyclines and taxanes are up to 70%, the response rate falls to only 20 to 30% after disease progression. Besides metastasis, this acquired chemoresistance is a major obstacle in the treatment of breast cancer (12, 13). Hence, an advancement of the treatment by avoiding drug resistance and a better prediction of chemotherapy efficacy would improve the clinical outcome for breast cancer patients.

miRNAs are shown to be dysregulated in many cancers, such as breast, prostate, colon and lung. Thereby, miRNAs can function as onco-miRs or tumor-suppressor-miRs depending on their respective target genes (3, 7). Previous studies have also shown that miRNAs are able to modulate the sensitivity of cancer cells to chemotherapeutic drugs and therefore contribute to the acquisition of chemoresistance (14-18).

The human miR-200 family, which consists of miR-200a/b/c, miR-141 and miR-429, is located in two fragile chromosomal regions and can be divided into two seed-clusters depending on the sequence of the seed region (Figure 2).

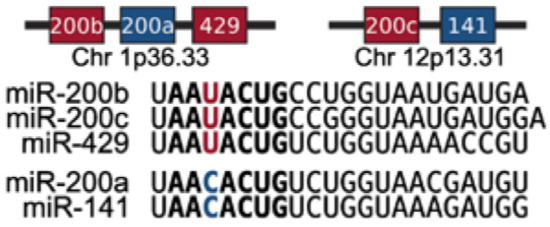

Figure 2. *Chromosomal location and seed-clusters of the miR-200 family*

The miR-200 family displays two sequence clusters, which differ in only one single nucleotide (U to C) in the seed region: miR-200bc/429 (red) and miR-200a/141(blue). The human miR-200 family is located in two fragile chromosomal regions on 1p36.33 (miR-200b, miR-200a and miR-429) and 12p13.31 (miR-200c and miR-141). (Adapted from Uhlmann S, Zhang JD, Schwager A, Mannsperger H, Riazalhosseini Y, Burmester S, et al. Oncogene. 2010 Jul 29;29(30):4297-306. © by Nature publishing group)

In breast cancer, the miR-200 family is known to be differentially expressed and several of its functions are well described. The miR-200 family, in particular miR-200c, has been reported to regulate epithelial-mesenchymal transition (EMT) by targeting ZEB1 and ZEB2, the transcriptional repressors of the epithelial marker E-cadherin (19-21). Hence, high miR-200c levels in cancer cells determine an epithelial phenotype, which is defined by an elevated E-cadherin expression, a low migratory capacity and a cobble-stone-like cell morphology (22-24). By the inhibition of EMT and the regulation of several other genes important for cell motility, such as FHOD1, PPM1F, MSN and FN1, miR-200c reduces the migration and invasion of cancer cells preventing tumor dissemination and metastases (25-29). It has also been shown that miR-200c links breast cancer stem cells with normal stem cells and that the down-regulation of the miR-200 family is required for the formation and maintenance of cancer stem cells (30, 31). Recent findings have furthermore suggested that a loss of miR-200c may regulate resistance to chemotherapeutics, such as paclitaxel or cisplatin (32, 33). However, an exact mechanism of miR-200c-dependent acquired chemoresistance has yet to be elucidated.

1.4 The proto-oncogene KRAS and its regulation by microRNAs

In cancer, many cellular processes, such as differentiation, growth, migration and survival, are regulated by GTPases of the RAS family. Amongst them K-ras plays a pivotal role in oncogenesis due to its capability of transforming human cells into malignant tumor cells, particularly if harboring an activating mutation in codon 12 or 13. KRAS mutations frequently occur in many types of human tumors, for example in 70 – 90% in pancreas, 30 – 60% in colon and 15 – 50% in lung making KRAS one of the most prominent oncogenes (34, 35). Furthermore, activating oncogenic KRAS mutations are often associated with resistance to chemotherapy and targeted therapies (35-39). Due to the poor prognosis for cancer patients with mutated KRAS, much effort has been spent on developing specific therapies for targeting oncogenic KRAS. However, apart from specific RNAi methods, up to now there are no small molecules available which can specifically target K-ras.

miRNAs represent endogenous regulators of KRAS and many other oncogenic pathways. Their differential expression in various cancerous tissues compared to normal tissues influences tumorigenesis (40), turning them either into tumor suppressors or oncogenes (8, 41). It has been shown that the let-7 family inhibits KRAS (42) resulting in slower proliferation and tumor growth of lung cancer cells (43-45). Moreover, miR-143 has been demonstrated to regulate tumorigenesis in colorectal and prostate cancer cells by targeting KRAS (46, 47). In pancreatic carcinogenesis it has been reported that the oncogene EVI1 leads to the activation of the KRAS pathway through suppression of the KRAS suppressor miR-96 (48). A recent study has revealed that miR-30c targets the KRAS oncogene as well and is deregulated in hereditary breast cancer (49). In contrast to these tumor suppressor miRNAs, which generally display a low expression level in cancer cells, miR-200c is differentially expressed among cancer cells and acts as molecular switch by modulating a multitude of cellular processes (50). Moreover, in resistant cancer cells miR-200c is able to restore sensitivity to anti-EGFR therapy (51, 52) as well as to classical chemotherapeutics (22, 32, 33). Therefore, a direct interaction of miR-200c and KRAS is of great interest in order to understand and predict tumor progression and therapy susceptibility of cancer patients.

1.5 Metastasis formation and the cancer stem cell-specific drug salinomycin

Distant metastases are the major cause of death in patients suffering from cancer. In spite of this, there is a lack of effective treatments for patients with metastatic disease. Tumor spreading is driven by the two fundamental processes epithelial-mesenchymal transition (EMT) and mesenchymal-epithelial transition (MET). As an early step of metastasis tumor cells undergo EMT, thereby acquiring an increased invasive and migratory capacity. Subsequently, these cells migrate into adjacent tissues, circulate in blood vessels and the lymphatic system and finally cause micrometastases in distant well-vascularized organs. To colonize and to form macrometastases, migrated tumor cells undergo MET and revert to an epithelial phenotype. (53-56)

miRNAs are a potent class of molecules modulating a multitude of cellular pathways (3). It has been shown that miR-200c regulates various processes in cancer cells, such as stemness, apoptosis, MET and chemosensitivity (50). In the early phase of metastasis the loss of miR-200c promotes tumor dissemination by modulating migration-regulatory target genes (27, 28) as well as by inducing EMT. The latter results in tumor cells with low miR-200c and E-cadherin but high vimentin levels thus displaying mesenchymal traits with an elevated migratory potential (19-25).

It has been reported that mesenchymal cancer cells are dedifferentiated and hence exhibit properties of cancer stem cells (CSC) (57). These CSC are important targets of cancer therapeutic approaches as they are assumed to be one of the major causes of relapse. Gupta *et al.* have recently found salinomycin to be a selective inhibitor of CSC obtained from immortalized transformed HMLER cells by a stable E-cadherin knockdown. Salinomycin reduced the proportion of CSC more than 100-fold compared to paclitaxel, a commonly used chemotherapeutic breast cancer drug (58).

Subsequent studies in a variety of different cancer types including breast, blood, lung, pancreas and colon have revealed diverse mechanisms of salinomycin action against cancer cells and CSC (Figure 3), such as induction of apoptosis and cell death, interference with cytoplasmic and mitochondrial ion transport as well as with ABC transporters, differentiation of CSC, and inhibition of oxidative phosphorylation and Wnt signaling (59-62). It has been also suggested that salinomycin inhibits

malignant traits in colorectal and prostate cancer cells either by selectively targeting CSC or by inducing oxidative stress (63, 64). When considering the mechanism of metastasis formation and the mesenchymal-like traits of CSC the question arises whether salinomycin is able to inhibit migration and metastasis by restraining cancer cells in an epithelial state.

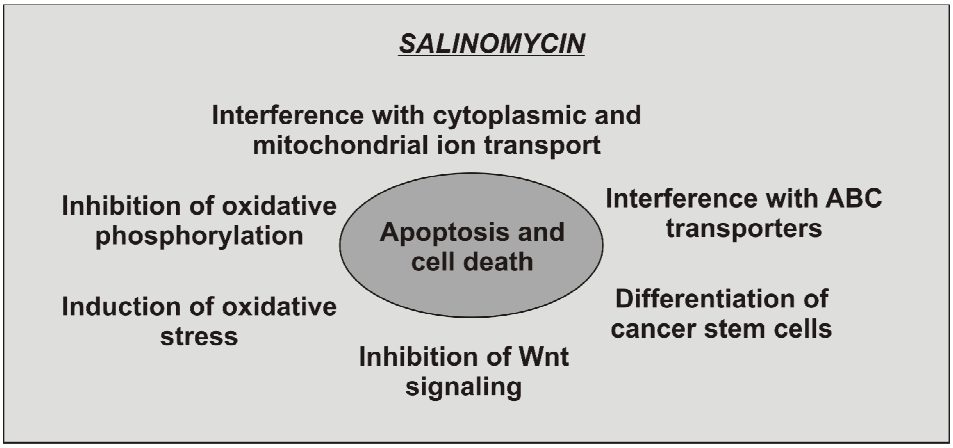

Figure 3. *Mechanisms of salinomycin action*

All mechanisms of salinomycin-induced apoptosis and cell death, which are published so far, are depicted in the graph.

1.6 microRNAs in cancer gene therapy

Besides the replacement of tumor-suppressor-miRs or the inhibition of onco-miRs by various methods, miRNAs and their differential expression can be also utilized for tumor-specific gene therapy. Tumor restricted transgene expression is a well suited approach to minimize side effects of cancer gene therapy. One possibility is to de-target the expression of toxic transgenes from non-cancerous tissues and hence protect them. miRNAs appear to be a suitable tool as they can regulate the expression of their target genes. miRNAs are highly conserved modulators of gene expression functioning as negative regulators of gene expression at the posttranscriptional level (1) affecting more than 60% of protein encoding genes (65). Malfunctioning miRNAs were found to be involved in several pathological processes including cancer (6) being either up- or down-regulated.

For example, miR-143 is found in abundance in most human and murine tissues, but considerably down-regulated in many cancer types including colon (66), liver (67) and gastric cancer (68). Several proteins involved in cell survival, proliferation and differentiation, such as KRAS (46) and Ras-responsive element-binding protein 1 (RREB1) (69), NFκB and BCL2 (70) are regulated by miR-143, indicating a function as tumor suppressor. As miR-143 is also involved in suppressing invasion and metastasis, amongst others in colon (71, 72) and prostate cancer (73), it represents a suitable target for therapeutic intervention. Attempts have been conducted to overexpress miR-143 in cancer cells which have low levels or no expression of miR-143 either by transfecting tumor cells prior to implantation with plasmids encoding for pri-miR-143 (74) or by delivering nanoparticles with miR-143 (75).

Alternatively, differential miR-143 expression between non-cancerous and cancerous tissue can be harnessed to de-target transgene expression from tissues with high miR-143 levels. For this purpose, multiple target sequences complementary to the sequence of miR-143 can be cloned into the 3'UTR of plasmid vectors encoding for different reporter or therapeutic genes. Thus, transgene transcription is only facilitated in miR-143 low-expressing cancer cells. This was shown for an oncolytic Herpes simplex virus 1 (HSV-1), where five miR-143 binding sites were placed between the 3'UTR and the polyadenylation signal of ICP4, an essential gene for HSV-1 replication (76). Albeit using the constitutively active CMV promoter driving ICP4 expression, the miR-143 binding sites inhibited virus replication in non-

malignant prostate tissue, whereas virus replication in prostate cancer cells was unaffected. Similarly, several reports have shown miRNAs successfully controlling virus replication (77-81) as well as regulating transgene expression of viral vectors (82-85). However, this de-targeting approach has not yet been applied to non-viral gene delivery systems, which possess certain advantages over viral carriers in terms of design flexibility, production and safety (86).

1.7 Aims of the thesis

Despite of improved early detection methods and novel targeted therapy approaches in the past 15 years, tumor progression including the formation of metastases and the acquisition of chemoresistance in response to conventional anti-cancer drugs still represents one of the largest hurdles in the successful treatment of cancer patients. A better understanding of the underlying pathological mechanisms is therefore needed to conceive novel treatment strategies, which will improve the clinical outcome of patients suffering from cancer.

In this thesis, the first aim was to investigate the mechanism of acquired chemoresistance to doxorubicin (Adriamycin ®), a commonly used chemotherapeutic drug from the group of the anthracyclines. The focus was thereby laid on miRNAs and their regulated target genes and pathways. In particular, the aim was to elucidate the role of miR-200c in chemoresistance as well as to generally broaden its relevance in tumorigenesis. Therefore, the physiological effects of the miR-200c-target interactions should be examined in order to evaluate its potential use in diagnosis and therapy.

In addition, the antibiotic drug salinomycin, which has been reported to be a selective inhibitor of cancer stem cells and which has hence raised hope for an improved cancer treatment, should be evaluated for its therapeutic potential against advanced stages of cancer. The aim was thereby to investigate the role of salinomycin in inhibiting tumor progression with regard to therapy resistance and metastasis formation.

Apart from classical therapeutic interventions including cytostatic drugs, antibodies or small molecules against certain oncogenic targets, the field of oligonucleotide based medicines, such as siRNAs, miRNAs or antagomiRs, has emerged in the last years. Here, the aim was to exploit the differential miRNA expression in healthy and cancerous tissue for tumor-specific non-viral gene therapy. Therefore, miR-143 as a prominent tumor suppressor miRNA was chosen. Plasmids which encode for reporter genes as well as for a therapeutic gene and which contain five binding sites complementary to the sequence of miR-143 should be investigated regarding their ability to specifically induce transgene expression in tumor cells by de-targeting non-malignant cells.

2. MATERIALS AND METHODS

2.1 miR-200c sensitizes breast cancer cells to doxorubicin

2.1.1 Primary antibodies

Primary antibodies against the following proteins were used: E-cadherin (C20820, Transduction Laboratories); vimentin (V9) (SC-6260, Santa Cruz); TrkB (H-181) (SC-8316, Santa Cruz); Akt (#9272, Cell Signaling); p-Akt (S-473) (#4051, Cell Signaling); Bmi1 (PAI-16973, Thermo Scientific); p53 (DO-1) (SC-126, Santa Cruz), actin (I-19) (SC-1616, Santa Cruz); α-tubulin (DM-1A) (T9026, Sigma).

2.1.2 Cell culture

The breast cancer cell lines BT-474 and MDA-MB-436 were cultivated according to supplier's instructions (ATCC). Briefly, BT-474 cells were grown in RPMI 1640 medium (Gibco) supplemented with 10% fetal calf serum (FCS) and 2mM glutamine (Gibco) at 37°C and 5% CO_2. MDA-MB-436 cells were cultivated in L-15 Leibovitz's medium (Biochrom) supplemented with 10% FCS and 2mM glutamine at 37°C without CO_2.

2.1.3 Molecular evolution assay

The epithelial breast cancer cell line BT-474 was treated with 50nM doxorubicin (doxorubicin hydrochloride, Sigma) for 72h when cells reached a confluency of 80%. After treatment doxorubicin containing medium was replaced by fresh medium. As soon as the cells recovered, they were seeded for RNA isolation, cell lysis (protein), cytotoxicity assays and the next treatment cycle. In this manner four rounds of the molecular evolution assay were performed. To obtain the appropriate rate of cell death in the molecular evolution assay, several doxorubicin concentrations were

tested in a preliminary experiment. Thereby, 50nM was obtained as the most suitable concentration.

For cytotoxicity assays 5000 cells were seeded in 96-well plates after each round of the molecular evolution assay. 24h after seeding cells were treated with different concentrations of doxorubicin for 72h. After incubation a CellTiter Glo assay (Promega) was performed following manufacturer's instructions.

2.1.4 Quantitative RT-PCR

For mRNA quantification total RNA was isolated with the miRCURY RNA Isolation Kit (Exiqon) followed by a reverse transcription using Transcriptor High Fidelity cDNA Synthesis Kit (Roche) according to manufacturers' protocols.

Primer	Sequence (5' – 3')
miR-141 SLP	GTTGGCTCTGGTGCAGGGTCCGAGGTATTCGCACCAGAGCCAACCCATCT
miR-141 F	GCGTAACACTGTCTGGTAAAGA
miR-200a SLP	GTTGGCTCTGGTGCAGGGTCCGAGGTATTCGCACCAGAGCCAACACATCG
miR-200a F	GAGTAACACTGTCTGGTAACGA
miR-200b SLP	GTTGGCTCTGGTGCAGGGTCCGAGGTATTCGCACCAGAGCCAACTCATCA
miR-200b F	GCGTAATACTGCCTGGTAATGA
miR-200c SLP	GTTGGCTCTGGTGCAGGGTCCGAGGTATTCGCACCAGAGCCAACTCCATC
miR-200c F	GCGTAATACTGCCGGGTAAT
miR-429 SLP	GTTGGCTCTGGTGCAGGGTCCGAGGTATTCGCACCAGAGCCAACACGGTT
miR-429 F	GAGTAATACTGTCTGGTAAAACC
miR-143 SLP	GTTGGCTCTGGTGCAGGGTCCGAGGTATTCGCACCAGAGCCAACGAGCTA
miR-143 F	GCGTGAGATGAAGCACTG
miR-191 SLP	GTTGGCTCTGGTGCAGGGTCCGAGGTATTCGCACCAGAGCCAACCAGCTG
miR-191 F	GCGCAACGGAATCCCAAAAG
universal R	GTGCAGGGTCCGAGGT

Table 2. Primers used for the quantitative RT-PCR of miRNAs. (F = forward primer; R = reverse primer; SLP = stem loop primer)

Quantitative RT-PCR was performed on a LightCycler 480 system (Roche) using UPL Probes (Roche) and Probes Master (Roche). Genes of interest were normalized to GAPDH as reference. The following probes and primer sequences were used: E-cadherin, UPL Probe #35, left primer: CCCGGGACAACGTTTATTAC, right primer: GCTGGCTCAAGTCAAAGTCC; TrkB, UPL Probe #2, left primer: AGTGCCTCTCGGATCTGGT, right primer: TTTCTGGTTTGCGATGAAAAT; Bmi1, UPL Probe #54, left primer: TGTAAAACGTGTATTGTTCGTTACC, right primer: CAATATCTTGGAGAGTTTTATCTGACC; GAPDH, UPL Probe #60, left primer: AGCCACATCGCTCAGACAC, right primer: GCCCAATACGACCAAATCC.
For miRNA quantification total RNA was isolated with the miRCURY RNA Isolation Kit. cDNA synthesis was carried out by a miRNA-specific reverse transcription using Transcriptor High Fidelity cDNA Synthesis Kit and a stem loop primer (SLP) which was specific for only one particular miRNA (87-89). Quantitative RT-PCR was then performed on a LightCycler 480 system using SYBR Green I Master (Roche). The expression of miR-200 family members (miR-141, miR-200a, miR-200b, miR-200c, miR-429) was normalized to miR-191 as reference (90). All sequences of the primers used for the miRNA quantification are shown in Table 2. Expression levels were normalized using the $2^{-\Delta Ct}$ or $2^{\Delta\Delta Ct}$ method.

2.1.5 miR-200c inhibition

BT-474 and MDA-MB-436 cells were seeded in 96-well plates at a density of 3000 cells per well. The following day cells were transfected with 50nM miRCURY LNA miRNA Inhibitor for hsa-miR-200c (miR-200c inhibitor) (Exiqon) or miRCURY LNA miRNA Inhibitor Control Negative Control A (scrambled control) (Exiqon) using Lipofectamine 2000 (Invitrogen) according to manufacturer's protocol.
24h after transfection cells were treated with different concentrations of doxorubicin for 72h followed by a CellTiter Glo assay.

2.1.6 miR-200c overexpression

MDA-MB-436 and BT-474 cells were transfected in 6-well plates with 100pmol Pre-miR miRNA Precursor of hsa-miR-200c (pre-miR-200c) (Ambion) or Pre-miR

miRNA Negative Control (scrambled control) (Ambion) using Lipofectamine 2000 according to manufacturer's protocol. After three consecutive transfections, cells were harvested for RNA isolation, cell lysis (protein) and cytotoxicity assays.
For cytotoxicity experiments transfected cells were seeded on 96-well plates at a density of 3000 cells per well. 24h after seeding cells were treated with different concentrations of doxorubicin for 72h followed by a CellTiter Glo assay.

2.1.7 Cell lysis and immunoblotting

Cells were washed with phosphate buffered saline (PBS) (Gibco) and incubated at 4°C with lysis buffer (Promega) supplemented with phosphatase and protease inhibitors (Santa Cruz and Roche). Cellular debris was removed by centrifugation. Protein estimation was performed using the Micro BCA Protein Assay Kit (Thermo Scientific). Samples were suspended in SDS sample buffer (50mM Tris-HCl (pH 6.8), 2% SDS, 10% glycerol, 1% β-mercaptoethanol, 12.5mM EDTA and 0.02% bromophenol blue), boiled for 5min and subjected to SDS-PAGE. For Western blot analysis, proteins were transferred to nitrocellulose membranes (Bio-Rad), which were subsequently blocked with NET-gelatine (150mM NaCl, 5mM EDTA, 50mM Tris-HCl (pH 8.0) and 0.05% Triton X-100, gelatine 0.25%) and incubated with the appropriate antibodies. After three steps of washing with NET-gelatine signals were developed using either Peroxidase Horse Anti-Rabbit IgG Antibody or Peroxidase Goat Anti-Mouse IgG Antibody (Vector Laboratories) and Lumi-Light^{PLUS} Western Blotting Substrate (Roche). Western blot quantification was done with ImageJ (91).

2.1.8 Immunofluorescence

Cells were seeded on a cover slip and fixed with 4% paraformaldehyde. Cover slips were blocked with 10% FCS, 1% gelatine and 0.05% Triton X-100 and incubated with indicated primary antibodies. Immunofluorescence was visualized using Donkey anti-Mouse IgG (Cy3) (PA1-29773, Thermo Scientific). Counterstaining was performed using 4'-6-diamidino-2-phenylindole (DAPI) (Sigma). Results were analyzed using Zeiss Laser Scanning Microscope LSM 510 Meta and Axiovert 200 software (Zeiss).

2.2 miR-200c targets KRAS

2.2.1 Oligonucleotides

The following oligonucleotides were used: miRCURY LNA miRNA Inhibitor for hsa-miR-200c (inh) (Exiqon), miRCURY LNA miRNA Inhibitor Control Negative Control A (ctr) (Exiqon), Pre-miR miRNA Precursor of hsa-miR-200c (pre) (Ambion), Pre-miR miRNA Negative Control (ctr) (Ambion), ON-TARGETplus SMARTpool siRNA against human KRAS consisting of four different siRNAs (Dharmacon) (siRas) and the non-targeting control siRNA (siCtr), which was previously described (92).

2.2.2 Cell culture

The breast cancer cell lines MDA-MB-157, MDA-MB-436, MDA-MB-231, MDA-MB-435 (formerly regarded as breast cancer, in fact melanoma), MDA-MB-453, MDA-MB-468, MCF-7, BT-474 and 4T1 as well as the lung cancer cell lines A549 and Calu-1 were cultivated according to supplier's instructions (ATCC).

2.2.3 Quantitative RT-PCR

Total RNA was isolated followed by a reverse transcription and a quantitative RT-PCR as described previously (93). The following primers (Metabion) and hydrolysis probes (Roche) were used for mRNA quantification: KRAS, UPL Probe 42, left primer: TGGACGAATATGATCCAACAAT, right primer: TCCCTCATTGCACTGTACTCC; GAPDH, UPL Probe #60, left primer: AGCCACATCGCTCAGACAC, right primer: GCCCAATACGACCAAATCC. All primers used for the miR-200c quantification are listed in Table 2.

2.2.4 Cell lysis and immunoblotting

Western blot experiments were performed as previously described (93) using the primary antibodies against the following proteins: K-ras (415700, Invitrogen), actin (I-19) (SC-1616, Santa Cruz) and α-tubulin (DM-1A) (T9026, Sigma).

2.2.5 Molecular evolution assay

BT-474 cells were treated with 50nM doxorubicin (doxorubicin hydrochloride, Sigma) for 72h as described previously (93). As soon as the cells recovered (confluency of 80%) the next treatment round was started. After each cycle cells were harvested for RNA isolation and protein lysates.

2.2.6 Oligonucleotide transfections

Indicated cell lines were transfected with the above mentioned oligonucleotides using Lipofectamine 2000 (Invitrogen) according to manufacturer's protocol. The following nucleotide amounts were thereby used: in 6-well plates (used for quantitative RT-PCR and Western blot) 75pmol, in 24-well plates (used for cell cycle) 15pmol, in 48-well plates (used for proliferation) 7.5pmol and in 96-well plates (used for luciferase assays) 3pmol.

2.2.7 Luciferase reporter assays

A renilla luciferase reporter plasmid containing the almost entire 3'UTR of the KRAS gene was obtained from Addgene (Addgene plasmid 44571). This plasmid was generated by Frank Slack and is based on the plasmid with the let-7 mutated binding site LCS6m from the publication Chin *et al*. (94). The renilla luciferase reporter containing the 3'UTR of KRAS (RLuc) or the firefly luciferase control plasmid pGL3 (Promega) (FLuc) were transfected into the indicated cell lines using Lipofectamine 2000 (Invitrogen) according to manufacturer's instructions. All RLuc signals were normalized to the respective FLuc signals as ratio (RLuc/FLuc).

Additionally, MDA-MB-436 cells were transfected with either pre-miR-200c (pre) or pre-miR-control (ctr) (Ambion) together with the reporter plasmid RLuc and the control plasmid FLuc for normalization. BT-474 cells were transfected with either the LNA miR-200c inhibitor (inh) or the LNA control inhibitor (ctr) (Exiqon) together with the reporter plasmid RLuc and the control plasmid FLuc for normalization.
All luciferase assays were performed in 96-well plates at 48h post transfection. Firefly luciferase assays were in principle carried out as previously described (92). The renilla luciferase assays were analogously performed with the exception that coelenterazine (SynChem) was used as substrate instead of luciferin. Thereby, the alcoholic coelenterazine solution was prediluted in phosphate buffered saline (PBS) and used in a final concentration of 50µM.

2.2.8 Proliferation assay

To examine proliferation, cells were seeded in 48-well plates. The following day, cells were transfected with indicated oligonucleotides and starting with day one after transfection proliferation was measured over seven days at indicated time points using a Scepter cell counter (Millipore).

2.2.9 Cell cycle analysis

For the acquisition of the cell cycle, cells were seeded in 24-well plates and transfected with the indicated oligonucleotides the following day. At 48h or 72h after transfection the cells were subjected to flowcytometry. For this purpose, cells were trypsinized, centrifuged and incubated on ice for four hours in propidium iodide staining solution consisting of 0.1% sodium citrate, 0.1% Triton X-100 and 50µg/ml propidium iodide. Thereafter, cells were centrifuged, resuspended in phosphate buffered saline and analyzed with a CyAn ADP flowcytometer (Beckman Coulter). Doublets were discriminated by gating forward versus sideward scatter and forward scatter versus pulse width. The DNA content was measured through excitation of the dye at 488nm and detection of the emission with a 613/20 bandpass filter. Cell cycle analysis was carried out using FlowJo software.

2.2.10 Target prediction and KEGG pathway analysis

Target prediction was achieved by utilizing the three different prediction algorithms TargetScan (95), miRanda (96) and DIANA microT (97, 98). A pathway analysis of all potential targets of miR-200c predicted by TargetScan was carried out, using the Database for Annotation, Visualization and Integrated Discovery (DAVID), and visualized by the Kyoto Encyclopedia of Genes and Genomes (KEGG)-pathway maps (99, 100).

2.3 Salinomycin targets migratory miR-200c^{low} tumor cells

2.3.1 Primary antibodies and reagents

Primary antibodies against the following proteins were used: actin (I-19) (SC-1616, Santa Cruz) for Western blot (WB); vimentin (D21H3) XP (#5741, Cell Signaling) for WB and *in vivo* immunohistochemistry (IHC)/ immunofluorescence (IF); E-cadherin (24E10) (#3195, Cell Signaling) for WB and *in vivo* IHC/IF; E-cadherin (DECMA-1) (ab11512, Abcam) for *in vitro* IF; vimentin (V9) (SC-6260, Santa Cruz) for *in vitro* IF. Salinomycin (S6201) and doxorubicin hydrochloride (D1515) were obtained from Sigma.

2.3.2 Cell culture

The breast (BT-474, MCF-7, MDA-MB-231, MDA-MB-436 and 4T1) and lung (NCI-H1299 and Lewis lung carcinoma) cancer cell lines were cultivated according to supplier's instructions (ATCC). 4T1-luc cells were a kind gift from Prof. Dr. Angelika Vollmar (LMU Munich).

2.3.3 Transfections

For miR-200c overexpression experiments cells were transfected either with Pre-miR miRNA Precursor of hsa-miR-200c (pre-miR-200c) (Ambion) or Pre-miR miRNA Negative Control (control) (Ambion) using Lipofectamine 2000 (Invitrogen) according to manufacturer's protocol.

2.3.4 Quantitative RT-PCR

Total RNA was isolated with the miRCURY RNA Isolation Kit (Exiqon) according to manufacturer's instructions. miRNA or mRNA was reversely transcribed and subjected to quantitative RT-PCR as described previously (93). All experiments were done in triplicates and the following primers (Metabion) and hydrolysis probes

(Roche) were used: E-cadherin (hsa), UPL Probe #35, left primer: CCCGGGACAACGTTTATTAC, right primer: GCTGGCTCAAGTCAAAGTCC; vimentin (hsa): UPL Probe #56 left primer: GTTTCCCCTAAACCGCTAGG, right primer: AGCGAGAGTGGCAGAGGA; Zeb2 (hsa): UPL Probe #68, left primer: AAGCCAGGGACAGATCAGC, right primer: CCACACTCTGTGCATTTGAACT; GAPDH (hsa), UPL Probe #60, left primer: AGCCACATCGCTCAGACAC, right primer: GCCCAATACGACCAAATCC; E-cadherin (mmu): UPL Probe #18, left primer: ATCCTCGCCCTGCTGATT, right primer: ACCACCGTTCTCCTCCGTA; vimentin (mmu): UPL Probe #79, left primer: TGCGCCAGCAGTATGAAA, right primer: GCCTCAGAGAGGTCAGCAAA; Zeb2 (mmu): UPL Probe #42, left primer: CCAGAGGAAACAAGGATTTCAG, right primer: AGGCCTGACATGTAGTCTTGTG; GAPDH (mmu): Universal ProbeLibrary Mouse GAPD Gene Assay (Roche). All primers used for the miR-200c quantification are depicted in Table 2.

2.3.5 Cell lysis and immunoblotting

Western blot experiments were performed as previously described (93) using the respective antibodies from the reagents section.

2.3.6 Cell viability assay

For cytotoxicity experiments cells were seeded on 96-well plates at a density of 5000 cells per well. After 24h cells were incubated with respective drugs for 72h unless otherwise indicated. Subsequently, a CellTiter Glo (Promega) assay was performed according to manufacturer's protocol. Cell viability was normalized to the respective mock-treated control cells and presented as percent of control. IC_{50} values for doxorubicin and salinomycin were obtained from several different drug concentrations using GraphPad Prism software for analysis. All experiments were done in triplicates.

2.3.7 Tumor cell co-culture

MCF-7 and MDA-MB-436 cells were co-cultured in a DMEM/ Leibovtiz's L-15 medium (1/1). For cytotoxicity assays 5000 co-cultured cells per well were seeded in a 96-well plate and incubated overnight. Subsequently, cells were treated with 0.25µM salinomycin, 0.25µM doxorubicin or the combination of 0.25µM salinomycin and 0.25µM doxorubicin for 72h. For immunofluorescence cells were seeded on cover slips at a density of 50 – 60%.

2.3.8 *In vitro* salinomycin long-term treatment

MDA-MB-436 cells received a pulsed salinomycin long-term treatment similarly as it was described previously for the molecular evolution assay of BT-474 cells with doxorubicin (93). Briefly, MDA-MB-436 cells were treated with 50nM salinomycin for 72h when cells reached a confluency of 80%. After treatment salinomycin was removed and replaced by fresh medium. As soon as cells recovered they were treated again with salinomycin. After the fourth treatment cycle the recovered salinomycin-treated cells were harvested for RNA isolation, cell lysis (protein), cytotoxicity and migration assays.

2.3.9 Boyden chamber migration assay

Transwells (8µm pore size, Millipore) were placed in 24-well plates containing 10% fetal calf serum (FCS) (Gibco) in medium plus or minus doxorubicin or salinomycin. Cells were suspended in 250µl serum free medium plus or minus chemotherapeutic drugs, added to the top of each chamber and incubated for 18h. Subsequently, chambers were washed and cells were removed from the upper side of the chamber with a cotton swab. Migrated cells were fixed and stained using the cell stain solution (Chemicon International). The average number of migrated cells from 15 representative fields (3 replicates per condition) was counted under a phase contrast microscope. For treatment experiments only drug concentrations causing approximately 10% cell death (as determined by a CellTiter Glo assay) were used. Microscopic pictures (phase contrast) show representative stained transwells.

2.3.10 Time-lapse microscopy and wound healing assay

Time-lapse microscopy was performed utilizing a live-cell imaging setup consisting of a microscope (Carl Zeiss MicroImaging) equipped with a Pln Apo 10x/0.45 DICII objective, motorized scanning table and a stage incubator at 37°C with or without CO_2. Images were captured with an AxioCamMR Rev3 camera using the Axiovision Rel 4.8 software for microscope control and data acquisition. Indicated cells were seeded in 24-well plates at a density of 50 – 70% and grown overnight. For wound healing assays MDA-MB-436 cells were seeded in 24-well plates and grown until a confluency of 90 – 95%. Subsequently, a scratch was placed in the middle of the well with a sterile 200µl pipette tip (Eppendorf). After washing once with serum-free media, the respective treatments were performed. Media with FCS was added to control wells and media with different drugs was added to respective wells before starting the time-lapse imaging. The images were captured every 15min for 72h. Each reading was performed in triplicates. 10 random cells/ well, i.e. 30 random cells per condition, were manually tracked using ImageJ (91) and the data was analyzed using the 'chemotaxis and migration tool' plugin for ImageJ.

2.3.11 *In vitro* immunofluorescence

Cells were seeded on cover slips. At a confluency of 50 – 60% cells were fixed with 4% paraformaldehyde and blocked with 10% FCS, 1% gelatine and 0.05% Triton X-100. After permeabilizing with 0.2% Triton X-100, cover slips were incubated with the respective primary antibodies. Immunofluorescence was visualized using goat anti-mouse Alexa 488 (Life Technologies) or donkey anti-rat Cy TM3 (Jackson ImmunoResearch) and DAPI for counterstaining the nuclei. Images were captured using 63x1.4 Oil DIC objective of Carl Zeiss Laser Scanning Microscope LSM 510 Meta and analyzed using LSM Image Browser (Carl Zeiss). Representative images are shown.

2.3.12 Animal experiments

All animal experiments were approved by the local ethical committee and performed according to the guidelines of the German law of protection of animal life.

2.3.13 Salinomycin treatment of SpC-c-MYC transgenic mice

All SpC-c-MYC mice were obtained from Dr. Chitra Thakur and Prof. Dr. Ulf Rapp (Max-Planck-Institute, Martinsried). Animals were genotyped through tail DNA at the age of three weeks. They have similar genetic background (>90% C57Bl/6) and were maintained heterozygous. Mice develop multifocal hyperplasias, and bronchioloalveolar adenomas and carcinomas derived from alveolar type II (ATII) cells within 10 – 14 months. At the average age of 7 months mice develop early stages of tumor characterized by multifocal hyperplasias originating in the alveolar epithelium (101).
A group of 11 SpC-c-MYC mice (72 weeks old) were injected intraperitoneally every second day with 5mg/kg salinomycin (2mg/ml in dimethyl sulfoxide (DMSO) stock solution was diluted in phosphate buffered saline) for three weeks. At the end of the experiment mice were sacrificed and organs were collected for further analysis. Mice at the same age from the previous study by Rapp *et al*. (102) served as controls.

2.3.14 Subcutaneous 4T1-luc mouse model

$2x10^6$ 4T1-luc cells were subcutaneously injected into the left flank of 18 female BALB/c mice (Janvier). 9 animals were treated either with mock (DMSO in phosphate buffered saline) or 5mg/kg salinomycin (2mg/ml in DMSO stock solution was diluted in phosphate buffered saline) on day 3, 6, 8, 10, 13 and 15. Tumor growth was monitored for 17 days at indicated time points using a caliper. At the end of the experiment mice were sacrificed and tumors resected for further experiments.

2.3.15 Intravenous 4T1-luc mouse model

$1x10^5$ 4T1-luc cells were injected intravenously into the tail vein of 20 female BALB/c mice. 10 animals were treated either with mock (DMSO in phosphate buffered saline) or 5mg/kg salinomycin (2mg/ml in DMSO stock solution was diluted in phosphate buffered saline) on day 0, 3, 6 and 9. Tumor growth was monitored for 13 days at indicated time points using bioluminescence imaging (BLI). BLI was performed as described previously (103). One mouse in the control group was missing for the last BLI (day 13) as this mouse had to be sacrificed earlier due to severe medical condition. At the end of the experiment mice were sacrificed and lung, brain, spleen, kidneys and liver were resected for subsequent *ex vivo* luciferase assays. For this purpose, the obtained tissue was pulverized in liquid nitrogen and an aliquot homogenized in cell lysis buffer (Promega) using a tissue and cell homogenizer (FastPrep-24, MP Biomedicals). Luciferase activity was quantified as described previously (104).

2.3.16 *In vivo* immunohistochemistry and immunofluorescence

Immunohistochemistry (haematoxylin & eosin and marker stainings) of transgenic lung tumors and subcutaneous 4T1-luc tumors as well as immunofluorescence of 4T1-luc tumors were performed as described previously (102). Representative images are shown.

2.3.17 Statistical analysis

All values are stated as mean ± SD unless otherwise indicated. For statistical analysis, student's t-tests were performed (*p<0.5; **p<0.01; ***p<0.001; ****p<0.0001). Outliers were identified using the ROUT (robust regression and outlier removal) method of GraphPad Prism.

2.3.18 MIRUMIR analysis

For the evaluation of miR-200c as prognostic marker for patients, the recently published online tool MIRUMIR (105) was used. It provides Kaplan-Meier plots along with Cox regression survival analyses. Reported p-values are corrected by False Discovery Rate (FDR) control procedure, thus accounting for multiple datasets used in the analysis.

2.4 miR-143-controlled transgene expression

2.4.1 Quantitative RT- PCR

Total RNA was isolated with the miRCURY RNA Isolation Kit (Exiqon) according to manufacturer's instructions. miRNA was reversely transcribed and subjected to quantitative RT-PCR as described previously (93). The obtained average C_T values of miR-143 were normalized to the C_T values of miR-191 using the $2^{-\Delta CT}$ method and presented as ratio. All sequences of the primers used for the miRNA quantification are shown in Table 2.

2.4.2 Cloning and propagation of plasmids

All CpG-depleted plasmids were based on the commercially available plasmid pCpG-MCS (Cayla Invivogen). The EGFP expression cassette was obtained from pEpito-hCMV/EF1-EGFP (106) by restriction with NheI and BglII, subcloned into pMOD-ZGFP (Invivogen), excised with AvrII and BamHI and ligated into the BglII and NheI digested pCpG-hCMV/EF1-LucSH (107) generating pCpG-hCMV/EF1-EGFP. The mCherry ORF from pRVmCherry was PCR amplified, BglII and NheI restriction sites were added and cloned into pGEM-T (Promega). Finally, the LucSH expression cassette in pCpG-hCMV/EF1-LucSH was exchanged for mCherry. The EF1 promoter element in all vectors was exchanged for the synthetic CMV-EF1α hybrid promoter (SCEP) (108) by digestion with SpeI and either HindIII or NcoI.
A plasmid vector containing five tandem copies of complementary miR-143 binding sites was synthesized by Geneart as specified (76). miR-143 binding sites were excised by digestion with XbaI and NheI and inserted into the NheI site of pCpG-hCMV/SCEP-mCherry, pCpG-hCMV/SCEP-LucSH and pCpG-hCMV/SCEP-TNFα, generating plasmids with five copies of the sequence complementary to miR-143. All plasmids were propagated in E.coli DB 3.1λ pir under zeocin selection pressure and purified using the Qiagen Plasmid Maxi Kit (Qiagen).

2.4.3 Cell culture

PC3 (human prostate cancer, ATCC CRL-1435) were cultured in RPMI-1640, Neuro2A (murine neuroblastoma ATCC CCL-131) in DMEM, HUH7 (human hepatoma, JCRB 0403) in DMEM/Ham's F-12 1:1, all supplemented with 10% fetal calf serum (FCS) (Gibco), 2mM stable glutamine, 100U/ml penicllin and 100µg/ml streptomycin (Biochrom). Primary porcine smooth muscle cells (PSMC) were cultivated in Ham's F12 (Biochrom)/ Waymouth (Gibco) medium 1:1 with $3.75x10^{-3}$% sodium bicarbonate, 10mM HEPES, 10% FCS, 40mM stable glutamine, 100U/ml penicillin, 100µg/ml streptomycin and 1.25µg/ml amphotericin B (Sigma).

2.4.4 SpC-c-MYC transgenic mice

SpC-c-MYC mice were described and characterized by Rapp *et al.* (102). All mice were of similar genetic background (≥90% C57BL/6 mouse strain).

2.4.5 *In vitro* transfections with EGFP and mCherry plasmids

Cells were seeded 24h prior to transfection in 6-well (PC3, $1.25x10^5$ cells; HUH7, PSMC, 10^5 cells) or 12-well plates (Neuro2A, $5x10^4$ cells) and co-transfected with pCpG-hCMV/SCEP-EGFP and the indicated mCherry plasmid harboring either five or no copies of the miR-143 binding site using X-tremeGENE HP DNA (Roche) according to manufacturer's protocol. 48h after transfection cells were trypsinised, washed and resuspended in phosphate buffered saline (PBS) and analyzed on a BD FACS Canto II Flow Cytometer (BD Bioscience). EGFP fluorescence was excited with the 488nm laser line and detected with a 530/30 bandpass filter. mCherry was excited with 635nm and emission was detected using a 660/20 bandpass filter. Cells were gated by forward versus sideward scatter to exclude cell debris and cell clusters. Data were recorded by BD FACSDiva Software and evaluated using Summit 4.3 software (Summit).

2.4.6 *In vitro* transfections with TNFα plasmids

Cells were seeded 24h prior to transfection in 24-well plates at a density of $2.5x10^4$ (HUH7, PSMC), $3.125x10^4$ (PC3) and $7.0x10^4$ (Neuro2A) cells per well. Subsequently, cells were transfected with indicated plasmids using the G3-HD-OEI (polypropylenimine generation three grafted with oligoethylenimine *via* 1,6-hexandioldiacrylate) polymer as previously described (109). 4h upon transfection medium was replaced by 500µL growth medium and 48h after transfection the conditioned medium was collected and frozen. TNFα was quantified using the Mouse TNF alpha ELISA Ready-SET-Go Kit (eBioscience) according to manufacturer's protocol.

2.4.7 L929 TNFα bioassay

Cytotoxicity of soluble TNFα was tested on murine fibroblasts (L929). The assay was in principle carried out as described by Su *et al*. (110). Indicated cell lines were seeded 24h prior to transfection in 24-well plates at a density of $2.5x10^4$ (HUH7, PSMC), $3.125x10^4$ (PC3) and $7.0x10^4$ (Neuro2A) cells per well. Subsequently, cells were transfected with indicated plasmids under optimized transfection conditions. After 4h of transfection medium was replaced by 500µL growth medium and 48h after transfection the conditioned medium was collected and stored frozen at -80°C. L929 murine fibroblasts were seeded in a 96-well tissue plate at a density of $1.25x10^4$ cells per well and cultured overnight at 37°C. The next day, the conditioned medium from transfected test cell lines was collected and supplemented with 1µg/mL actinomycin D (Sigma). The growth medium of L929 cells was replaced by 100µL per well of the conditioned medium. After an incubation time of 24h TNFα-mediated cytotoxicity of L929 cells was detected using the MTT (3-(4,5-dimethylthiazol-2-yl)-2,5-diphenyltetrazolium bromide) assay as previously described (111).

2.4.8 *In vitro* transfections with luciferase plasmids

Cells were seeded in their respective growth media 24h prior pDNA delivery in 96-well plates (10^4 cells) and transfected with 200ng of the indicated plasmid using Lipofectamine 2000 (Invitrogen) according to manufacturer's protocol. 24h after transfection luciferase activity was quantified as described previously (92).

2.4.9 *In vivo* transfections

All animal experiments were approved by the local ethical committee and performed according to the guidelines of the German law of protection of animal life. $6.5x10^6$ HUH7 cells were subcutaneously injected into the right flank of 8 weeks old female NMRI nude mice (Janvier). Animals received plasmids complexed with linear polyethylenimine (50µg plasmid in 250µl: pDNA/LPEI 1:0.78 (w:w) (N/P=6/1) in 20mM HEPES, 5% glucose, pH7.4) *via* the lateral tail vein when tumors reached a size of approximately 10mm in diameter. 48h after application organs (lung, heart, liver, kidney and spleen) and tumors were resected, the tissue was pulverized in liquid nitrogen and an aliquot homogenized in cell lysis buffer (Promega) using a tissue and cell homogenizer (FastPrep-24, MP Biomedicals). Luciferase activity was quantified as previously described (104). To determine the miR-143 levels of murine tissues and HUH7 xenografts, 30mg pulverized sample was subjected to above described RNA isolation and cDNA synthesis followed by a quantitative RT-PCR.

3. RESULTS

3.1 miR-200c sensitizes breast cancer cells to doxorubicin

3.1.1 Molecular evolution of breast cancer cells leads to a chemoresistant phenotype and down-regulation of miR-200c

Occurrence of chemoresistance is one of the major obstacles in chemotherapy of breast cancer patients. Thus, the pulse therapy of cancer patients applied in the clinics was mimicked by using an *in vitro* cell culture system. Therefore, the molecular evolution assay was established, in which the epithelial breast cancer cell line BT-474 was treated with doxorubicin for several cycles (Figure 4A). After each treatment round cells were harvested for cytotoxicity assays as well as RNA and protein isolation to investigate changes in chemosensitivity and gene expression. The cytotoxicity assays revealed that cells became more resistant from the third treatment cycle on. This effect did not get more significant after the fourth treatment round, indicating that the chemoresistant phenotype was obtained within three treatments (Figure 4B). In addition, the cell morphology changed from cells with a cobble-stone-like appearance to spindle-like cells, which also showed more scattering (Figure 4C). To further characterize the altered phenotype of the doxorubicin-treated cells, the protein expressions of E-cadherin and vimentin were determined in the rounds of the molecular evolution assay. In accordance with the microscopic pictures, a decrease of E-cadherin and an increase of vimentin was observed suggesting an EMT-like mechanism (Figure 4D). As the miR-200 family is regulating EMT by inhibiting transcriptional repressors of E-cadherin (20, 21, 112, 113), the expression levels of all family members (miR-141, miR-200a, miR-200b, miR-200c and miR-429) was analyzed in BT-474 cells. Thereby, miR-200c was the most abundantly expressed family member, showing a more than 10-fold higher expression (Figure 4E). Hence, the miR-200c levels during the molecular evolution assay were determined and a significant down-regulation within three rounds without any further decrease after the fourth treatment was observed (Figure 4F).

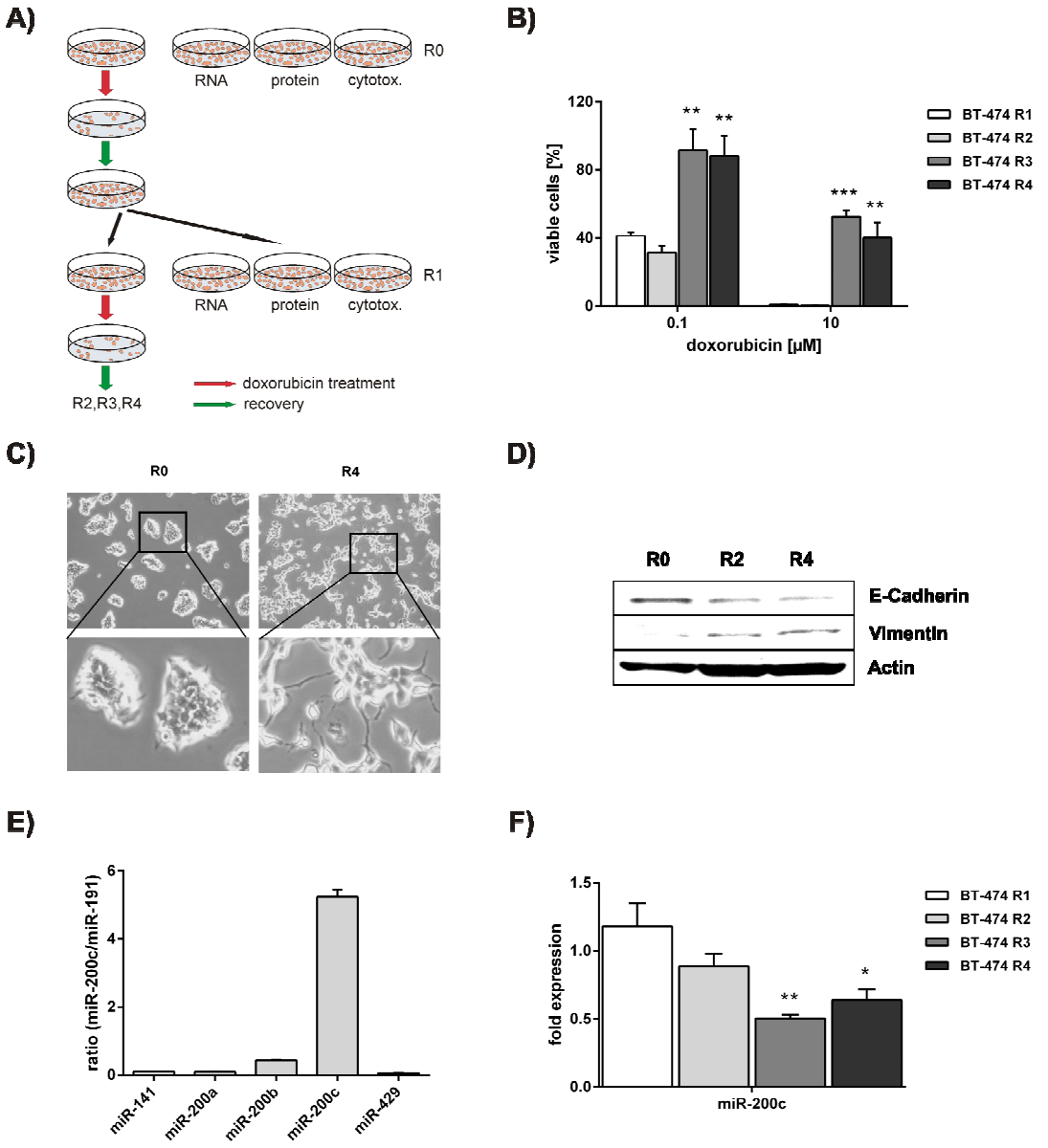

Figure 4. *Molecular evolution of breast cancer cells leads to a chemoresistant phenotype and down-regulation of miR-200c*

A) Molecular evolution assay. The epithelial breast cancer cell line BT-474 was sequentially treated with 50nM doxorubicin for 72h. Subsequently, medium was replaced by fresh medium until cells recovered and reached a confluency of 80%. Finally, cells were harvested for RNA isolation, cell lysis (protein), cytotoxicity assays and the next treatment round. R0 represents the untreated control cell line, whereas R1, R2, R3 and R4 represents BT-474 cells which are treated for one, two, three and four times, respectively.
B) Susceptibility to doxorubicin treatment. BT-474 cells of R1 to R4 were treated with 0.1 and 10µM doxorubicin for 72h. A CellTiter Glo assay was carried out to determine cell viability. Results are indicated as percentage of viable cells normalized to mock-treated cells.
C) Cell morphology of untreated and treated BT-474 cells. Microscopic pictures (phase contrast) were taken from untreated BT-474 cells (R0) and from doxorubicin-treated and recovered cells of R4.
D) Epithelial and mesenchymal marker expression in BT-474 cells of R0, R2 and R4 of the molecular evolution assay. E-cadherin and vimentin protein levels were determined by Western blot analysis. Actin was used as loading control.
E) miR-200 family screen in BT-474 cells. Quantitative RT-PCR was performed to analyze the levels of miR-141, miR-200a, miR-200b, miR-200c and miR-429. The expression of the respective miRNA was normalized to miR-191 as reference and depicted as ratio.
F) miR-200c expression in BT-474 cells which have undergone molecular evolution. Quantitative RT-PCR was performed to analyze miR-200c levels in BT-474 cells of R1 to R4. miR-200c expression was thereby normalized to miR-191. Results are depicted as fold expression compared to the untreated control cell line (R0). Experiments were done in triplicates. For statistical analysis a student's t-test was performed (*p<0.05; **p<0.01; ***p<0.001).

3.1.2 Characterization of the epithelial and the mesenchymal breast cancer cell line BT-474 and MDA-MB-436

To investigate the role of miR-200c in chemoresistance, a panel of different breast cancer cell lines was tested for the abundance of miR-200c. The mesenchymal cell lines (MDA-MB-436, MDA-MB-231 and MDA-MB-157) showed no expression of miR-200c, whereas the epithelial cell lines (MCF-7, MDA-MB-468 and BT-474) displayed high levels of miR-200c (Figure 5A). The cell line with the highest miR-200c expression (BT-474) and one with no miR-200c expression (MDA-MB-436) were further characterized.

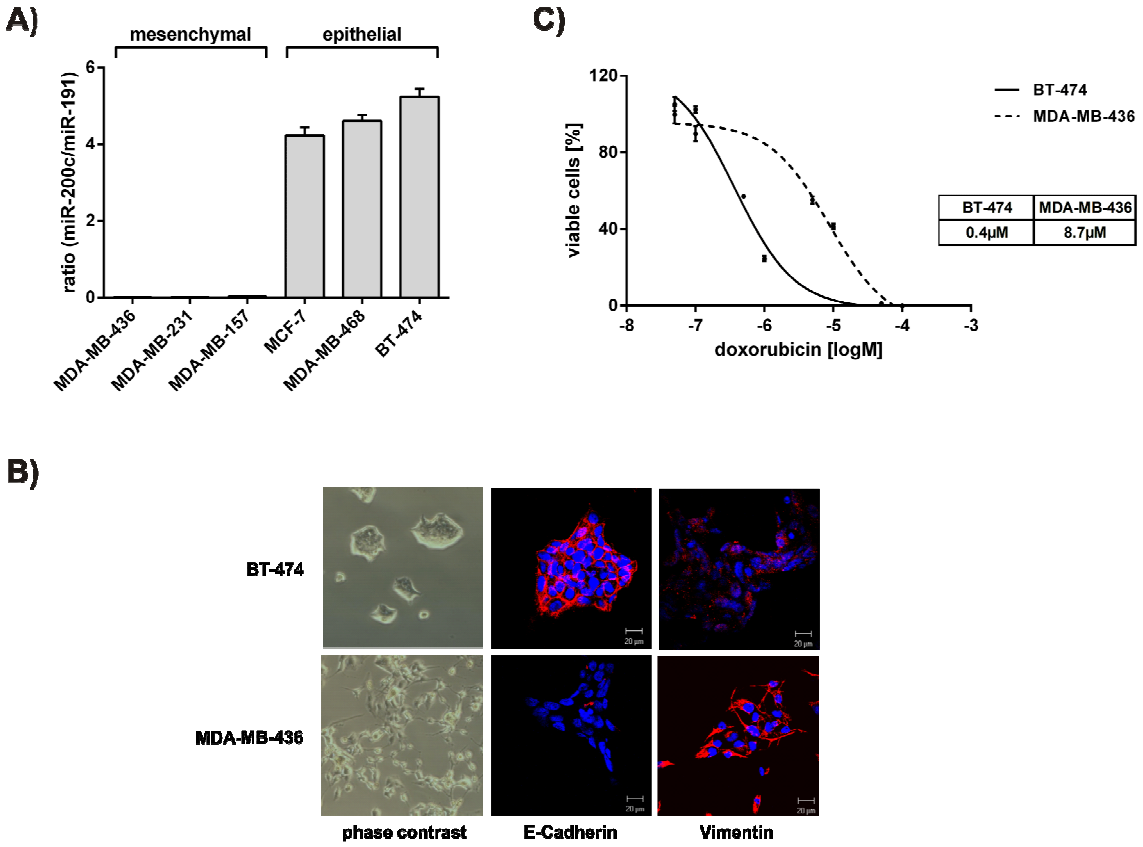

Figure 5. *Characterization of the epithelial and the mesenchymal breast cancer cell line BT-474 and MDA-MB-436*

A) miR-200c levels in a panel of mesenchymal (MDA-MB-436, MDA-MB-231, MDA-MB-157) and epithelial (MCF-7, MDA-MB-468, BT-474) breast cancer cell lines. Quantitative RT-PCR was performed to assess the levels of miR-200c. Expression was normalized to miR-191 and presented as ratio.
B) Epithelial and mesenchymal phenotype of BT-474 and MDA-MB-436 cells. To confirm the different phenotypes, microscopic pictures were taken from both cell lines (phase contrast, left panel). Furthermore, immunofluorescence and laser scanning microscopy was carried out to determine E-cadherin (red, middle panel) and vimentin (red, right panel) expression. Nuclei were stained with DAPI (blue).
C) Dose reponse curves and IC_{50} values for doxorubicin. BT-474 and MDA-MB-436 cells were treated with different concentrations of doxorubicin for 72h. Subsequently, a CellTiter Glo assay was performed to determine the percentage of viable cells (normalized to mock-treated cells). IC_{50} values are shown in the table.
Experiments were done in triplicates. Immunofluorescence stainings and microscopy were carried out by Prajakta Oak (PhD 2012, LMU Munich).

Consistent with the miR-200c expression, BT-474 cells grew in clusters with tight cell-cell junctions representing an epithelial cell type, whereas MDA-MB-436 cells grew as single spindle-shaped cells resembling a mesenchymal morphology (Figure 5B) (114). Immunofluorescence confirmed the epithelial phenotype of BT-474 in terms of high membrane localized E-cadherin and low cytoplasmic vimentin expression. On the other hand, MDA-MB-436 exhibited high vimentin and only low E-cadherin levels (Figure 5B) (114). Finally, the IC_{50} values for doxorubicin in BT-474 and MDA-MB-436 were determined. Dose response curves revealed that BT-474 cells were approximately 22-fold more susceptible to doxorubicin treatment as compared to MDA-MB-436 cells (Figure 5C).

Thus, BT-474 represents an epithelial breast cancer cell line with high levels of miR-200c and E-cadherin. On the contrary, MDA-MB-436 displays a mesenchymal phenotype with no expression of miR-200c, but with a high expression of the mesenchymal marker vimentin. Along with these findings, BT-474 cells were significantly more susceptible to doxorubicin treatment as compared to MDA-MB-436 cells. These two cellular systems were suitable to investigate the role of miR-200c in chemoresistance by either inhibiting or overexpressing this particular miRNA.

3.1.3 Inhibition of miR-200c in BT-474 cells causes chemoresistance to doxorubicin treatment

BT-474 and MDA-MB-436 cells were transfected with a miR-200c inhibitor (a locked nucleic acid (LNA) antisense molecule) as well as a scrambled control to prove whether there is a direct involvement of miR-200c in regulating chemosensitivity. As MDA-MB-436 cells have no miR-200c expression, this cell line served as a control to exclude off-target effects of the used LNAs.

Transfection of BT-474 cells with the miR-200c inhibitor led to significantly reduced levels of miR-200c as compared to those cells transfected with the scrambled control (Figure 6A). miR-200c inhibition in BT-474 cells also resulted in a more elongated and spindle-shaped cell morphology (Figure 6B). There was no change in cell morphology in MDA-MB-436 cells (data not shown). Most notably, the transfection of BT-474 cells with miR-200c inhibitor resulted in significantly more resistant cells, when treated with doxorubicin. As expected, there was no significant effect observable in MDA-MB-436 cells (Figure 6C).

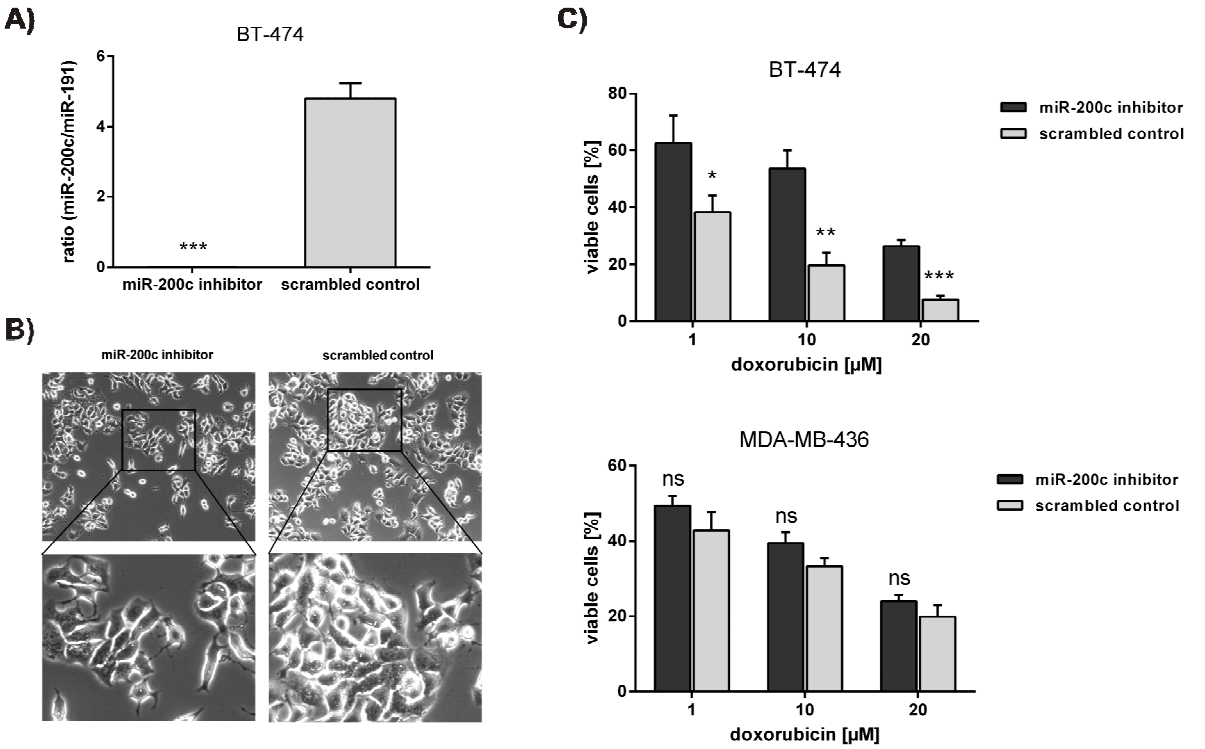

Figure 6. *Inhibition of miR-200c in BT-474 cells causes chemoresistance to doxorubicin treatment*

A) miR-200c expression after inhibiton. 24h after transfection with either miR-200c inhibitor or scrambled control, BT-474 cells were harvested for RNA isolation and quantitative RT-PCR. miR-200c expression was normalized to miR-191 and presented as ratio.
B) Cell morphology. Micrographs (phase contrast) of BT-474 cells were taken 24h after transfection with either miR-200c inhibitor or scrambled control.
C) Susceptibility to doxorubicin treatment. BT-474 and MDA-MB-436 cells, transfected with inhibitor or scrambled control, were treated with 1, 10 and 20µM doxorubicin for 72h. Cell viability was analyzed using CellTiter Glo.
Experiments were done in triplicates with at least two biological replicates. For statistical analysis a student's t-test was performed (ns = not significant; *p<0.05; **p<0.01; ***p<0.001).

3.1.4 Overexpression of miR-200c in MDA-MB-436 cells increases susceptibility to doxorubicin

As demonstrated, miR-200c inhibition in BT-474 cells resulted in chemoresistance to doxorubicin. Hence, the question was raised whether it was possible to sensitize the miR-200c-negative and doxorubicin-resistant cell line MDA-MB-436 to doxorubicin treatment by overexpressing miR-200c. Thus, MDA-MB-436 cells were transfected with the miR-200c precursor (pre-miR-200c), resulting in a high ectopic overexpression of miR-200c (Figure 7A). In accordance with previous studies (19, 20, 22, 23), cell morphology of pre-miR-200c-transfected cells changed to a more epithelial-like phenotype with cells growing in clusters (Figure 7B). Finally, a cytotoxicity assay was performed to investigate whether the miR-200c overexpressing cells were more susceptible to doxorubicin treatment. In all

doxorubicin concentrations the miR-200c overexpressing cells displayed a higher sensitivity to the treatment. On the other hand, susceptibility of BT-474 cells did not increase by further overexpressing miR-200c (Figure 7C).

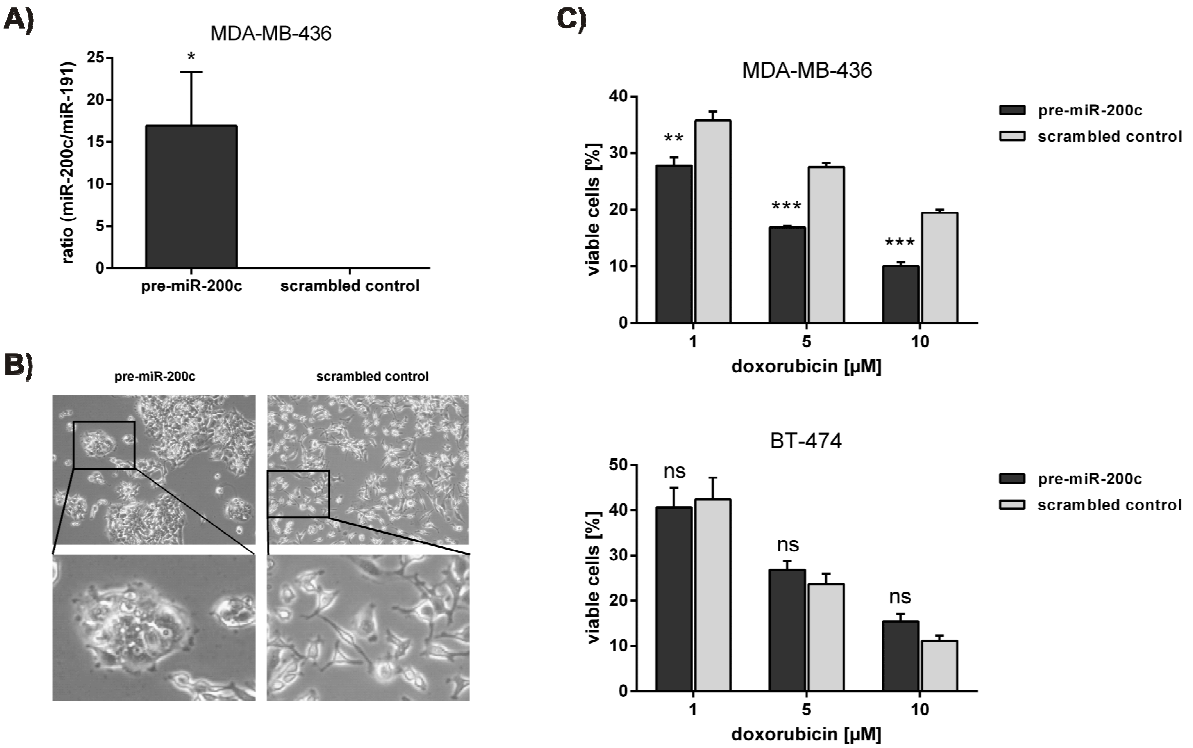

Figure 7. *Overexpression of miR-200c in MDA-MB-436 cells increases susceptibility to doxorubicin*

A) miR-200c levels after overexpression. After three consecutive transfections with either pre-miR-200c or scrambled control, MDA-MB-436 cells were harvested for RNA isolation and quantitative RT-PCR. miR-200c expression was normalized to miR-191 and presented as ratio.
B) Cell morphology. Micrographs (phase contrast) of MDA-MB-436 cells were taken after three consecutive transfections with either pre-miR-200c or scrambled control.
C) Susceptibility to doxorubicin treatment. With pre-miR-200c or scrambled control transfected MDA-MB-436 and BT-474 cells were treated with 1, 5 and 10µM doxorubicin for 72h. Cell viability was determined by a CellTiter Glo assay.
Experiments were done in triplicates with at least two biological replicates. For statistical analysis a student's t-test was performed (ns = not significant; *p<0.05; **p<0.01; ***p<0.001).

3.1.5 TrkB and Bmi1 protein expression is hampered by overexpression of miR-200c in MDA-MB-436 cells

miRNAs endogenously regulate gene expression by degrading mRNA or by inhibiting the translational process. Therefore, biological functions and physiological effects of miRNAs can be directly attributed to the silencing of their particular target genes. Thus, it was searched for candidates that are targeted by miR-200c and can interfere with cell survival or chemoresistance.

Howe *et al.* (27) have recently reported that TrkB (NTRK2), a member of the neurotrophic tyrosine receptor kinase family, is a direct target of miR-200c and responsible for anoikis resistance in breast cancer. It has also been shown that in neurons TrkB is involved in differentiation, proliferation and particularly in survival (115). To clarify whether TrkB can be silenced in the cell line MDA-MB-436 upon miR-200c overexpression, MDA-MB-436 cells were transfected with pre-miR-200c or scrambled control. As expected, the protein expression of two TrkB isoforms (gp145 and gp95) was decreased in pre-miR-200c-transfected cells as compared to scrambled control-transfected cells (Figure 8A). On the contrary, TrkB mRNA levels were not altered suggesting that TrkB translation was repressed by miR-200c without degradation of the mRNA (Figure 8B). The receptor tyrosine kinase TrkB is signaling amongst other pathways *via* PI3K and Akt (115), which plays a pivotal role in cell survival. Thus, the phosphorylation status of Akt was analyzed upon miR-200c modulation. However, there were no detectable differences in the p-Akt levels of pre-miR-200c- and scrambled control-transfected cells. Hence, pre-miR-200c- as well as scrambled control-transfected MDA-MB-436 cells were treated with doxorubicin for 24h to induce Akt-dependent survival signaling. Here, the phosphorylation of Akt was enhanced in the scrambled control-transfected cells, whereas miR-200c overexpressing cells still showed low levels of p-Akt (Figure 8C).

Another target of miR-200c is Bmi1, a regulator of stem cell self-renewal and senescence (31). It has been reported that Bmi1 confers cisplatin and docetaxel resistance in osteosarcoma and prostate cancer, respectively (116, 117). Thus, the mesenchymal cell line MDA-MB-436 was transfected with either pre-miR-200c or scrambled control. As hypothesized, Bmi1 was silenced in the pre-miR-200c-transfected cells as compared to the scrambled control-transfected cells (Figure 8D). Consistent with TrkB, Bmi1 mRNA was also not degraded by miR-200c (Figure 8E). Bmi1 functions as transcriptional repressor leading to the repression of a variety of genes including $p16^{Ink4a}$ and $p19^{Arf}$ of the Ink4a locus. Since repression of $p19^{Arf}$ results in the degradation of p53 by MDM2 leading to anti-apoptotic effects (118), the protein expression of p53 was determined in pre-miR-200c-transfected cells. However, no regulation of p53 protein was observed in MDA-MB-436 as this cell line lacks intrinsic p53 (Figure 8F).

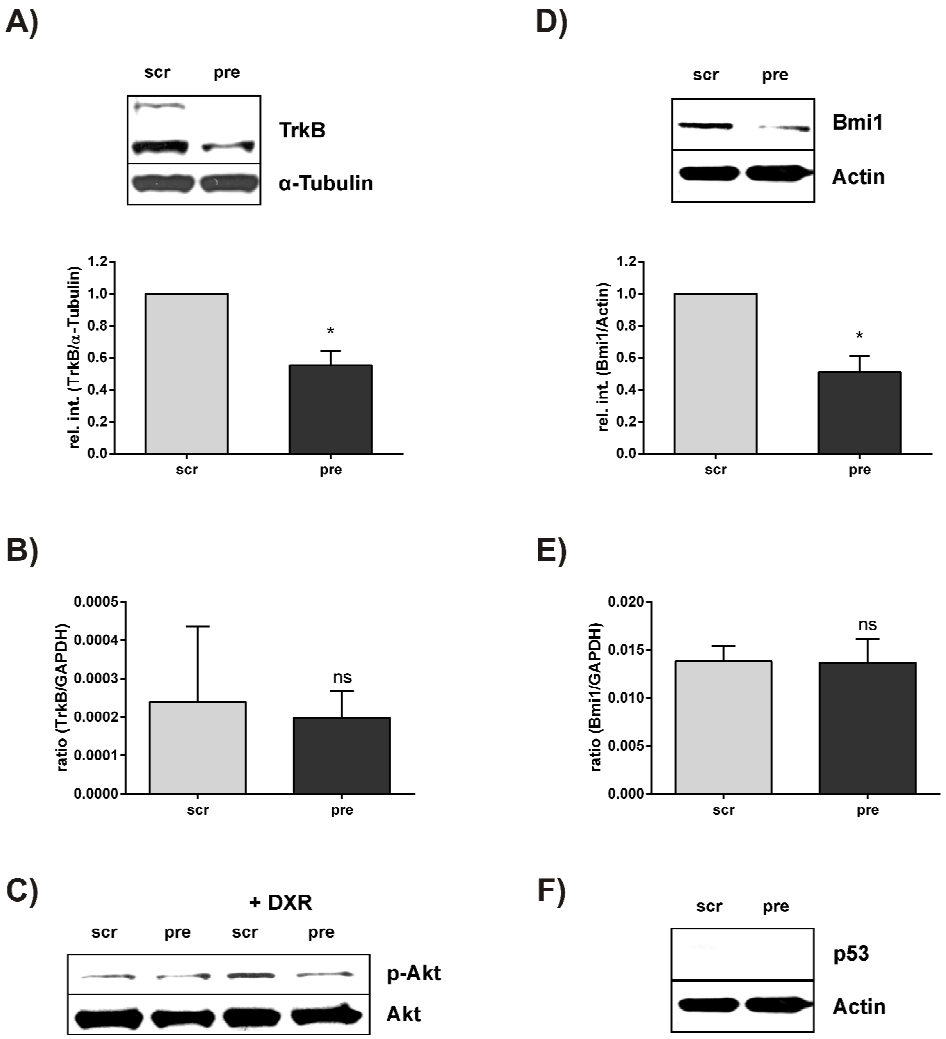

Figure 8. *TrkB and Bmi1 protein expression is hampered by overexpression of miR-200c in MDA-MB-436 cells*

Total cell lysates of pre-miR-200c- (pre) and scrambled control- (scr) transfected MDA-MB-436 cells were subjected to Western blot analysis and quantitative RT-PCR to determine expression of A) TrkB (gp145 and gp95) protein, B) TrkB mRNA, C) p-Akt protein either after treatment with 0.5µM doxorubicin for 24h (right panel) or untreated (left panel), D) Bmi1 protein, E) Bmi1 mRNA and F) p53 protein. α-Tubulin or actin was used as loading control. Western blot quantification of three independent experiments was carried out by analyzing the relative intensities (rel. int.) of TrkB or Bmi1 normalized to the rel. int. of α-tubulin or actin using ImageJ software. For quantitative RT-PCR TrkB and Bmi1 expressions were normalized to GAPDH as reference and presented as ratio. A student's t-test was performed to assess statistical significance (ns = not significant; *p<0.05). DXR = doxorubicin.

3.1.6 The protein expression of TrkB and Bmi1 is regulated during the rounds of the molecular evolution assay in BT-474 cells

After demonstrating the effects of miR-200c on the target genes TrkB and Bmi1, it was analyzed whether these proteins were also regulated in the molecular evolution assay. BT-474 cells showed a slight elevation of TrkB in the second round (R2) followed by a down-regulation in the last round (R4) (Figure 9A). Moreover, the

phosphorylation status of Akt, a downstream target of TrkB and an important regulator of cell survival, was determined. Consistent with the regulation of TrkB expression, p-Akt was considerably increased in round 2 (R2) and decreased in round 4 (R4) (Figure 9B).

Bmi1 levels were also assessed in the protein lysates of the molecular evolution assay of BT-474 cells. An up-regulation of Bmi1 was observed with no protein expression in the control round (R0), a slight expression in the second (R2) and a high expression in the fourth round (R4) (Figure 9C). Consequently, the protein expression of p53 was determined and a decline of p53 in round 4 (R4) was observed (Figure 9D). The molecular evolution assay of BT-474 cells resulted in a regulation of TrkB and Bmi1 protein expression. The respective downstream targets p-Akt and p53 were modulated in accordance, presumably conferring the observed chemoresistance.

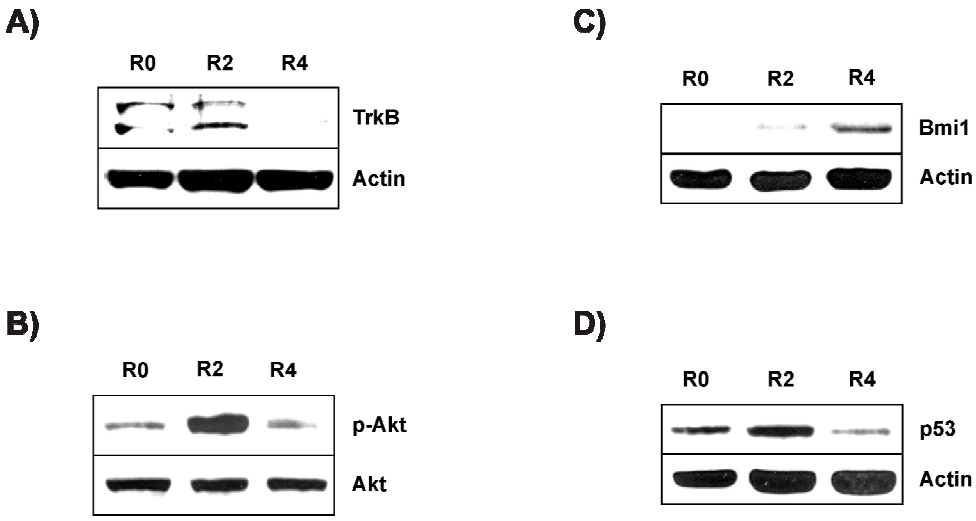

Figure 9. *The protein expression of TrkB and Bmi1 is regulated during the rounds of the molecular evolution assay in BT-474 cells*

Total cell lysates of BT-474 cells derived from R0, R2 and R4 of the molecular evolution assay were subjected to Western blot analysis to determine protein expression of A) TrkB isoforms, B) p-Akt, C) Bmi1 and D) p53. Actin was used as loading control.

3.2 miR-200c targets KRAS

3.2.1 KRAS is a predicted target of miR-200c and its protein expression inversely correlates with miR-200c expression in breast cancer cells

In order to examine whether miR-200c has any predicted target site in the 3'UTR of the KRAS gene, online prediction tools were utilized, which were based on the three different algorithms TargetScan (95), miRanda (96) and DIANA microT (97, 98). All applied algorithms uniformly predicted one specific binding site, which is broadly conserved among several species. This predicted site is located at position 305-311 of the KRAS 3'UTR and comprises a 7mer-m8 seed, i.e. a perfect base pairing between the nucleotides 2-7 (seed region) and the nucleotide 8 of the mature miRNA and its target mRNA (Figure 10A). As miR-200c is well established and known to be differentially expressed in breast tumors, miR-200c (Figure 10B) and K-ras (Figure 10C) expression levels were analyzed in a panel of different breast cancer cell lines. The expression of miR-200c was found to inversely correlate with the K-ras protein expression (Figure 10D); i.e. breast cancer cells, which displayed a high miR-200c expression, had low protein levels of K-ras (Pearson r = -0.80). A typical characteristic of advanced cancer is acquired chemoresistance. miR-200c as well as particularly mutated K-ras have both been implicated in resistance to classical chemotherapy and targeted therapies (22, 32, 37, 38, 51, 52, 93, 119), but their direct interaction has not been shown yet. Therefore, it was investigated whether a reduction of miR-200c increases K-ras protein expression in an assay for induced chemoresistance, which was previously described as molecular evolution assay (93). The miR-200c-positive breast cancer cell line BT-474 was treated with doxorubicin for three rounds, which resulted in reduced miR-200c levels (Figure 10E) and an elevated K-ras protein expression (Figure 10F) suggesting a miR-200c-dependent regulation of KRAS.

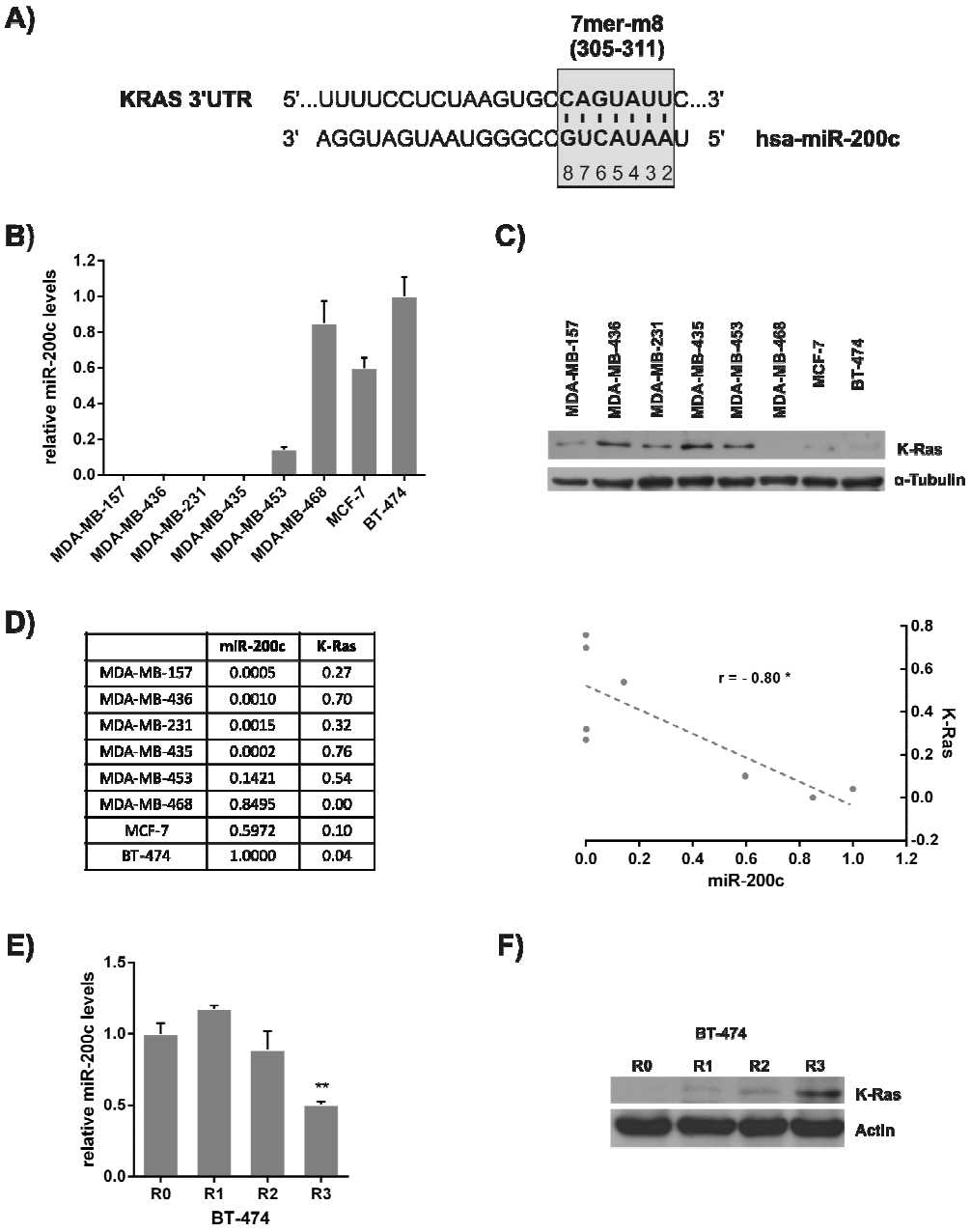

	miR-200c	K-Ras
MDA-MB-157	0.0005	0.27
MDA-MB-436	0.0010	0.70
MDA-MB-231	0.0015	0.32
MDA-MB-435	0.0002	0.76
MDA-MB-453	0.1421	0.54
MDA-MB-468	0.8495	0.00
MCF-7	0.5972	0.10
BT-474	1.0000	0.04

Figure 10. *KRAS is a predicted target of miR-200c and its protein expression inversely correlates with miR-200c expression in breast cancer cells*

A) Target site prediction of miR-200c in the 3'UTR of the KRAS gene. By means of the three different prediction algorithms TargetScan, miRanda and DIANA microT, a unique conserved binding site with a 7mer-m8 seed at position 305 – 311 of the 3'UTR of the KRAS gene was found.
B) miR-200c expression in a panel of breast cancer cell lines. miR-200c expression was normalized to miR-191 and values are stated as mean ± SD (n=3).
C) K-ras protein expression in a panel of breast cancer cell lines. Total cell lysates were subjected to Western blot analysis and incubated with indicated antibodies.
D) Correlation of K-ras protein and miR-200c expression. The relative intensities of the Western blot were quantified using ImageJ software. K-ras signals were then normalized to the loading control α-tubulin and depicted as ratio. The values of the relative K-ras protein and miR-200c expression are listed in the table. The graph shows the Pearson correlation scatter plot of the relative K-ras and miR-200c levels in the different breast cancer cell lines (*p<0.05).
Chemotherapeutic treatment of the miR-200c^{high} cell line BT-474. Cells were treated with 50nM doxorubicin as described for the molecular evolution assay. After each cycle cells were harvested for RNA isolation and protein lysates to determine E) the relative miR-200c expression and F) the K-ras protein levels of the indicated round. Values are stated as mean ± SD (n=3). For statistical analysis a student's t-test was performed (**p<0.01; R0 compared to R3).

3.2.2 miR-200c inhibits K-ras protein expression without affecting KRAS mRNA levels

For the validation of KRAS as a new target of miR-200c, a luciferase reporter assay was performed using a vector encoding for renilla luciferase and almost the entire 3'UTR of the KRAS gene including the predicted miR-200c binding site. Ectopic expression of this reporter in two miR-200c^{low} (MDA-MB-231 and MDA-MB-436) and two miR-200c^{high} (BT-474 and MCF-7) breast cancer cell lines showed high and low luciferase activities, respectively (Figure 11A). This correlation indicates a direct inhibition of the luciferase reporter *via* the KRAS 3'UTR by miR-200c. Next, it was examined whether miR-200c was able to regulate the luciferase reporter when overexpressed or inhibited. The luciferase reporter was therefore transfected together with pre-miR-200c in MDA-MB-436 cells or miR-200c inhibitor in BT-474 cells. As expected, overexpression of miR-200c led to a decreased luciferase activity, whereas its inhibition resulted in an enhanced bioluminescence (Figure 11B).

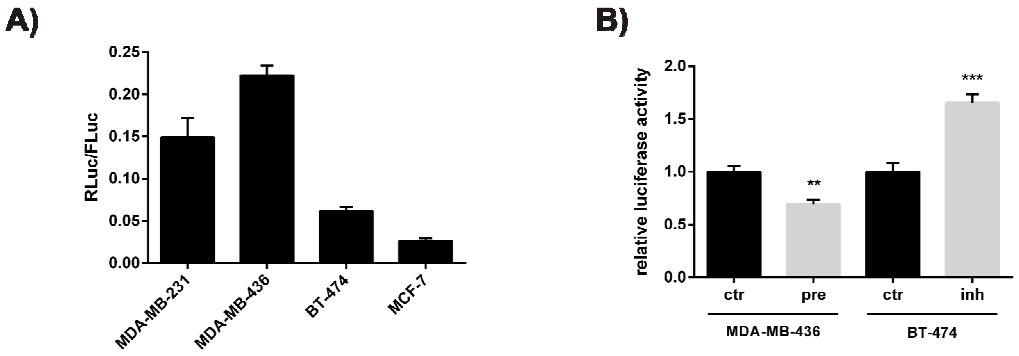

Figure 11. *miR-200c targets the 3'UTR of the KRAS mRNA*

A) Luciferase reporter assay with different breast cancer cell lines. The renilla luciferase reporter containing the 3'UTR of KRAS including the predicted target site of miR-200c (RLuc) or the firefly luciferase control plasmid pGL3 (FLuc) were transfected into the indicated cell lines. Renilla reporter luciferase activity was normalized to the activity of the firefly control as ratio. Values are stated as mean ± SEM (n=5).
B) Luciferase reporter assay upon miR-200c modulation. MDA-MB-436 cells were transfected with either pre-miR-200c (pre) or scrambled control (ctr). BT-474 cells were transfected with either miR-200c inhibitor (inh) or scrambled control inhibitor (ctr). Relative luciferase activities (RLuc/FLuc) are depicted in the graph. Values are stated as mean ± SEM (n=5). For statistical analysis a student's t-test was performed (**p<0.01; ***p<0.001).

To further prove the inhibition of KRAS expression by miR-200c, protein and mRNA levels were checked after either miR-200c inhibition or overexpression. Inhibition of miR-200c in BT-474 and MCF-7 cells led to an elevated K-ras protein expression, while KRAS mRNA levels were not changed (Figure 12A). Overexpression of miR-200c resulted in decreased K-ras protein and unaltered KRAS mRNA levels in MDA-MB-231 and MDA-MB-436 cells (Figure 12B).

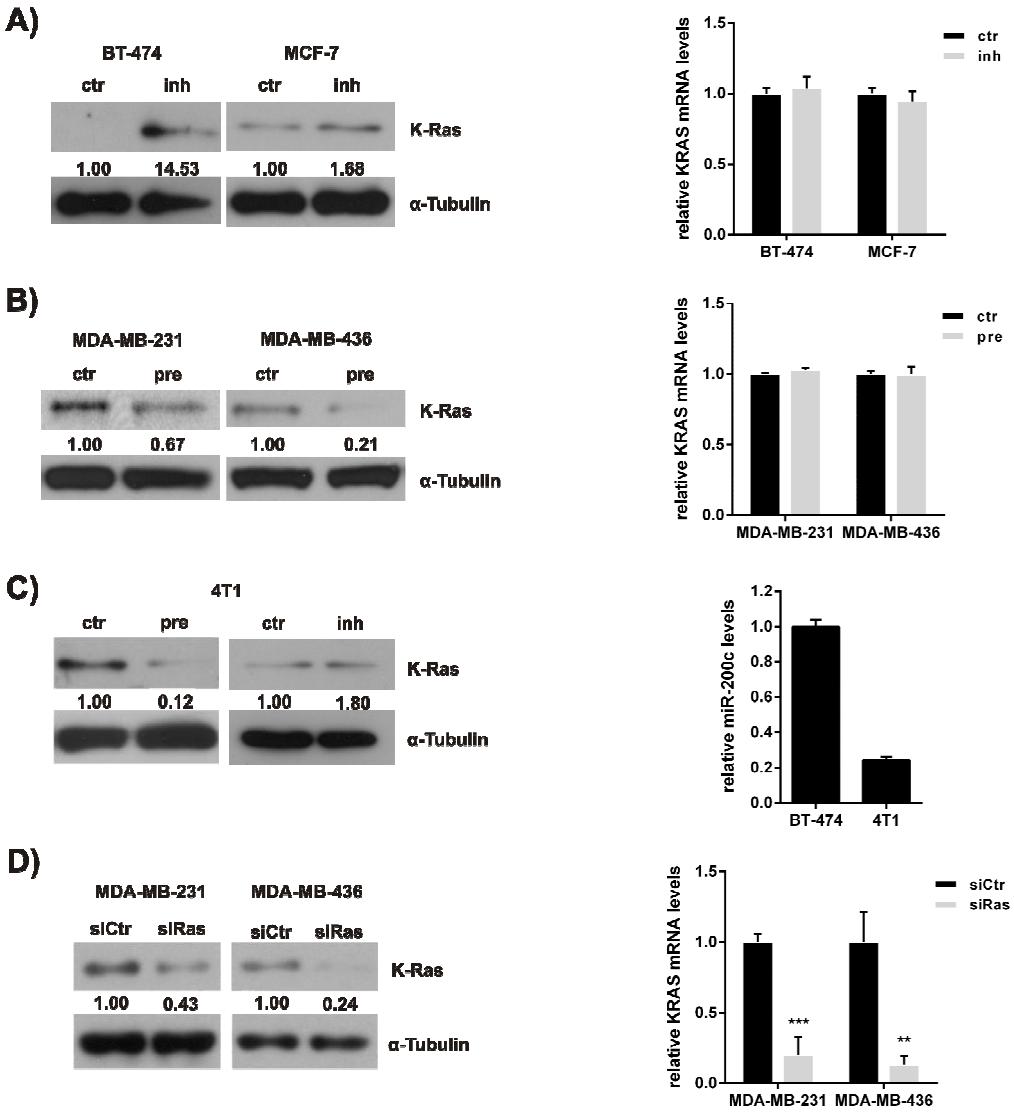

Figure 12. *miR-200c inhibits K-ras protein expression without affecting KRAS mRNA levels*

A) miR-200c inhibition in the miR-200c^{high} cell lines BT-474 and MCF-7. Indicated cell lines were transfected with either miR-200c inhibitor (inh) or scrambled control inhibitor (ctr) and at 72h post transfection subjected to Western blot analysis (left panel) or quantitative RT-PCR (right panel). Values are stated as mean ± SD (n=3).
B) miR-200c overexpression in the miR-200c^{low} cell lines MDA-MB-231 and MDA-MB-436. Indicated cell lines were transfected with either pre-miR-200c (pre) or scrambled pre-miR-control (ctr) and at 72h after transfection subjected to Western blot analysis (left panel) or quantitative RT-PCR (right panel). Values are stated as mean ± SD (n=3).
C) K-ras regulation by miR-200c in the miR-200c^{medium} cell line 4T1. K-ras protein levels were examined by Western blot analysis at 72h after transfection with either pre-miR-200c (pre) or miR-200c inhibitor (inh). The relative miR-200c expression of 4T1 cells was determined by quantitative RT-PCR in comparison to the miR-200c^{high} cell line BT-474 (right panel).
D) KRAS-specific knockdown in MDA-MB-231 and MDA-MB-436. Cells were transfected either with a siRNA pool against human KRAS (siRas) or with a non-targeting control siRNA (siCtr). After 72h K-ras protein (left panel) and KRAS mRNA levels (right panel) were determined. Values are stated as mean ± SD (n=3). For statistical analysis a student's t-test was performed (**p<0.01; ***p<0.001).

Moreover, in the murine breast cancer cell line 4T1, which endogenously displayed a medium expression of miR-200c, it was demonstrated that K-ras protein levels were both down- and up-regulated after miR-200c overexpression and inhibition (Figure 12C). As there was no regulation on the mRNA level in the cell lines tested before, the mRNA expression of KRAS upon miR-200c manipulation was not determined in 4T1 cells. In order to assess the silencing efficiency and the mechanism of the miR-200c-induced KRAS knockdown, the effects of miR-200c were compared with those of a siRNA-pool against KRAS (siRas). While the siRNA knockdown was similar on protein level, siRas also remarkably reduced KRAS mRNA (Figure 12D), consistent with the different known modes of action of miRNA and siRNA-induced gene silencing. Although it has been reported that miRNAs can also down-regulate target mRNAs by affecting their stabilities (120), miR-200c primarily inhibits the translation of KRAS, whereas siRas causes the expected mRNA cleavage.

3.2.3 KRAS silencing by miR-200c and siRas leads to reduced proliferation and changed cell cycle of breast cancer cells dependent on the KRAS mutation status

The significance of the oncogene KRAS is underlined by frequently occurring activating mutations in numerous tumors and cancer cell lines. According to the respective mutation status, different physiological effects were expected upon KRAS knockdown. Thus, the cell line MDA-MB-231, which harbors an activating G13D mutation in the KRAS gene, and the cell line MDA-MB-436, which expresses the wild-type KRAS gene (121, 122), were chosen for further experiments. By using pre-miR-200c as well as siRas for the silencing of KRAS, the particular role of KRAS should be dissected from the role of all the other potential targets of miR-200c. Several reports have shown that oncogenic K-ras stimulates proliferation in various cell types, highlighting its role in tumorigenesis (123-125). Therefore, the proliferation of the two breast cancer cell lines was analyzed upon transfection with pre-miR-200c or siRas. In the KRAS mutated cell line MDA-MB-231 the proliferation of pre-miR-200c- and siRas-transfected cells was similarly decreased (Figure 13A), whereas in the KRAS wild-type cell line MDA-MB-436 only pre-miR-200c was able to significantly reduce proliferation (Figure 13B).

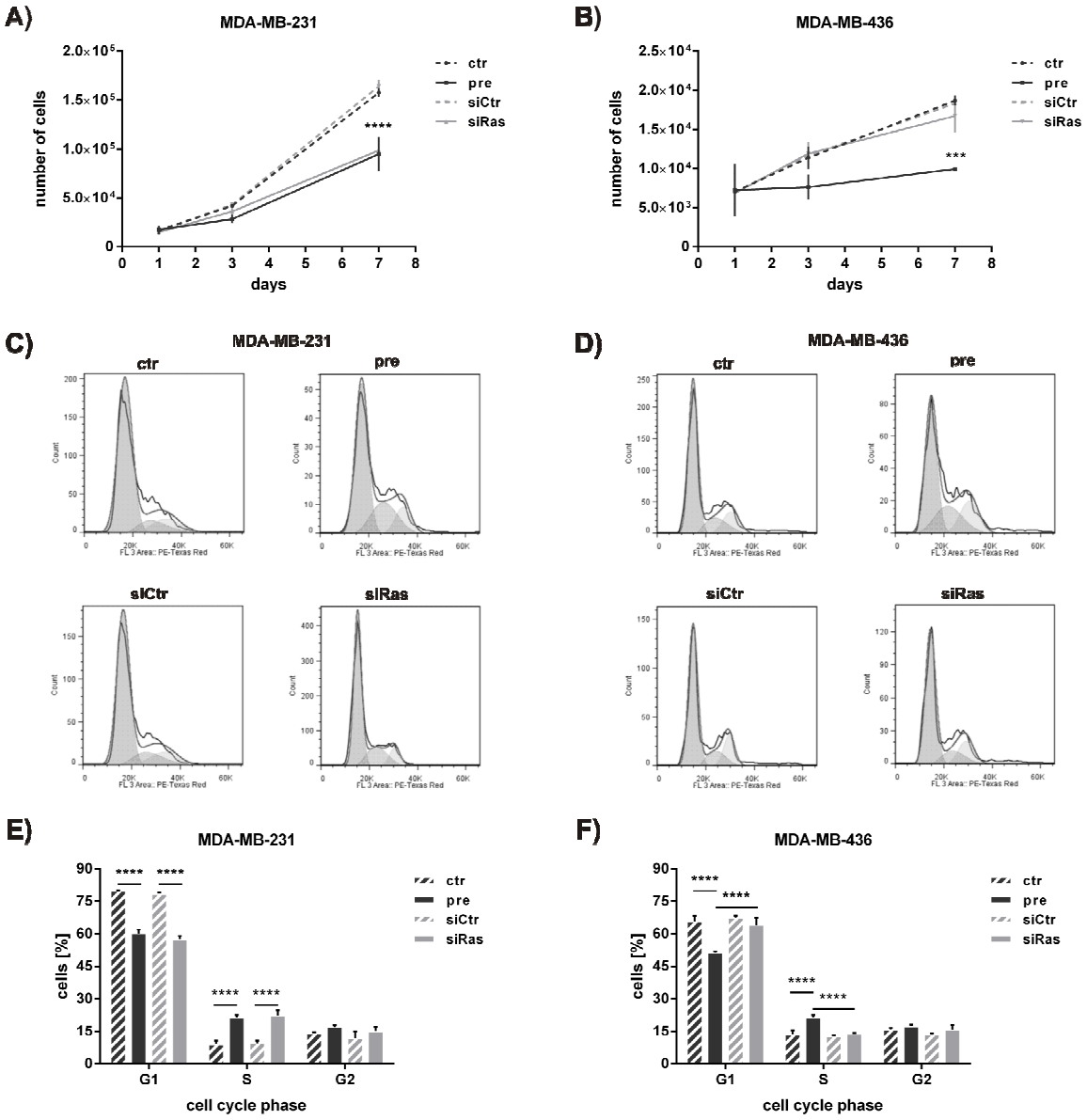

Figure 13. *KRAS silencing by miR-200c and siRas leads to reduced proliferation and changed cell cycle of breast cancer cells dependent on the KRAS mutation status*

Proliferation of different breast cancer cell lines upon KRAS knockdown. A) MDA-MB-231 cells which harbor an activating (G13D) KRAS mutation and B) MDA-MB-436 cells which express wild-type KRAS were transfected with the indicated oligonucleotides. Values are stated as mean cell number ± SD (n=3). For statistical analysis a student's t-test was performed (***p<0.001; ****p<0.0001).
Cell cycle of different breast cancer cell lines upon KRAS knockdown. C) MDA-MB-231 cells and D) MDA-MB-436 cells were subjected to flowcytometry at 72h after transfection with the indicated oligonucleotides. Cell cycle analysis was carried out using FlowJo software. Results are presented as histograms (y-axis: counts; x-axis: PE-Texas Red indicative for propidium iodide).
Statistical analysis of the cell cycle phases upon KRAS silencing. The percentage of E) MDA-MB-231 and F) MDA-MB-436 cells in the respective cell cycle phase upon indicated oligonucleotide transfection was determined. Values are stated as mean ± SD (n=3). For statistical analysis a student's t-test was performed (****p<0.0001).

As it has been demonstrated that oncogenic K-ras drives cell cycle progression by enabling cells to enter the S-phase and thereby promotes tumorigenesis (126, 127), cell cycle analyses were additionally performed to investigate whether the cell cycle was differentially affected. Consistent with the proliferation, the cell cycle of MDA-MB-231 cells was considerably changed upon both pre-miR-200c and siRas transfection (Figure 13C), whereas only pre-miR-200c changed the cell cycle of MDA-MB-436 cells (Figure 13D). Quantification of the cell cycle phases revealed that in MDA-MB-231 cells pre-miR-200c as well as siRas led to a decrease of the G1-phase and an increase of the S-phase (Figure 13E). In MDA-MB-436 cells, however, only pre-miR-200c achieved a reduction of the G1-phase and an increase of the S-phase, whereas siRas did not affect the cell cycle (Figure 13F).

3.2.4 miR-200c and siRas also affect the cell cycle in lung cancer cells by inhibiting KRAS

As the relevance of KRAS mutations in breast cancer remains elusive, the physiological effects of miR-200c-dependent KRAS silencing were explored in a more relevant cancer type. Besides in pancreas and colon cancer, KRAS mutations occur very frequently in non-small cell lung cancer (NSCLC) (15-50%) (35, 37).
Thus, the two NSCLC cell lines A549 and Calu-1 were used, which harbor the activating KRAS mutations G12S and G12C, respectively (128, 129). Both lung cancer cell lines displayed low miR-200c levels (Figure 14A) but a considerable K-ras protein expression (Figure 14B) as compared to the miR-200c^{high} breast cancer cell line BT-474. The cell cycle upon KRAS knockdown was determined in the two lung cancer cell lines to examine whether the effects were comparable to those of the KRAS mutated breast cancer cell line MDA-MB-231. Interestingly, the cell cycle of pre-miR-200c- as well as siRas-transfected A549 (Figure 14C) and Calu-1 (Figure 14D) cells was similarly changed. In accordance with MDA-MB-231 cells, the G1-phase was decreased, whereas the S-phase was increased in A549 (Figure 14E) and Calu-1 (Figure 14F) cells.

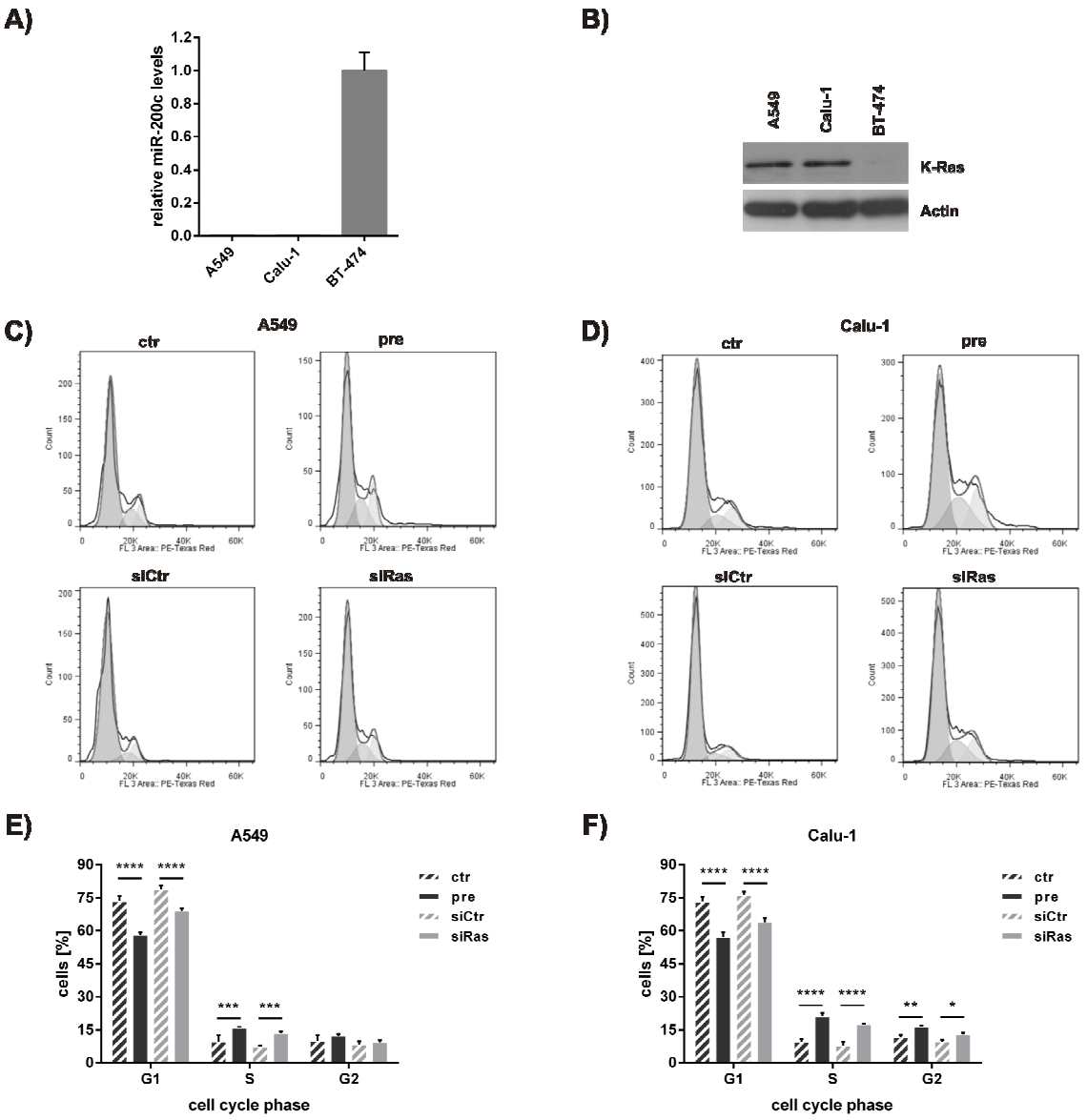

Figure 14. *miR-200c and siRas also affect the cell cycle in lung cancer cells by inhibiting KRAS*

A) miR-200c expression and B) K-ras protein levels of the two KRAS mutated lung cancer cell lines A549 (G12S) and Calu-1 (G12D) in comparison to the breast cancer cell line BT-474. Values are stated as mean ± SD (n=3).
Cell cycle of different lung cancer cell lines upon KRAS knockdown. C) A549 cells and D) Calu-1 cells were subjected to flowcytometry at 72h after transfection with the indicated oligonucleotides. Cell cycle analysis was carried out using FlowJo software. Results are presented as histograms (y-axis: counts; x-axis: PE-Texas Red indicative for propidium iodide).
Statistical analysis of the cell cycle phases upon KRAS silencing. The percentage of E) A549 and F) Calu-1 cells in the respective cell cycle phase upon indicated oligonucleotide transfection was analyzed. Values are stated as mean ± SD (n=3). For statistical analysis a student's t-test was performed (*p<0.05; **p<0.01; ***p<0.001; ****p<0.0001).

These data suggest that miR-200c can generally interfere with cell proliferation and cell cycle by directly targeting oncogenic KRAS independent of the respective cancer type. Furthermore, these results highlight the prominent role of the miR-200c-dependent regulation of KRAS, especially if applied to cell lines which are driven by oncogenic KRAS.

3.3 Salinomycin targets migratory miR-200c^{low} tumor cells

3.3.1 Salinomycin targets migrating cancer cells

To investigate whether salinomycin is a potent inhibitor of migrating cancer cells, several breast and lung cancer cell lines were characterized in terms of their migratory capacity as well as their mesenchymal or epithelial marker expression.

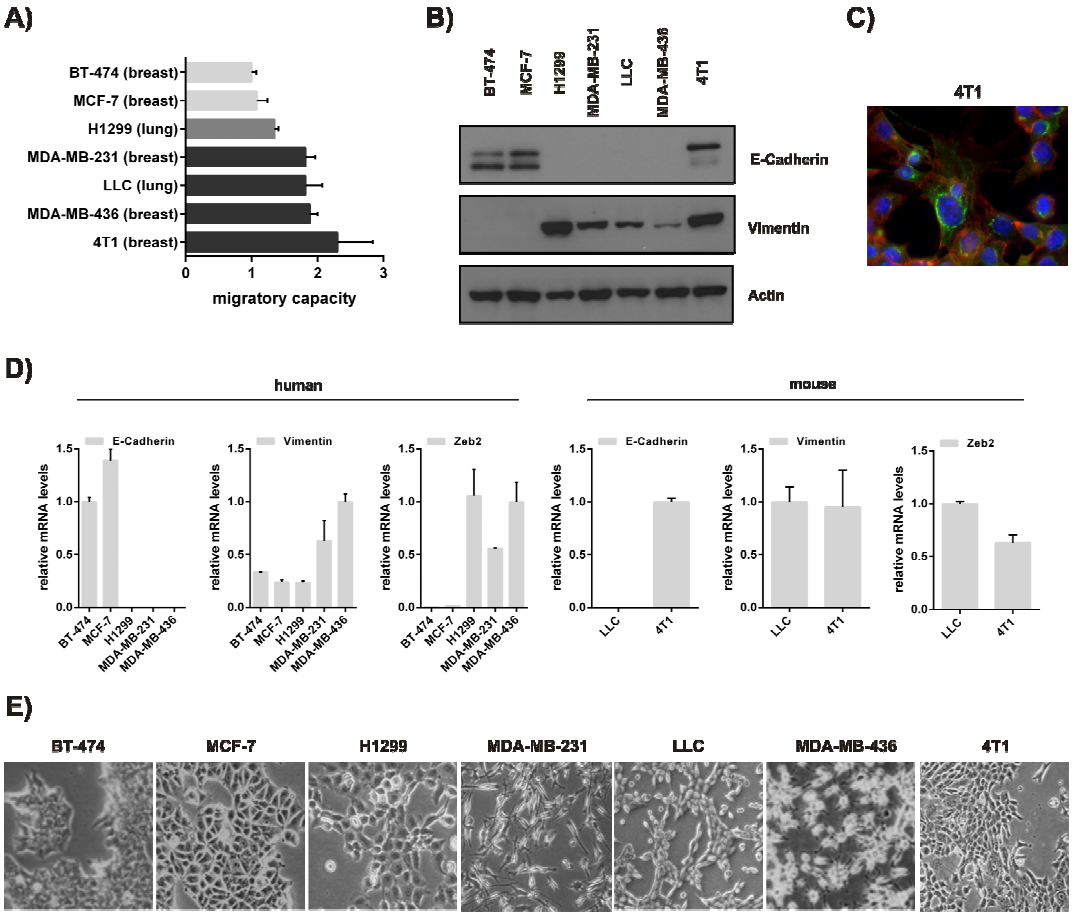

Figure 15. *Characterization of a panel of breast and lung cancer cell lines*

A) Boyden chamber migration assays of different breast and lung cancer cell lines. The number of migrated BT-474 cells was set to a migratory capacity of one and the remaining cell lines were normalized as fold of the migratory capacity of BT-474 cells.
B) Western blot analysis of different breast and lung cancer cell lines. Total cell lysates from indicated cell lines were analyzed for the protein expression of E-cadherin and vimentin.
C) Heterogeneous cell population in the 4T1 cell line. Immunofluorescence staining was performed to assess the distribution of E-cadherin (red) and vimentin (green) in the murine breast cancer cell line 4T1. Nuclei were counterstained with DAPI (blue).
D) Relative mRNA levels of EMT markers in the panel of cancer cell lines. Quantitative RT-PCR was carried out to determine the relative mRNA expression of E-cadherin, vimentin and Zeb2. The left panel presents all human cancer cell lines using human-specific primers, whereas the right panel shows the two murine cancer cell lines using mouse-specific primers.
E) Cell morphology of different cancer cell lines. Microscopic pictures (phase contrast) were taken from the indicated cell lines.
Migration assays and the microscopy of the cell lines were conducted by Adam Hermawan (PhD study, LMU Munich).

The migratory potential of the panel of breast (BT-474, MCF-7, MDA-MB-231, MDA-MB-436 and 4T1) and lung (H1299 and LLC) cancer cell lines was determined by Boyden chamber assays (Figure 15A). Cell lines with an increased migratory capacity displayed a high vimentin and in most cases a low E-cadherin expression on both the protein and mRNA level (Figure 15B and Figure 15D). This was in line with their mesenchymal cell morphology (Figure 15E). 4T1 cells, however, displayed high vimentin and significant E-cadherin levels representing a heterogeneous cell population consisting of mesenchymal and epithelial cells (Figure 15C); i.e. cells which highly express vimentin have rather low levels of E-cadherin and *vice versa*.

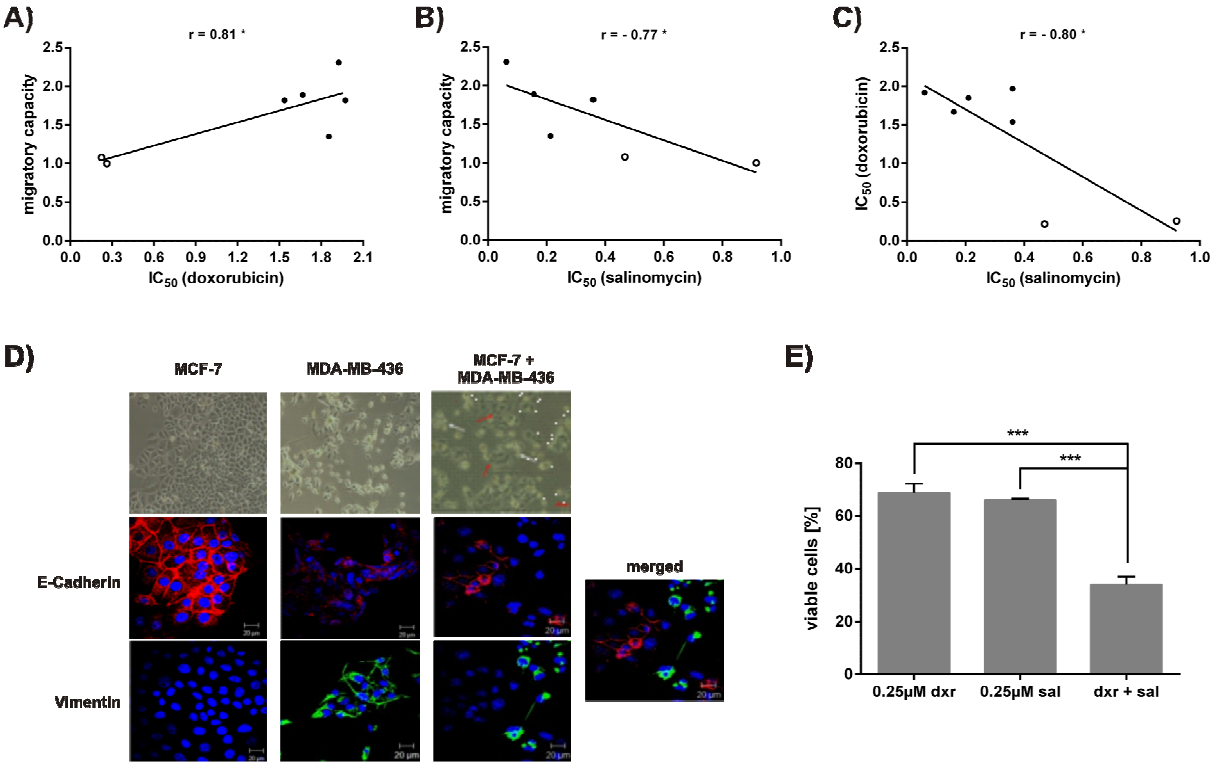

Figure 16. *Salinomycin targets migrating cancer cells*

A) Correlation between migratory capacity and susceptibility to doxorubicin. IC_{50} values of doxorubicin were determined by a CellTiter Glo assay and correlated with the migratory capacity of the respective cell lines (Pearson r = 0.81; *p<0.05). Open circles represent the epithelial cell lines BT-474 and MCF-7.
B) Correlation between migratory capacity and susceptibility to salinomycin. IC_{50} values of salinomycin were analogously obtained and correlated with the migratory capacity of the respective cell lines (Pearson r = -0.77; *p<0.05).
C) Correlation of doxorubicin and salinomycin susceptibility. The IC_{50} values of doxorubicin were correlated with the IC_{50} values of salinomycin (Pearson r = -0.80; *p<0.05).
D) Microscopy of single and co-cultured MCF-7 and/or MDA-MB-436 cells. Phase contrast and immunofluorescence pictures for E-cadherin (red) and vimentin (green) were taken either from MCF-7, MDA-MB-436 or MCF-7 (red arrows) + MDA-MB-436 (white arrows). Nuclei were stained with DAPI (blue).
E) Treatment of co-cultured MCF-7 and MDA-MB-436 cells. Co-cultured cells were treated with indicated concentrations of salinomycin (sal) and/or doxorubicin (dxr). (Student's t-test, two-tailed; ***p<0.001)
Imunofluorescence and treatment experiments of the co-cultured cell lines were done by Prajakta Oak (PhD 2012, LMU Munich).

In order to examine the sensitivity of these differentially migrating cancer cell lines to doxorubicin, a classical chemotherapeutic, and to salinomycin, a new class of CSC-specific drugs, the IC_{50} values of both drugs were determined for each cell line and correlated with the respective migratory capacity (a numerical table is provided in Table 3). Cell lines with a high migratory potential were resistant to doxorubicin (Pearson r = 0.81) (Figure 16A), whereas they were sensitive to salinomycin (Pearson r = -0.77) (Figure 16B). Accordingly, the susceptibility to doxorubicin inversely correlated with the salinomycin sensitivity of the respective cell lines (Pearson r = -0.80) (Figure 16C). To further prove the selective targeting of epithelial and mesenchymal cells by doxorubicin and salinomycin, the epithelial non-migratory breast cancer cell line MCF-7 was co-cultured with the mesenchymal highly migratory breast cancer cell line MDA-MB-436. The obtained cell mix reflected the cellular heterogeneity in tumors comprising epithelial and mesenchymal cells as shown by immunofluorescence staining for E-cadherin and vimentin (Figure 16D). Single treatment as well as combined treatment with doxorubicin and salinomycin revealed that the combination of both drugs proved most beneficial, confirming the selective efficacy on the different cell types (Figure 16E).

	4T1	MDA-MB-436	LLC	MDA-MB-231	H1299	MCF-7	BT-474
Migratory cap.	2.31	1.89	1.82	1.82	1.35	1.08	1.00
IC_{50} (dxr) [µM]	1.92	1.67	1.97	1.54	1.85	0.22	0.26
IC_{50} (sal) [µM]	0.06	0.16	0.36	0.36	0.21	0.47	0.92
miR-200c exp.	0.24	0.00	0.00	0.00	0.00	0.81	1.00

Table 3. Migratory capacity, treatment susceptibility and miR-200c expression of the different cancer cell lines. Migratory capacity (Migratory cap.) was determined by Boyden chamber assays, IC_{50} values for doxorubicin (dxr) and salinomycin (sal) were analyzed using CellTiter Glo and relative miR-200c expression levels (miR-200c exp.) were assessed by quantitative RT-PCR.

3.3.2 miR-200c is a marker for migration and therapy response

miR-200c as key regulator of EMT/MET and modulator of several migration-relevant proteins represents a promising marker for cellular transitions and response upon chemotherapeutic treatment (27, 28, 130).

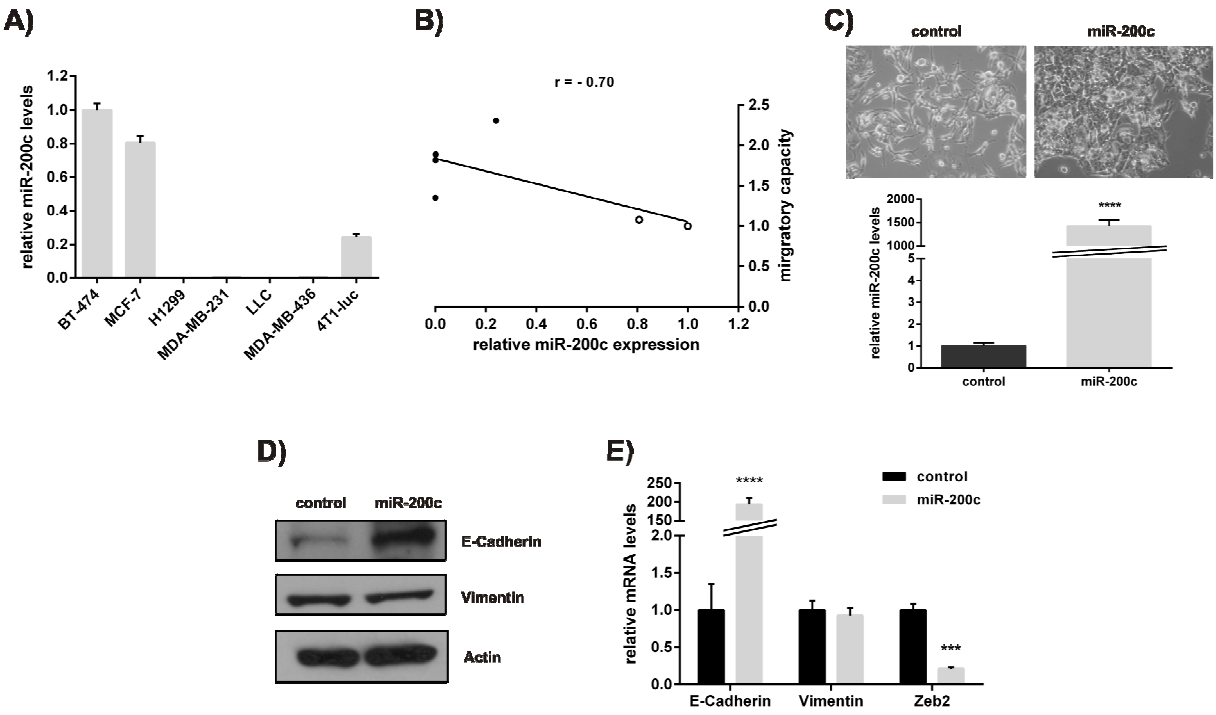

Figure 17. *miR-200c expression correlates with the migratory capacity of cancer cells and its ectopic overexpression induces MET in MDA-MB-436 cells*

A) miR-200c expression in different cancer cell lines. Relative miR-200c levels were determined by quantitative RT-PCR.
B) Correlation between migratory capacity and relative miR-200c expression. A Pearson correlation was carried out to compare migratory capacity and relative miR-200c expression of the respective cell lines (Pearson r = -0.70). Open circles represent the epithelial cell lines BT-474 and MCF-7.
C) miR-200c overexpression in MDA-MB-436 cells. Microscopic pictures (phase contrast) show the cell morphology of control- and miR-200c-transfected cells. Relative expression levels of miR-200c were determined by quantitative RT-PCR. (Student's t-test, two-tailed; ****p<0.0001)
D) Western blot analysis upon ectopic miR-200c overexpression in MDA-MB-436 cells. Total cell lysates were analyzed for the protein expression of E-cadherin and vimentin.
E) Quantitative RT-PCR analysis upon miR-200c overexpression in MDA-MB-436 cells. Relative mRNA levels of the EMT markers E-cadherin, vimentin and Zeb2 were quantified. (Student's t-test, two-tailed; ***p<0.001; ****p<0.0001)

Hence, the relative miR-200c levels were assessed in the panel of cancer cell lines (Figure 17A) and correlated with the respective migratory capacity (Figure 17B and Table 3). Thereby, the less migratory cells comprised cells with higher miR-200c levels. However, the murine breast cancer cell line 4T1 differed from this pattern as these cells displayed a medium expression of miR-200c. By ectopically overexpressing miR-200c, MET was induced in the mesenchymal breast cancer cell line MDA-MB-436 resulting in a more cobble-stone-shaped cell morphology (Figure 17C) and an epithelial-like marker expression with increased E-cadherin and slightly reduced vimentin levels (Figure 17D and Figure 17E). In addition, mRNA expression of Zeb2, a transcriptional repressor of E-cadherin and a direct target of miR-200c, was significantly reduced, which confirmed the induction of MET by miR-200c (Figure 17E).

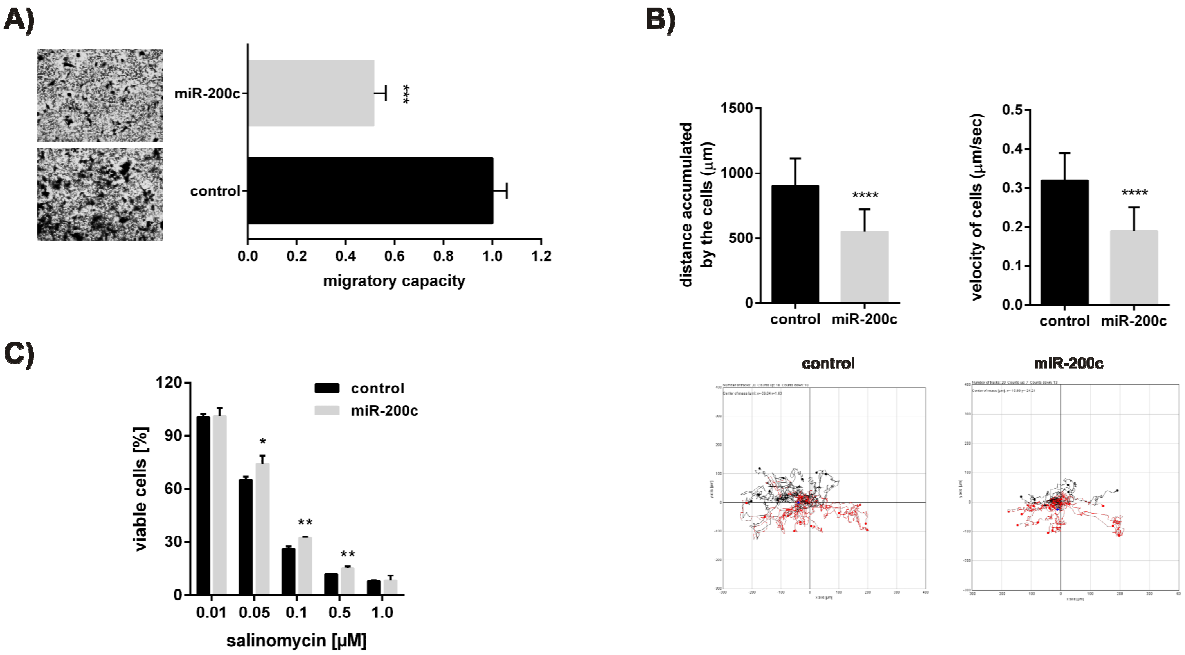

Figure 18. *miR-200c is a functional marker for migration and salinomycin susceptibility in MDA-MB-436 cells*

A) Boyden chamber migration assay of MDA-MB-436 cells overexpressing miR-200c. The number of migrated control-transfected MDA-MB-436 cells was set to a migratory capacity of one. (Student's t-test, two-tailed; ***p<0.001)
B) Time-lapse microscopy of MDA-MB-436 cells. Control and miR-200c overexpressing cells were monitored using time-lapse microscopy. The accumulated distance, the velocity and the direction of movement were analyzed. (Student's t-test, two-tailed; ****p<0.0001)
C) Cytotoxicity assay of miR-200c overexpressing MDA-MB-436 cells. Cells were treated with indicated concentrations of salinomycin and cell viability was assessed. (Student's t-test, two-tailed; *p<0.05; **p<0.01)
Migration assays were conducted by Adam Hermawan (PhD study, LMU Munich). Time-lapse microscopy was performed by Prajakta Oak (PhD 2012, LMU Munich).

In addition, miR-200c overexpressing cells had a lower migratory capacity as determined by Boyden chamber assay (Figure 18A) and time-lapse microscopy. For the latter, the accumulated distance, the velocity and the direction of movement of MDA-MB-436 cells transfected with either pre-miR-200c or scrambled control were analyzed (Figure 18B). In a previous study, it has been shown that induction of MET in MDA-MB-436 cells by overexpressing miR-200c leads to an increased susceptibility to the classical chemotherapeutic drug doxorubicin (93). To prove that salinomycin selectively targets migrating mesenchymal cancer cells, miR-200c overexpressing MDA-MB-436 cells were tested for their salinomycin sensitivity (Figure 18C). Of note, these cells, which displayed more epithelial-like properties and were sensitized to doxorubicin, were less susceptible to salinomycin treatment. This confirmed the inverse correlation that highly migratory cells were sensitive to salinomycin but resistant to doxorubicin.

3.3.3 Short-term salinomycin treatment hampers migration in cancer cells

To examine whether salinomycin has an immediate anti-migratory effect on highly migrating cancer cells, Boyden chamber assays were performed, in which MDA-MB-436, Lewis lung carcinoma (LLC) and 4T1 cells were treated with low concentrations of doxorubicin or salinomycin causing a comparable cytotoxicity (Figure 19B). In all salinomycin-treated cells migration was significantly reduced as compared to mock- or doxorubicin-treated cells (Figure 19A). Moreover, the immediate effect of salinomycin on MDA-MB-436 cells was characterized by time-lapse microscopy. It was observed that mock- (control) as well as doxorubicin-treated cells migrated into the scratch, whereas salinomycin prevented wound closure (Figure 19C). Subsequent analysis revealed that the accumulated distance and the velocity of salinomycin-treated cells were significantly reduced as compared to mock- or doxorubicin-treated cells (Figure 19D and Figure 19E). This effect became even more evident when looking at the direction of the cells treated with salinomycin (Figure 19F). Although these results were in line with the anti-migratory effects of miR-200c in MDA-MB-436 cells, there was no immediate regulation of miR-200c upon salinomycin treatment (Figure 19G). The lack of miR-200c regulation was ascribed to the short treatment duration which may have prevented any phenotypic alterations.

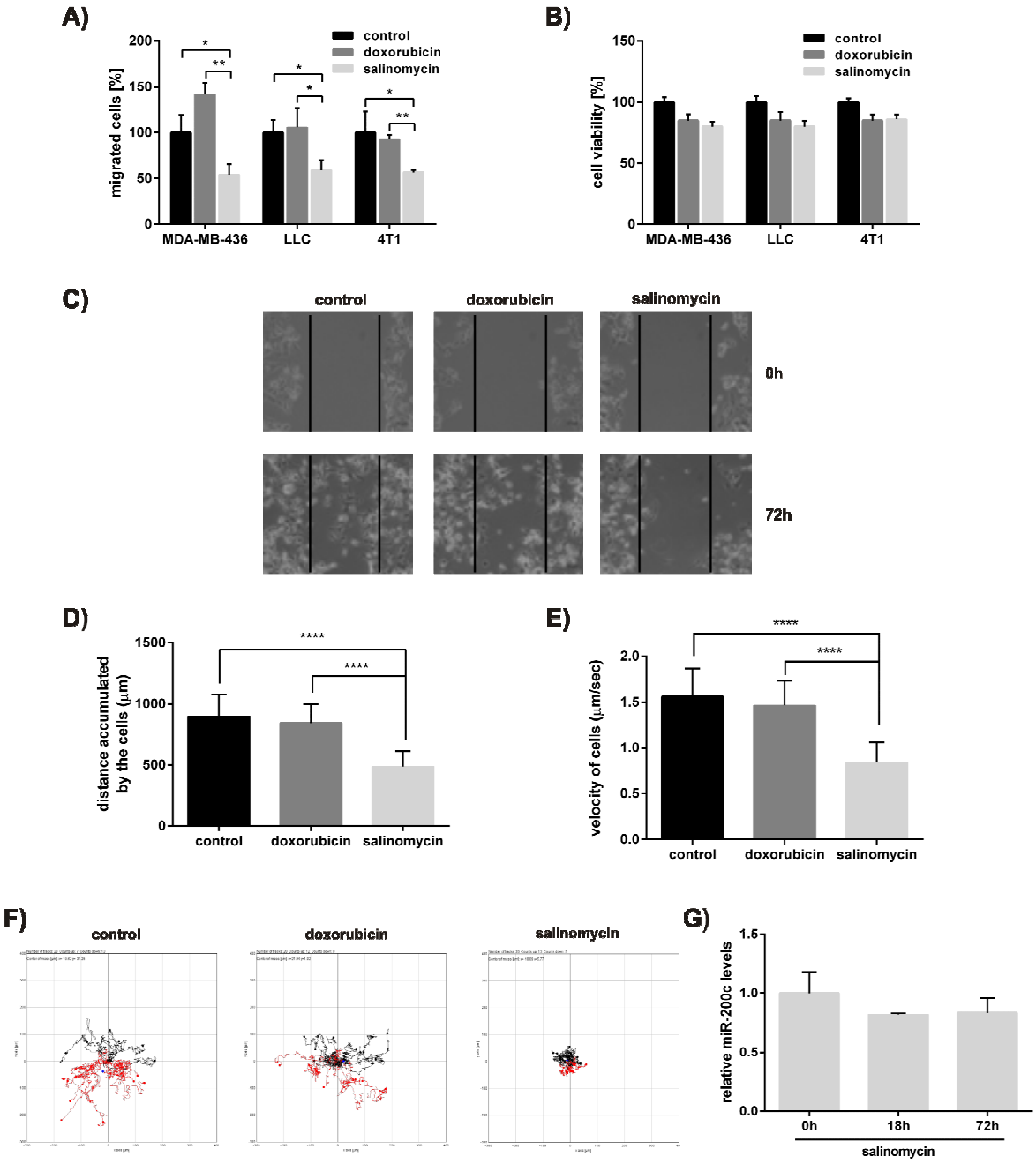

Figure 19. *Short-term salinomycin treatment hampers migration in cancer cells*

A) Boyden chamber migration assays of different cancer cell lines during treatment. MDA-MB-436 (breast), LLC (lung) and 4T1 (breast) cells were treated for 18h with indicated drugs at a concentration resulting in approximately 90% viable cells (B). The number of migrated mock-treated (control) cells was set to 100%. (Student's t-test, two-tailed, *p<0.05; **p<0.01)

B) Cell viability upon doxorubicin or salinomycin short-term treatment. MDA-MB-436, LLC and 4T1 cells were treated for 18h with 10µM, 0.5µM and 0.5µM doxorubicin and 0.05µM, 0.5µM and 0.05µM salinomycin, respectively. Cell viability was determined by a CellTiter Glo assay and normalized to mock-treated control cells.

C) Wound healing assay of MDA-MB-436 cells. Cells were treated either with mock (control), doxorubicin (0.05µM) or salinomycin (0.05µM).

Time-lapse microscopy of MDA-MB-436 cells. The same cells as for the wound healing assay were used for time-lapse microscopy. Manually tracked cells were analyzed for D) the accumulated distance, E) the velocity and F) the direction of movement. (Student's t-test, two-tailed, ****p<0.0001)

G) miR-200c expression upon short-term salinomycin treatment in MDA-MB-436 cells. Cells were treated with 0.05µM salinomycin for the indicated period of time. Subsequently, relative miR-200c levels were determined using quantitative RT-PCR.

Migration assays were performed by Adam Hermawan (PhD study, LMU Munich). Time-lapse microscopy was carried out by Prajakta Oak (PhD 2012, LMU Munich).

3.3.4 Long-term salinomycin treatment reduces migratory capacity and modulates treatment susceptibility in MDA-MB-436 cells by inducing MET

In order to allow phenotypic changes upon salinomycin treatment, a pulsed long-term treatment was performed as described previously for BT-474 cells and doxorubicin treatment (93).

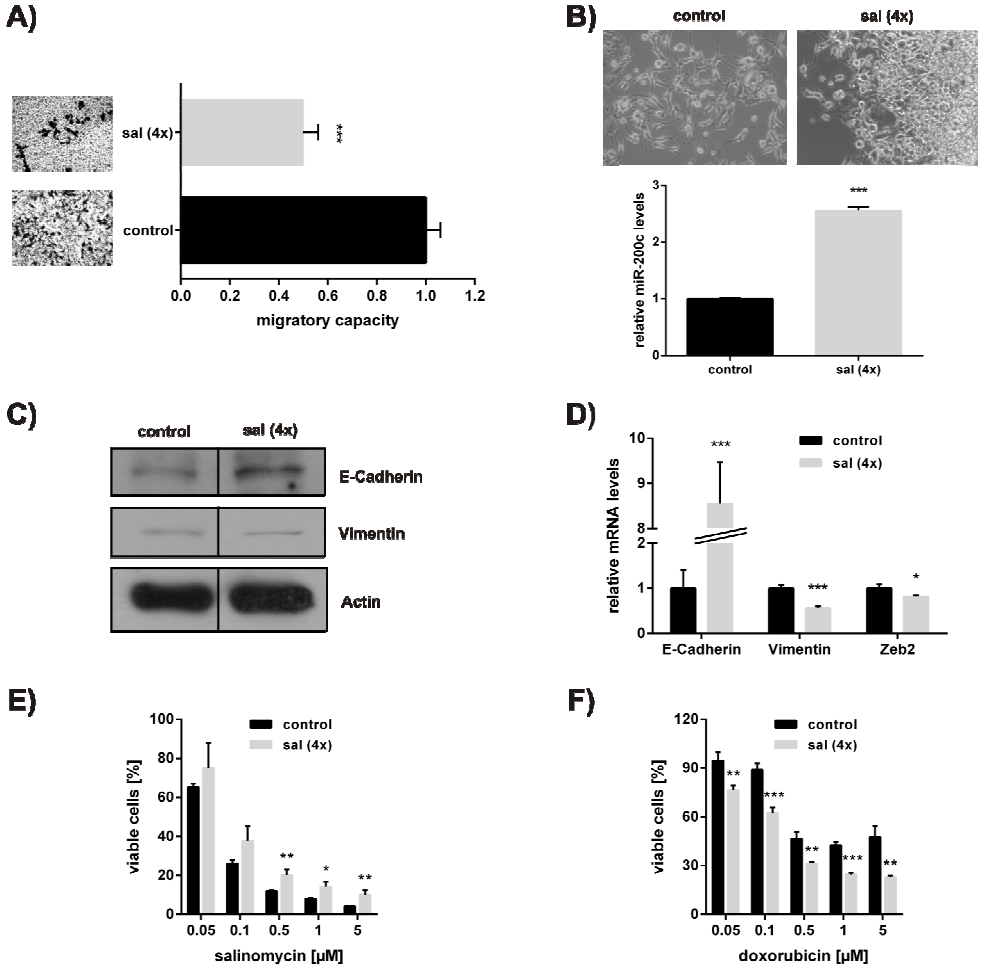

Figure 20. *Long-term salinomycin treatment reduces migratory capacity and modulates treatment susceptibility in MDA-MB-436 cells by inducing MET*

MDA-MB-436 cells were treated in rounds with 0.05µM salinomycin followed by a recovery phase until the next round started. Cells which had received four treatment rounds and which had completely recovered (sal 4x) were harvested for the following experiments.
A) Migratory capacity of control and salinomycin-treated cells (sal 4x). The migratory capacity of control cells was set to one. (Student's t-test, two-tailed; ***p<0.001)
B) miR-200c expression of salinomycin-treated MDA-MB-436 cells (sal 4x) compared to control cells. Relative miR-200c levels were determined by quantitative RT-PCR. Microscopic pictures (phase contrast) show the cell morphology of control and salinomycin-treated cells. (Student's t-test, two-tailed; ***p<0.001)
C) Western blot analysis. Total cell lysates of control and salinomycin-treated cells (sal 4x) were analyzed for the protein expression of E-cadherin and vimentin.
D) Quantitative RT-PCR analysis. Relative mRNA levels of the EMT markers E-cadherin, vimentin and Zeb2 were quantified in control and salinomycin-treated cells (sal 4x). (Student's t-test, two-tailed; *p<0.05; ***p<0.001)
Cytotoxicity assays for salinomycin and doxorubicin. Salinomycin-treated (sal 4x) as well as control cells were treated with indicated concentrations of either E) salinomycin or F) doxorubicin. (Student's t-test, two-tailed; *p<0.05; **p<0.01; ***p<0.001)
Migration assays and cytotoxicity assays with salinomycin and doxorubicin were conducted by Adam Hermawan (PhD study, LMU Munich).

Here, MDA-MB-436 cells were treated with salinomycin for several rounds, which was in each case followed by a recovery phase until the next cycle started. The recovered cells after four rounds of treatment (sal 4x) were then harvested and used for further experiments. Repeated long-term treatment of MDA-MB-436 cells with salinomycin significantly hampered migration as compared to control cells (Figure 20A). Consistent with the reduced migratory capacity, miR-200c levels were considerably increased and the cell morphology of salinomycin-treated cells changed to clones growing in clusters with an epithelial-like appearance (Figure 20B). Moreover, the mesenchymal expression pattern switched to a more epithelial-like expression pattern with an increase of E-cadherin and a decrease of vimentin on both the protein and mRNA level (Figure 20C and Figure 20D). In addition, the mRNA expression of Zeb2, a direct target of miR-200c and an inducer of EMT in mesenchymal cancer cells, was significantly reduced (Figure 20D). Finally, MDA-MB-436 cells subjected to a long-term treatment with salinomycin (sal 4x) were compared to untreated control cells in terms of their sensitivity to salinomycin or doxorubicin. Salinomycin-treated epithelial-like and less migratory MDA-MB-436 cells were significantly more resistant to salinomycin as compared to their mesenchymal and highly migratory counter parts (Figure 20E). However, in accordance with the inversely correlating susceptibilities of mesenchymal and epithelial cells, salinomycin-treated cells were now more sensitive to the classical chemotherapeutic drug doxorubicin (Figure 20F).

3.3.5 Salinomycin induces MET in a syn- and transgenic mouse tumor model

To evaluate the potential of salinomycin to induce MET *in vivo*, luciferase expressing 4T1 (4T1-luc) cells and syngenic BALB/c mice were utilized in a subcutaneous tumor model. Tumor-bearing mice were treated with either salinomycin or mock (control) every second or third day and monitored for 17 days. No significant effect on tumor growth was observed (Figure 21A). The minor effect on tumor growth of the salinomycin-treated mice can be explained by increased apoptosis, which was determined by immunohistochemistry of cleaved caspase 3 (Figure 21B). Of note, consistent with the *in vitro* results of salinomycin-treated MDA-MB-436 cells, salinomycin-treated tumors displayed an increased miR-200c expression

(Figure 21C) and elevated E-cadherin protein levels as determined by Western blot analysis (Figure 21D). Immunofluorescence stainings of 4T1-luc tumor sections revealed a heterogeneous cell population consisting of either E-cadherin-positive or vimentin-positive cells. The latter disappeared after salinomycin treatment, resulting in an epithelial-like tumor with considerable E-cadherin expression (Figure 21E).

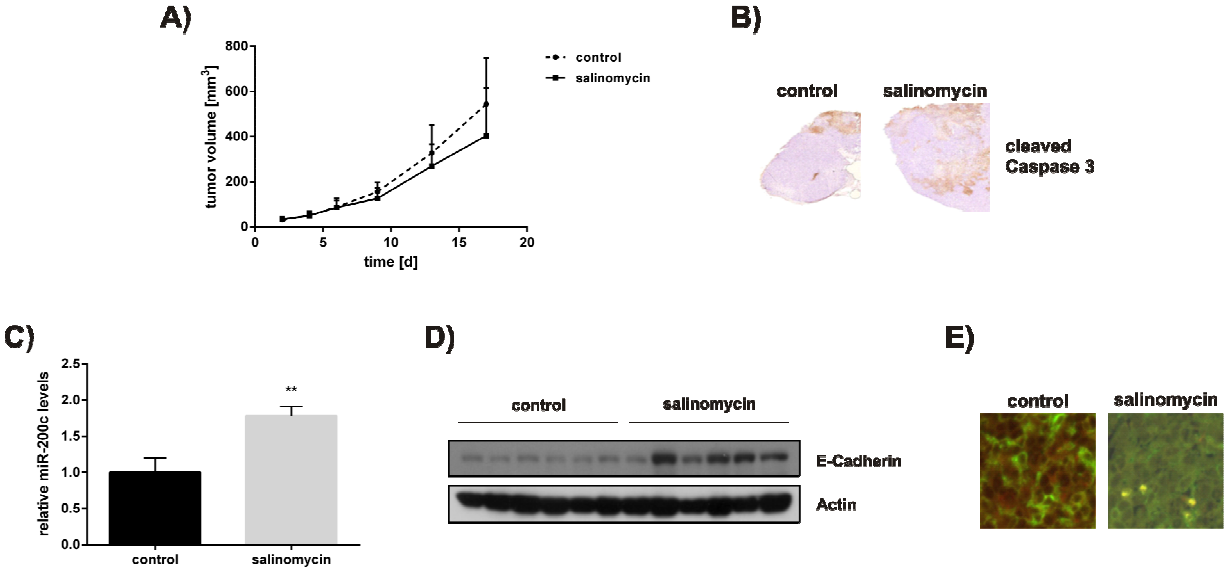

Figure 21. *Salinomycin induces MET in a syngenic mouse tumor model*

A) Tumor growth of subcutaneous 4T1-luc tumors. $2x10^6$ 4T1-luc cells were subcutaneously injected into the right flank of 9 female BALB/c mice per group. Animals were treated either with mock (control) or 5mg/kg salinomycin on day 3, 6, 8, 10, 13 and 15. Tumor growth was monitored for 17 days at indicated time points using a caliper and depicted as tumor volume [mm^3].
B) Immunohistochemistry of subcutaneous 4T1-luc tumors. On day 17 mice were sacrificed and tumors resected. Sections of paraffin embedded control and salinomycin-treated tumors were used for immunohistochemistry and stained for cleaved caspase 3.
C) miR-200c expression in 4T1-luc tumors. Relative miR-200c levels of salinomycin- and mock-treated (control) 4T1-luc tumors were determined by quantitative RT-PCR. (Mean ± SEM; student's t-test, two-tailed; **p<0.01)
D) Western blot analysis and immunofluorescence of 4T1-luc tumors. Lysates from representative control and salinomycin-treated tumors were analyzed for E-cadherin protein expression.
E) Immunofluorescence of 4T1-luc tumors. Respective sections were stained for E-cadherin (green) and vimentin (red).
Immunohistochemistry and immunofluorescence were performed by Vijay Ulaganathan (Max-Planck-Institute, Martinsried). Annika Herrmann (veterinary MD study, LMU Munich) assisted in the syngenic mouse model experiment.

Moreover, a c-MYC driven transgenic mouse model of non-small cell lung cancer (SpC-c-MYC mouse) was used, which was previously described by Rapp *et al*. (102). The animals received nine treatments with salinomycin every second day. Immunohistochemistry of salinomycin-treated and control SpC-c-MYC mice also demonstrated an epithelial-like expression pattern with increased E-cadherin levels upon salinomycin treatment (Figure 22A). Vimentin expression was low and could not be further down-regulated (Figure 22B). Consistent with the syngenic mouse model,

salinomycin-treated lung tumors showed increased PARP cleavage, indicating augmented apoptosis upon treatment (Figure 22C). Hence, salinomycin treatment of subcutaneous 4T1-luc as well as of transgenic SpC-c-MYC lung tumors led to an induction of MET with increased E-cadherin and miR-200c levels.

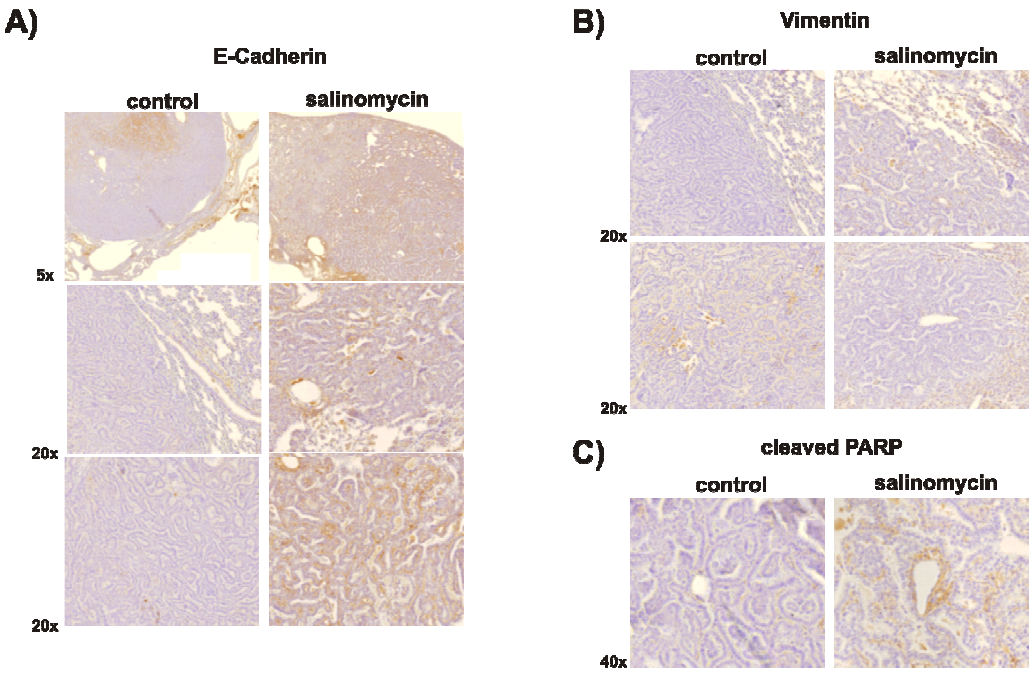

Figure 22. *Salinomycin induces MET in the transgenic SpC-c-MYC mouse model*

Immunohistochemistry of lung tumors obtained from tumor-bearing transgenic mice. SpC-c-MYC mice at the age of 72 weeks received 12 treatments with 5mg/kg salinomycin every second day. Untreated tumor-bearing SpC-c-MYC mice at nearly the same age were used as control group. Paraffin embedded sections were stained either for F) E-cadherin, G) vimentin or H) cleaved PARP.
SpC-c-MYC mice were obtained from Chitra Thakur and Ulf Rapp (Max-Planck-Institute, Martinsried). Salinomycin treatments were carried out by Nefertiti Elnikhely (Max-Planck-Institute, Bad Nauheim). Immunohistochemistry was done by Vijay Ulaganathan (Max-Planck-Institute, Martinsried).

3.3.6 Salinomycin hampers metastasis in a syngenic intravenous mouse tumor model

Based on these observations, the question was raised whether salinomycin was able to prevent metastasis *in vivo* by up-regulating miR-200c. The migratory capability of 4T1-luc cells after miR-200c overexpression was therefore investigated. Boyden chamber assay (Figure 23A) and time-lapse microscopy (Figure 23B) demonstrated that miR-200c significantly reduced the migratory capacity as well as the accumulated distance, the velocity and the movement of miR-200c overexpressing 4T1-luc cells.

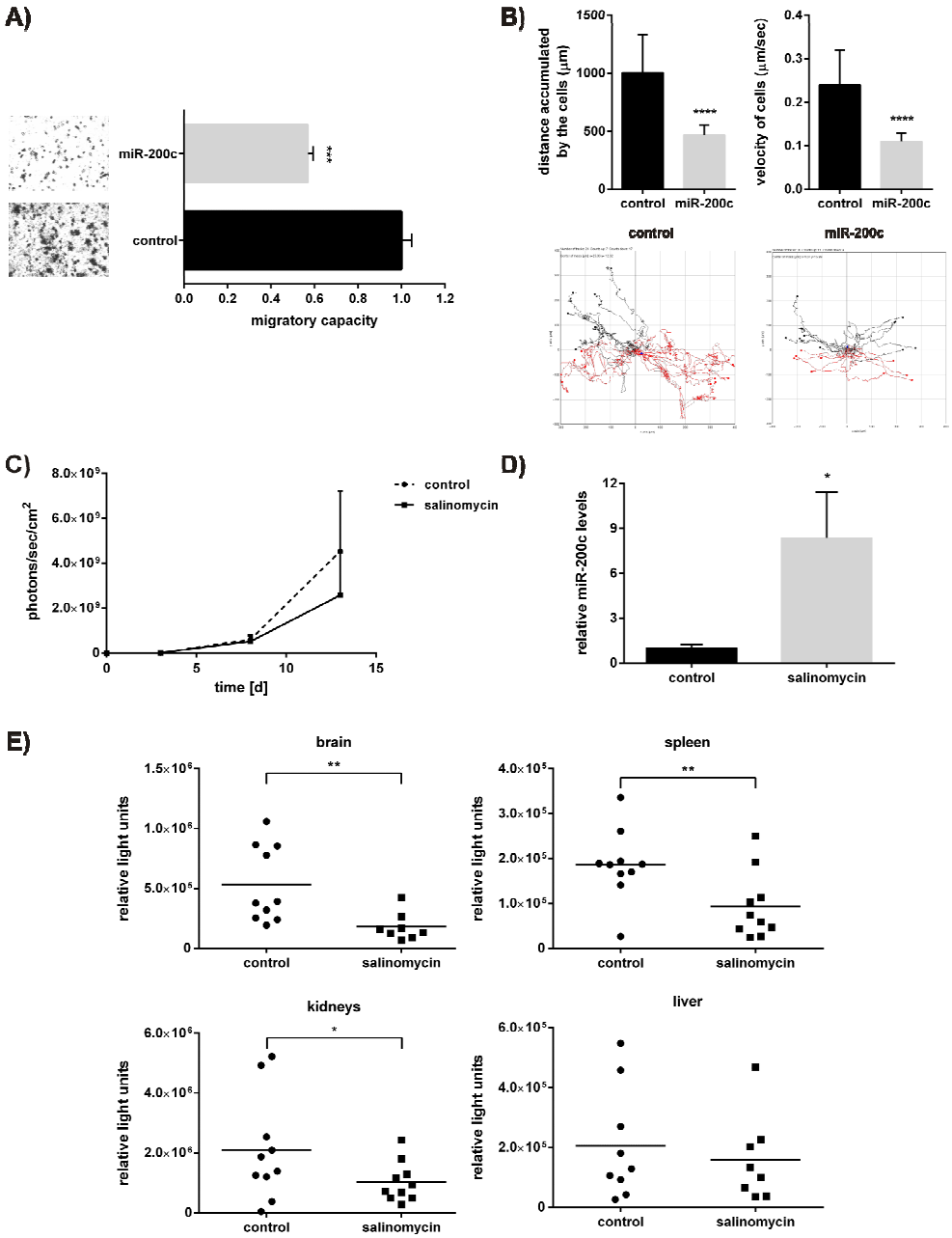

Figure 23. *Salinomycin hampers metastasis in a syngenic intravenous mouse tumor model*

A) Boyden chamber migration assay of 4T1-luc cells upon ectopic overexpression of miR-200c. The number of migrated control-transfected 4T1-luc cells was set to a migratory capacity of one. (Student's t-test, two-tailed, ***p<0.001)
B) Time-lapse microscopy of 4T1-luc cells. Cells transfected with control or miR-200c were monitored using time-lapse microscopy. The accumulated distance, the velocity and the direction of movement were analyzed. (Student's t-test, two-tailed; ****p<0.0001)
C) Tumor growth of 4T1-luc tumors in lungs. $1x10^5$ 4T1-luc cells were intravenously injected into 10 female BALB/c mice per group. Animals were treated either with mock (control) or 5mg/kg salinomycin on day 0, 3, 6 and 9. Tumor growth was monitored for 13 days at indicated time points using bioluminescence imaging.
D) miR-200c expression of 4T1-luc tumor-bearing lungs. Mice were euthanized on day 13 and the relative miR-200c levels in the resected lungs were analyzed by quantitative RT-PCR. (Mean ± SEM; Student's t-test, two-tailed; *p<0.05)
E) Metastasis in 4T1-luc tumor-bearing mice. Brain, spleen, kidneys and liver were analyzed for metastases using an *ex vivo* luciferase assay. (Student's t-test, one-tailed; *p<0.05; **p<0.01)
Migration assays were done by Adam Hermawan (PhD study, LMU Munich). Time-lapse microscopy was conducted by Prajakta Oak (PhD 2012, LMU Munich). Annika Herrmann (veterinary MD study, LMU Munich) assisted in the syngenic mouse model experiment.

Thus, 4T1-luc cells were injected into the tail vein of BALB/c mice and treated with mock or salinomycin at indicated time points. Primary tumor formation in the lungs was monitored *in vivo* using bioluminescence imaging. As observed in the subcutaneous model, there was no significant effect of salinomycin treatment on primary tumor formation and growth (Figure 23C). When analyzing the miR-200c expression after salinomycin treatment, considerably elevated miR-200c levels were observed, which was in concordance with the subcutaneous 4T1-luc tumors (Figure 23D). Notably, metastases were significantly reduced in brain, spleen and kidneys after salinomycin treatment as determined by an *ex vivo* luciferase assay (Figure 23E). These findings suggest that salinomycin is able to induce MET in a syngenic intravenous mouse tumor model resulting in a significantly smaller metastatic tumor burden.

3.4 miR-143-controlled transgene expression

3.4.1 miR-143 is down-regulated in a variety of cancer cell lines and cancerous tissues

Since miR-143 was reported as tumor suppressor miRNA in different cancer types, such as colon, gastric, prostate and cervical cancer, this supposed differential expression was utilized for tumor-specific gene therapy.

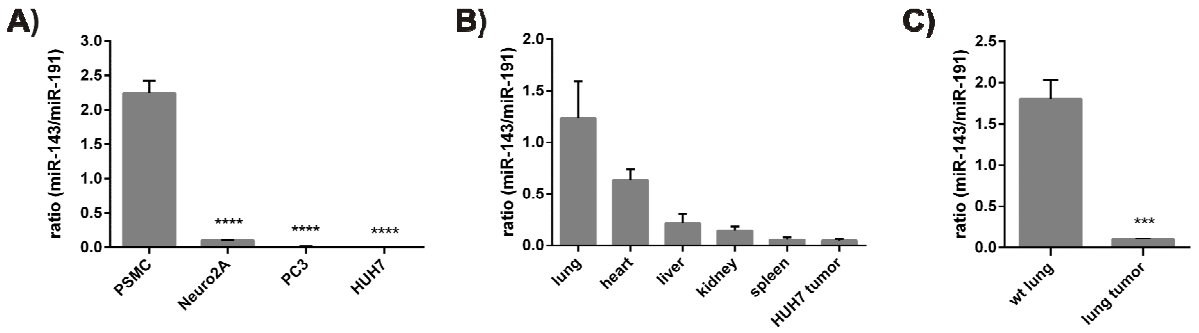

Figure 24. *miR-143 is down-regulated in a variety of cancer cell lines and cancerous tissues*

miR-143 was quantified by quantitative RT-PCR and the levels normalized to miR-191 either from cells *in vitro* (A) or from murine tissues (B-C). All values are stated as mean ± SD of relative miRNA levels.
A) Porcine smooth muscle cells (PSMC), murine neuroblastoma Neuro2A, human prostate carcinoma PC3 and human hepatoma HUH7; (****p<0.0001, ANOVA (Dunnett), n=4).
B) Lung, heart, liver, kidney, spleen and HUH7 tumor of NMRI nude mice bearing a subcutaneous HUH7 tumor; (n=4).
C) SpC-c-MYC transgenic mouse tumors (lung tumor) and wild type lungs (wt lung); (***p<0.001, student's t-test, two tailed, n=3).

Therefore, miR-143 levels were determined in the human hepatocellular cancer cell line HUH7, in the human prostate cancer cell line PC3, in the murine neuroblastoma cell line Neuro2A and in primary porcine smooth muscle cells (PSMC) representing cells from healthy tissue. PSMC showed the highest miR-143 expression, whereas an either low or moderate expression was observed in HUH7, PC3 or Neuro2A cells (Figure 24A). Furthermore, miR-143 levels of healthy mouse tissue and HUH7 xenografts were determined in a NMRI nude/ HUH7 mouse xenograft model to prove this differential expression *in vivo*. As expected, HUH7 xenografts showed the lowest miR-143 expression followed by mouse spleen, kidneys, liver, heart and most notably mouse lung (Figure 24B). Finally, miR-143 levels were investigated in lung tumors of SpC-c-MYC transgenic mice as well as in the respective wild type lungs (SpC-c-MYC transgenic mouse model for spontaneous non-small cell lung cancer has been

previously described (102)). Consistent with the previous findings, this transgenic mouse model illustrated the high expression of miR-143 in wild type lung tissue as compared to the low expression in cancerous tissue of SpC-c-MYC transgenic mice (Figure 24C). Here, it was demonstrated that the miR-143 is differentially expressed in healthy and cancerous tissue with high expression in PSMC as well as in wild type mouse organs. In contrast, the cancer cell lines PC3, HUH7 and Neuro2A showed only low or moderate expression levels of miR-143, confirming the role of miR-143 as tumor suppressor miRNA.

3.4.2 Reporter gene as well as therapeutic transgene expression can be controlled by miR-143

All vectors used for this study were based on the previously optimized combination of human cytomegalovirus (hCMV) enhancer and synthetic CMV-EF1α hybrid promoter (SCEP) in a backbone completely devoid of CpG motifs (108). To analyze the regulation by miR-143, several different reporter plasmids were developed. pCpG-hCMV/SCEP-mCherry encoding for red fluorescent protein was cloned containing either no (mCherry) or five miR-143 binding sites (mCherry-miR143-bs) in the 3'UTR (Figure 25A). pCpG-hCMV/SCEP-EGFP (EGFP) encoding for enhanced green fluorescent protein was employed as control for transfection efficiency. PSMC, Neuro2A, PC3 and HUH7 were co-transfected with pCpG-hCMV/SCEP-EGFP and one of the vectors encoding for mCherry. Flow cytometric analysis showed a considerable decrease of mCherry intensity in PSMC upon transfection with the mCherry plasmid containing five copies of the miR-143 target sequence. To a lesser extent, mCherry intensity was also decreased in Neuro2A and PC3 cells after transfection with the same plasmid. However, HUH7 cells were not able to down-regulate the expression of the plasmid with five miR-143 binding sites (Figure 25B). For quantitative analysis of the effects induced by the inclusion of miR-143 target sequences, the mCherry fluorescence of each sample was normalized to mean mCherry fluorescence of cells transfected with the plasmid without miR-143 binding sites (Figure 25C).

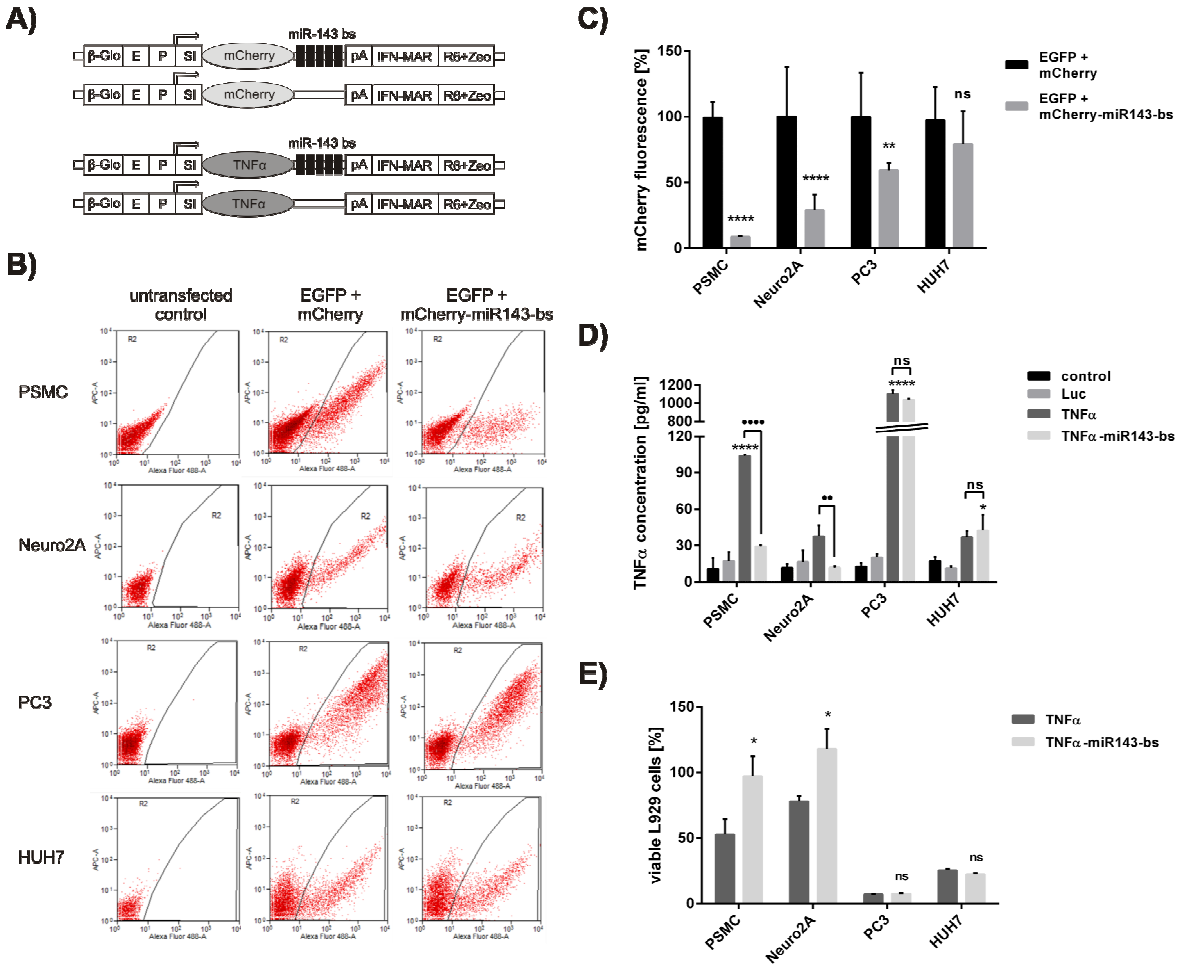

Figure 25. *Reporter gene as well as therapeutic transgene expression can be controlled by miR-143*

A) Scheme of mCherry and TNFα plasmids. Five tandem copies of the miR-143 binding sequence separated by a five nucleotide linker were inserted into the pCpG-hCMV/SCEP-mCherry or pCpG-hCMV/SCEP-TNFα vector. β-Glo=matrix attached region (MAR) from the β-globin gene; E=human cytomegalovirus (hCMV) enhancer; P=synthetic CMV-EF1α hybrid promoter (SCEP); SI=synthetic intron; pA=late simian virus 40 (SV40) polyadenylation signal; IFN-MAR=MAR from the 5' region of the human IFN-β gene; R6=R6K ori from E. coli; Zeo=Zeocin-resistance gene.
B) Representative density blots of transfected cells. PSMC, Neuro2A, PC3 and HUH7 cells were co-transfected with pCpG-hCMV/SCEP-EGFP (EGFP) and one of the plasmids encoding for mCherry containing either no (mCherry) or five miR-143 binding sites (mCherry-miR143-bs). After 48h cells were harvested for flow cytometric analysis. x-axis: Alexa Fluor 488 (indicative for EGFP-positive cells), y-axis: APC-A (indicative for mCherry-positive cells).
C) Intensity of mCherry fluorescence relative to mean mCherry fluorescence of cells transfected with the mCherry plasmid containing no miR-143 binding site. Transfection efficiency was normalized to EGFP expression and values are stated as mean ± SD of relative mCherry fluorescence; (**p<0.01, ****p<0.0001, ns = not significant, student's t-test, two-tailed, n=6-10).
D) Determination of soluble TNFα by ELISA. TNFα concentration in the supernatant of cells transfected with indicated plasmids were determined by ELISA 48h after transfection. Indicated plasmids were compared to untransfected control (*p<0.05, ****p<0.0001, ANOVA, Tukey, n=8) and TNFα was compared to TNFα-miR143-bs (¨p<0.01, ¨¨¨¨p<0.0001, ns = not significant, student's t-test, two-tailed, n=3).
E) Cytotoxicity of soluble TNFα on murine fibroblasts L929. PSMC, Neuro2A, PC3 and HUH7 cells were transfected either with the TNFα, TNFα-miR-143-bs or Luc plasmid. 48h post transfection supernatants were collected and transferred to L929 cells. After 24h cell viability was determined by a MTT assay. Results are presented as mean of viable L929 cells ± SEM normalized to Luc-transfected control cells; (*p<0.05, ns = not significant, student's t-test, one-tailed, n=8).
Experiments were done by Maria Schnoedt and adapted from her Master Thesis (LMU Munich, 2011).

To assess the suitability of the differential miR-143 expression for therapeutic transgene expression, PSMC, Neuro2A, PC3 and HUH7 cells were transfected with pCpG-hCMV/SCEP-TNFα plasmids containing either no (TNFα) or five miR-143 binding sites (TNFα-miR143-bs) (Figure 25A). pCpG-hCMV/EF1-LucSH (Luc), a plasmid coding for firefly luciferase, was used to determine the endogenous TNFα concentration in response to cell transfection. Soluble TNFα was analyzed in the supernatant by ELISA 48h after transfection (Figure 25D). TNFα gene expression was effectively suppressed in PSMC if the miR-143 binding sequences were included into the coding plasmid. Statistical analysis revealed no significant differences in TNFα protein concentration in supernatants of untransfected cells, cells transfected with the plasmid encoding for firefly luciferase and cells transfected with the TNFα plasmid containing five target sequences of miR-143. Similar results were obtained from Neuro2A cells, which were shown to express relatively high levels of miR-143 as compared to PC3 and HUH7 cells. Consistently, no significant decrease of TNFα production was observed in PC3 and HUH7 cells after transfection with either plasmid. To investigate the physiological effects of miRNA-regulated gene therapy, the TNFα-induced cytotoxicity was analyzed by utilizing a model system which was previously described by Su *et al.* (110). Murine fibroblasts (L929) were treated with supernatants of tumor cells transfected either with the TNFα, TNFα-miR-143-bs or Luc plasmid. The obtained L929 cell viabilities after TNFα treatment reflected the results of the TNFα ELISA (Figure 25E). Thus, the miR-143-dependent expression of the mCherry reporter as well as of the therapeutic gene TNFα was demonstrated, emphasizing the potential role of miR-143 in cancer cell-specific targeting. All plasmids were cloned by Maria Schnoedt and Rudolf Haase (LMU Munich). The flow cytometry, TNFα ELISA and TNFα cytotoxicity experiments were performed by Maria Schnoedt and adapted from her Master Thesis (LMU Munich, 2011).

3.4.3 miR-143-dependent silencing of a luciferase reporter system *in vitro* and *in vivo*

To test the ability of miR-143-regulated transgene expression *in vivo*, the mCherry coding sequence was exchanged for the luciferase sequence (Figure 26A). First, the effectiveness of miRNA regulation was investigated in an *in vitro* luciferase assay.

Therefore, all cell lines were transfected with either pCpG-hCMV/SCEP-LucSH (Luc) or pCpG-hCMV/SCEP-LucSH containing five miR-143 binding sites (Luc-miR143-bs). As expected, no significant difference in luciferase expression was observed between PC3 and HUH7 cells transfected with either plasmid. However, PSMC were able to effectively reduce luciferase activity to 40% if transfected with the plasmid containing the miR-143 target sequences. Neuro2A cells could still achieve a reduction of luciferase activity to 60% (Figure 26B).

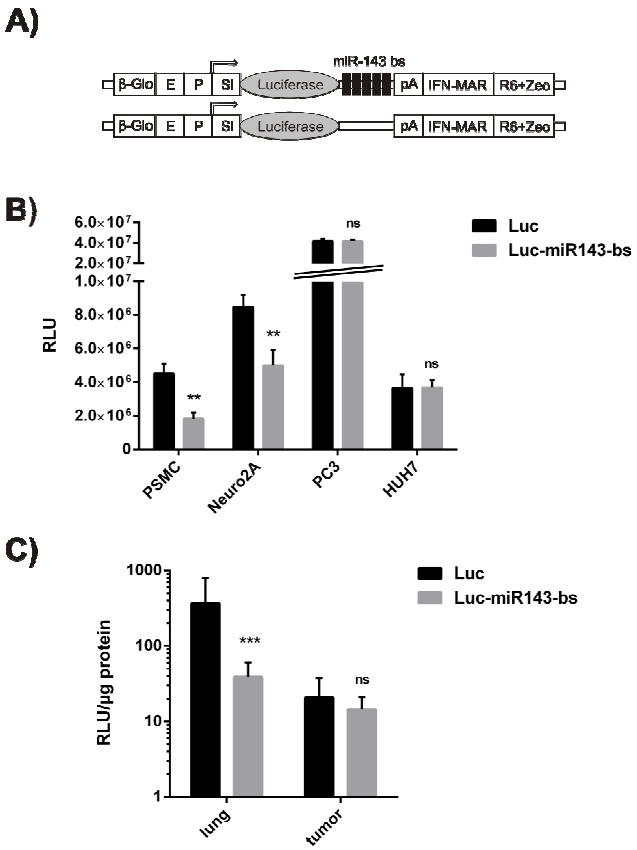

Figure 26. *miR-143-dependent silencing of a luciferase reporter system in vitro and in vivo*

A) Scheme of luciferase plasmids. Five tandem copies of the miR-143 binding sequence separated by a five nucleotide linker were inserted into the pCpG-hCMV/SCEP-LucSH vector.
β-Glo=matrix attached region (MAR) from the β-globin gene; E=human cytomegalovirus (hCMV) enhancer; P=synthetic CMV-EF1α hybrid promoter (SCEP); SI=synthetic intron; pA=late simian virus 40 (SV40) polyadenylation signal; IFN-MAR=MAR from the 5' region of the human IFN-β gene; R6=R6K ori from E. coli; Zeo=Zeocin-resistance gene.
B) Expression profile of luciferase reporter plasmids. PSMC, Neuro2A, PC3 and HUH7 cells were transfected with the luciferase reporter containing either no (Luc) or five copies of the miR-143 binding sequence (Luc-miR143-bs). Luciferase expression was monitored after 24h from whole cell lysates. Values are stated as mean ± SD of relative light units (RLU) per 10^4 seeded cells; (**p<0.01, ns = not significant, student's t-test, two-tailed, n=3).
C) Luciferase expression after *in vivo* transfections. HUH7 tumor-bearing mice were treated either with Luc or Luc-miR143-bs plasmids *via* the tail vein using LPEI as carrier. 48h after treatment luciferase signals were detected *ex vivo* by a luciferase assay of the resected lungs (lung) and HUH7 tumors (tumor); (***p<0.001, ns = not significant, u-test, Mann-Whitney, n=8).

For *in vivo* application linear polyethylenimine (LPEI) polyplexes were chosen, which have a strong preference of transfecting lungs after intravenous administration in mice (109). It was therefore interesting whether luciferase expression could be specifically regulated in an *in vivo* mouse xenograft tumor model by de-targeting the lungs. Thus, HUH7 cells, which display low miR-143 levels and which have been reported to result in well vascularized and transfectable tumors (131), were injected into the right flanks of NMRI nude mice. When tumors reached a diameter of 10mm, mice were treated with plasmids encoding either for Luc or Luc-miR143-bs complexed with LPEI or mock-treated (HEPES buffered glucose, pH 7.4). Luciferase activity was analyzed in all groups 48h after transfection with an *ex vivo* luciferase assay. In concordance with the miR-143 expression levels, a significant miR-143-dependent decrease of the luciferase signal was achieved in the lungs of Luc-miR143-bs-treated mice. In contrast, there was no significant regulation of the luciferase signal detectable in the miR-143 low-expressing tumor tissue (Figure 26C). All luciferase signals of Luc- and Luc-miR143-bs-treated mice were significantly above the background signal of mock-treated animals (3.9 RLU/µg protein).

Apparently, differential miR-143 expression could be used for specific tumor targeting by de-targeting the lung, suggesting that this might be suitable for tumor-specific gene therapy.

4. DISCUSSION

4.1 miR-200c sensitizes breast cancer cells to doxorubicin

In breast cancer treatment classical chemotherapy is largely used besides hormone therapy and novel targeted therapy approaches (12, 132). For instance, the anthracycline doxorubicin (Adriamycin®) is commonly used as single-agent or in combination with other drugs like docetaxel (Taxotere®) and cyclophosphamide (TAC regimen) in an adjuvant or neo-adjuvant setting (133). Generally, chemotherapy regimens are administered sequentially, i.e. in case of the TAC regimen patients are treated six times every three weeks (134, 135). In this study, this pulse chemotherapy of breast cancer was mimicked in an *in vitro* cell culture model by treating the epithelial breast cancer cell line BT-474 sequentially in four cycles with doxorubicin. The treatment of BT-474 cells with a recovery phase followed by the next treatment cycle resembles the therapy regimen of patients and thereby provides a model for acquired chemoresistance. The molecular evolution assay of BT-474 cells was demonstrated to result in significantly more resistant cells within three treatment cycles. Acquisition of chemoresistance was accompanied by a change in cell morphology and in the expression of the epithelial marker E-cadherin and the mesenchymal marker vimentin suggesting that an EMT-like mechanism might be involved. Besides the well investigated and established regulation of EMT (3, 19, 20, 119), recent findings also suggest that the loss of miR-200c regulates resistance to paclitaxel or cisplatin (22, 32, 33). However, an exact mechanism of miR-200c-dependent acquired chemoresistance had to be elucidated. Here, it was shown that the sequential doxorubicin treatment of the epithelial breast cancer cell line BT-474 led to an altered phenotype with decreased miR-200c levels resulting in doxorubicin resistance.

To further investigate the role of miR-200c in acquired chemoresistance, two different cell lines were utilized, with which it was possible to modulate chemoresistance by molecular manipulation of the respective miR-200c levels. First, miR-200c was inhibited in the epithelial, doxorubicin-sensitive and miR-200c high-expressing cell line BT-474. Thereby, the inhibition of miR-200c resulted in cells which were

significantly more resistant to doxorubicin treatment. Second, miR-200c was overexpressed in the mesenchymal, doxorubicin-resistant and miR-200c-negative cell line MDA-MB-436. Accordingly, miR-200c expressing MDA-MB-436 became significantly more susceptible to doxorubicin treatment. Thus, it was demonstrated in two different cell types that miR-200c alone was able to regulate sensitivity to doxorubicin, confirming the findings of the molecular evolution assay.

Since miRNAs are endogenously modulating gene expression by degrading mRNA or by inhibiting translation, biological functions of these tiny RNAs can be attributed to their targets (1-3, 7, 136). Howe *et al.* (27) have reported that TrkB is targeted by miR-200c in breast cancer conferring anoikis resistance. Moreover, Trk receptors including TrkB are essential for the development and functioning of the nervous system by mediating cell migration, proliferation and most notably survival. Thereby, TrkB is signaling *via* PLCγ, the MAP kinases or PI3K and Akt (115). Phosphorylation of Akt plays a pivotal role in cell survival and anti-apoptotic signaling by phosphorylating and thereby inhibiting pro-apoptotic factors like Bad or caspase 9 (137, 138). The molecular evolution assay of BT-474 cells resulted in a differential expression of TrkB over the cycles with an increase in the second round followed by a reduction in the fourth round. Consistent with the TrkB regulation, Akt phosphorylation was remarkably enhanced in the second round and reduced again in the fourth round. The discrepancy in the extent of TrkB and p-Akt regulation can be explained by other clonal selection events influencing the Akt survival pathway. As the molecular evolution assay is based on clonal selection processes, a linear regulation of resistance markers, such as TrkB or p-Akt, is not necessarily expected (139). Dependent on the particular condition of a treated cell, such as genetic background, phase of cell cycle or extent of DNA damage, distinct survival pathways are preferred to circumvent chemotherapy. To ascertain the role of TrkB as miR-200c-dependent resistance factor, miR-200c was overexpressed in the mesenchymal and doxorubicin-resistant cell line MDA-MB-436. In accordance with the increased susceptibility to doxorubicin, TrkB protein was silenced in miR-200c overexpressing cells. However, there were no differences in p-Akt levels between pre-miR-200c- and scrambled control-transfected cells. This was ascribed to a missing stimulus which may induce survival signaling in the transfected cells. Therefore, miR-200c overexpressing as well as control cells were treated with

doxorubicin to activate survival signaling. Thereafter, phosphorylation of Akt was induced by doxorubicin treatment in the scrambled control-transfected cells, whereas in the pre-miR-200c-transfected cells it was blocked at basal levels comparable to untreated cells.

Because miRNAs regulate the expression of numerous target genes (2, 3, 9), it was assumed that the down-regulation of miR-200c promotes chemoresistance by modulating more than one target gene. Shimono *et al.* (31) have reported that Bmi1, a member of the polycomb group proteins, is targeted by miR-200c linking breast cancer stem cells with normal stem cells. Furthermore, Bmi1 is involved in the maintenance of stemness and in the regulation of senescence (140-142). Thereby, Bmi1 functions as transcriptional repressor of a variety of genes including $p16^{Ink4a}$ and $p19^{Arf}$ of the Ink4a locus. Repression of $p19^{Arf}$ results downstream in the degradation of p53 by MDM2 leading to anti-apoptotic effects (118). Additionally, recent studies have shown that Bmi1 promotes cisplatin and docetaxel resistance in osteosarcoma and prostate cancer, respectively (116, 117). Thus, Bmi1 protein expression was investigated over the rounds in the molecular evolution assay of BT-474 cells and in miR-200c overexpressing MDA-MB-436 cells. Accordingly, a continuous up-regulation of Bmi1 over the rounds in BT-474 cells and a clear down-regulation after miR-200c overexpression in MDA-MB-436 cells were observed. Moreover, p53 levels were demonstrated to be decreased after the fourth cycle of doxorubicin treatment, which was in line with the increased chemoresistance in the molecular evolution assay. However, the mesenchymal and resistant cell line MDA-MB-436 was p53-negative independent of the miR-200c levels. This indicates that in MDA-MB-436 cells Bmi1 may mediate resistance *via* other pathways than p53, for instance *via* the PI3K/Akt pathway (117), and that p53 might be silenced through epigenetics, e.g. through promoter methylation. Additionally, miR-200c is a key modulator of a variety of genes which can potentially contribute to chemoresistance. Therefore, one has to be aware of the possibility that more than these two target genes described in this study can provide different resistance mechanisms dependent on the respective genetic background. Nevertheless, these findings illustrate how a single miRNA is able to regulate the circuitry of many pathways to render cancer cells susceptible or resistant to chemotherapy.

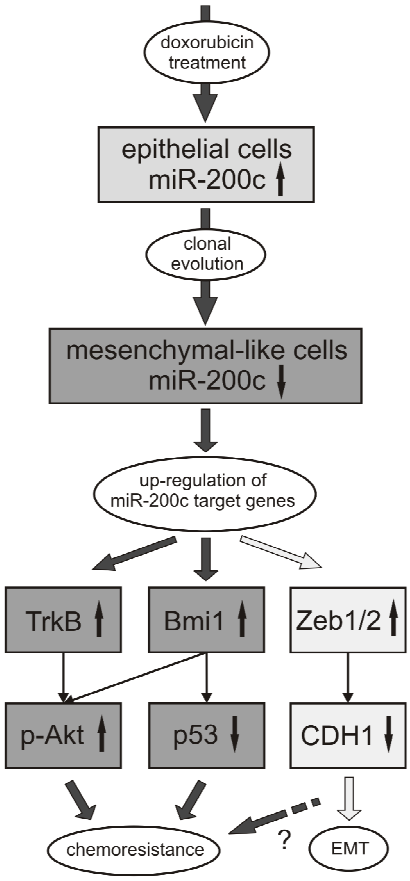

Figure 27. *Model of miR-200c-regulated chemoresistance*

Treatment of miR-200c high-expressing epithelial cancer cells with doxorubicin leads to clonal evolution of miR-200c low-expressing and mesenchymal-like cells. In consequence, a variety of miR-200c target genes are up-regulated. Besides the induction of EMT by the up-regulation of the E-cadherin (CDH1) repressors Zeb1 and Zeb2 (54, 119), this loss of miR-200c can cause an elevation of resistance factors like TrkB and Bmi1 resulting in enhanced cell survival. This leads to the activation of anti-apoptotic pathways like the phosphorylation of Akt or the degradation of p53, which can be further modulated by a complex crosstalk.

In conclusion, doxorubicin treatment of a heterogeneous cancer cell population leads to clonal evolution and selection of miR-200c low-expressing cells and subsequently to an up-regulation of various target genes including EMT inducing repressors like Zeb1 and Zeb2 (54, 119) as well as chemoresistance inducing factors like TrkB or Bmi1, resulting in enhanced survival signaling (Figure 27).

This study is one step forward in the understanding of miR-200c-dependent regulation of chemoresistance. Furthermore, these results provide an insight into the complex interaction network of miRNAs and their numerous target genes, highlighting the challenges in cancer therapy and supporting strategies utilizing miRNA-modulating anticancer drugs in the future.

4.2 miR-200c targets KRAS

The GTPase K-ras is involved in a variety of cellular processes, such as differentiation, proliferation and survival. However, activating mutations, which frequently occur in many types of cancer, turn KRAS into one of the most prominent oncogenes. Likewise, miR-200c plays an important role in tumorigenesis as a molecular switch between an epithelial, non-migratory, chemosensitive and a mesenchymal, migratory, chemoresistant state. While it has been reported that KRAS is regulated by several tumor suppressor miRNAs, this is the first report on the interaction of these two key players in oncogenesis.

In this study, it was shown that KRAS is a predicted target of miR-200c and that the protein expression of KRAS inversely correlates with the miR-200c expression in a panel of human breast cancer cell lines. KRAS was experimentally validated as a target of miR-200c by Western blot analyses and luciferase reporter assays. Interestingly, upon molecular evolution, an assay for acquired chemoresistance in which cancer cells were sequentially treated with doxorubicin, BT-474 cells displayed a significantly reduced miR-200c and a remarkably enhanced K-ras protein expression. Even though BT-474 cells express wild-type K-ras (121), the up-regulation of K-ras is a reasonable way to overcome the chemotherapeutic treatment as those cells have an amplification of the pro-survival gene encoding for the receptor tyrosine kinase HER2 (143), which signals downstream among others *via* the RAS/MAPK signaling pathway. This suggests that not only the presence of mutated but also the expression levels of wild-type K-ras are important for tumor progression and may serve as predictive marker for therapy efficacy, especially when occurring in combination with other genetic alterations such as EGFR mutations or HER2 amplifications.

Furthermore, the inhibitory effect of miR-200c-dependent KRAS silencing on proliferation and cell cycle was demonstrated in different breast and lung cancer cell lines. Thereby, the particular role of KRAS was dissected from the role of all other potential targets of miR-200c by specific knockdown experiments using siRNA against KRAS. Cell lines harboring an activating KRAS mutation (MDA-MB-231, A549 and Calu-1) were similarly affected by miR-200c as well as by the siRNA against KRAS. The observed decrease of the G1-phase together with the increase of

the S-phase indicates that the DNA replication upon K-ras knockdown might be slowed down, hence leading to the reduced proliferation. However, in the KRAS wild-type cell line MDA-MB-436 only miR-200c was able to change proliferation and cell cycle. Uhlmann *et al*. (144) have shown that in MDA-MB-231 cells the miR-200bc/429 seed-cluster, in particular miR-200c, inhibits EGF-driven invasion as well as proliferation and cell cycle progression, the latter by decreasing the G1-population. However, they ascribed the physiological effects to a miR-200c-induced down-regulation of PLCγ1, regardless of the KRAS mutation status. While the effects on invasion were nicely reflected by a specific knockdown of PLCγ1, the effects on proliferation were only mimicked in part. Here, it was shown that the effects on proliferation and cell cycle are coinciding for miR-200c and siRas if an activating KRAS mutation is present. These results indicate that in MDA-MB-231 cells, which harbor the activating KRAS mutation G13D, miR-200c inhibits proliferation and cell cycle progression more likely *via* a down-regulation of KRAS. On the contrary, in cells harboring wild-type KRAS, only miR-200c is able to alter proliferation and cell cycle presumably *via* other targets than KRAS, for instance BMI1. The polycomb group repressor Bmi1 induces transcriptional repression of a variety of genes including $p16^{Ink4a}$ of the Ink4a locus, which causes cell cycle arrest and senescence (118). Hence, miR-200c shows a broader efficacy against cancer cells by targeting multiple genes and pathways.

Activating mutations in the KRAS gene are important drivers of carcinogenesis in many types of cancer, such as lung, colon and pancreas (34, 35). However, it has been reported that human tumors display a remarkable intratumoral heterogeneity (145), which is furthermore associated with drug resistance and the failure of cancer therapies (146). Oncogenic K-ras might not necessarily be expressed across an entire tumor, but rather cellular subpopulations may exist, which display the wild-type KRAS gene. These cell populations can additionally contribute to tumor progression and to an aggressive phenotype including a high propensity of cancer cells to metastasize and to overcome drug treatment. Therefore, usage of miR-200c may be superior to that of a siRNA against KRAS as this miRNA has multiple targets (50), which regulate crucial events for tumor progression, e.g. epithelial-mesenchymal transition (EMT), acquisition of stem-like properties or therapy resistance (Figure 28).

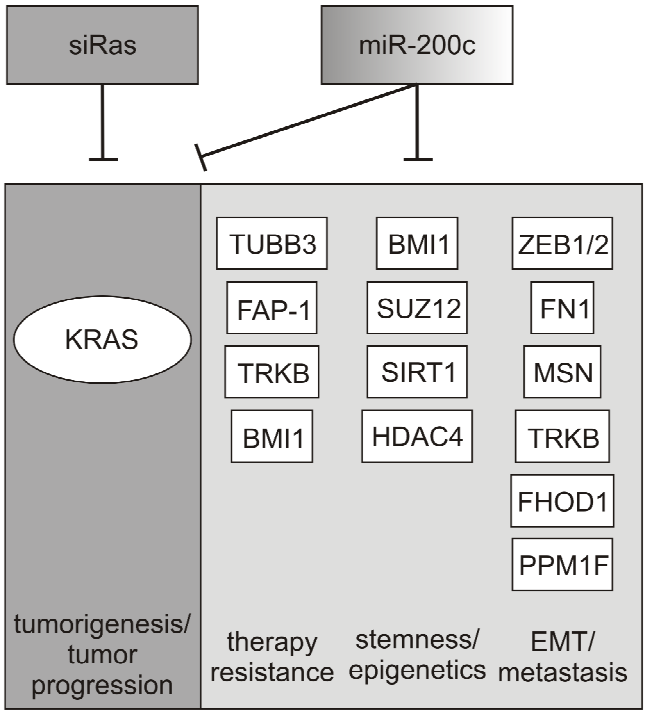

Figure 28. *Regulatory network of miR-200c*

While siRas can only specifically target KRAS mRNA, miR-200c regulates a variety of genes involved in tumor progression, metastasis and therapy resistance. By controlling a multitude of cellular processes, miR-200c causes stronger effects against various cancer cells independent of the mutational status of KRAS. The targets depicted in the diagram and their respective biological roles are reviewed in (50).

Moreover, KEGG-pathway analysis of all potential miR-200c targets predicted by TargetScan (95) revealed that miR-200c might strongly interact with the MAPK and ERBB signaling pathway by regulating a multitude of target genes, such as central adaptor proteins like Shc and Sos, kinases like MEKK1 and PKC or transcription factors like SRF and JUN. Although the direct regulation of these targets needs to be proven, these findings suggest that miR-200c may have additional regulating functions as a kind of gatekeeper of tumor progression and therapy resistance by controlling a complex network of oncogenic pathways including the RAS/MAPK pathway.

4.3 Salinomycin targets migratory miR-200c^{low} tumor cells

It has been suggested that intratumoral heterogeneity derived from genetic and non-genetic alterations can remarkably influence clinically important events, such as metastasis formation and therapy resistance (145). This implicates that a tumor comprises different cellular phenotypes amongst them migratory, mesenchymal, more chemoresistant cells, as well as non-migratory, epithelial, commonly chemosensitive cells. Developing novel therapeutic strategies for targeting all the different cell populations within a tumor is crucial for a successful cancer therapy. Hence, the discovery of the new class of CSC targeting drugs such as salinomycin raised hope for improved treatment options for cancer patients. Interestingly, Naujokat and Steinhart have reported promising case studies where patients with exhausted therapeutic options were treated with salinomycin (59).

Considering that CSC display traits of cells which have undergone epithelial-mesenchymal transition (EMT) (57) and that down-regulation of miR-200c induces EMT (26, 29) and links normal stem cells with breast cancer stem cells (31) implicates that miR-200c may represent a functional marker for therapy response, disease progression and tumor dissemination. In this study, it was demonstrated that miR-200c expression correlates with the migratory capacity in a panel of cancer cell lines and that ectopic overexpression leads to reduced migration and sensitivity to salinomycin due to the induction of mesenchymal-epithelial transition (MET). Moreover, the migratory potential of the cancer cell lines used in this study correlated directly with salinomycin susceptibility and inversely with doxorubicin susceptibility, i.e. highly migratory mesenchymal cells with low miR-200c levels were sensitive to salinomycin but resistant to doxorubicin. Combined treatment of co-cultured cancer cells consisting of epithelial non-migratory MCF-7 and mesenchymal migratory MDA-MB-436 cells with salinomycin and doxorubicin confirmed the selective targeting of the two cell types. Salinomycin had considerable inhibitory effects on cell migration in several different cancer cell lines including MDA-MB-436 (breast), LLC (lung) and 4T1 (breast) when applied at low dose for a short period of time. Short-term salinomycin treatment did not influence miR-200c expression levels in MDA-MB-436 cells, whereas long-term treatment inhibited migration and induced MET resulting in more differentiated epithelial cells with elevated miR-200c levels.

Thus, there are two consequences of salinomycin treatment: first, an immediate effect on mesenchymal cells blocking the migration and second, long-term survival and persistence of epithelial-type tumor cells. As suggested by recent publications (60, 61, 147), epithelial cells may have a higher capability than mesenchymal cells to initiate autophagy and thereby to circumvent salinomycin treatment, hence explaining the differential salinomycin susceptibility of these two cell types. Moreover, salinomycin-treated tumors may also acquire epithelial traits in several other ways. On the one hand, genetic instability and clonal selection as suggested by Cahill *et al*. (139) may determine surviving clones which display epithelial properties and elevated miR-200c levels when treated with salinomycin. One of the possible mechanisms for miR-200c up-regulation has been reported by Hur *et al.* (55). In their study, they have shown hypomethylation of the promoter region of the miR-200c/141 cluster in liver metastases of colorectal cancer. On the other hand, salinomycin treatment may induce miR-200c expression by transcriptional regulation *via* signaling cascades. Taking into account that there was no immediate response on miR-200c expression in salinomycin-treated MDA-MB-436 cells and that long-term treatment induced MET with elevated miR-200c levels, the first mechanism of a clonal selection of epithelial-like cancer cells appears to be more likely. Salinomycin was also able to increase miR-200c expression and induce MET in subcutaneously inoculated 4T1-luc cells and in the transgenic SpC-c-MYC mouse model of metastasizing non-small cell lung cancer (102), confirming the *in vitro* results. Of note, metastasis formation in brain, spleen and kidneys from primary 4T1-luc tumors in the lungs was considerably reduced by salinomycin treatment, even though the growth of the primary lesion was not significantly hampered.

In summary, the *in vitro* and *in vivo* results show that salinomycin - initially a cancer stem cell-specific drug - inhibits the migration of various cancer cells and restrains them in an epithelial state preventing tumor dissemination. Salinomycin treatment can hamper cancer cell migration and metastasis in two ways: an immediate short-term response on migration and a long-term effect resulting in MET and differentiated tumor cells. Therefore, treatment with salinomycin leads to less aggressive cancer cells and tumors in terms of lower migratory capacity, less metastasis and higher susceptibility to classical chemotherapy. Salinomycin treatment may therefore render cancer better controllable and improve the clinical outcome of patients suffering from metastatic cancer.

The analysis of two published studies on miRNA expression profiles in early primary breast cancers (148) and in high-risk estrogen receptor-positive (ER+) tamoxifen-treated breast cancers (149) revealed miR-200c as promising prognostic marker for survival. By means of the recently published online tool MIRUMIR (105) an overall survival probability of patients with high miR-200c levels (divided by the median miR-200c expression) was obtained which was slightly improved for early primary breast cancers and significantly superior for the high-risk ER+ breast cancers (Figure 29A).

In order to target all the heterogeneous cell populations, a treatment regimen is suggested which includes the combination of classical chemotherapeutics such as doxorubicin, targeted approaches such as tamoxifen or trastuzumab, and salinomycin for aggressive migratory cancer cells (Figure 29B). Since tumor heterogeneity increases upon cancer progression (145), and low miR-200c expression has been linked to high tumor stages with poor differentiation (150), the differential miR-200c expression was assigned to the respective stages of breast cancer (151). Accordingly, beneficial effects of a combined treatment with salinomycin and doxorubicin were particularly expected for tumors at higher stages, i.e. with lower miR-200c expression. Those patients who suffer from advanced breast cancer may benefit from salinomycin treatment in addition to classical chemotherapy as salinomycin prevents tumor progression and metastasis. Long-term salinomycin treatment selectively kills highly migratory mesenchymal cancer cells with low miR-200c levels, which are usually hard to target by conventional chemotherapies (93, 152-154). In addition, a sensitizing effect of salinomycin to DNA damaging and anti-mitotic drugs has been also suggested in recent studies (155, 156). Hence, the eradication of these chemoresistant subpopulations with low miR-200c expression by salinomycin treatment results in elevated miR-200c levels and MET, turning advanced cancers into less aggressive tumors with reduced migratory capacity and higher susceptibility to classical anti-cancer drugs. Such a therapeutic approach might improve the outcome and overall survival of cancer patients suffering from advanced and recurrent therapy-refractory malignancies, eventually rendering cancer controllable.

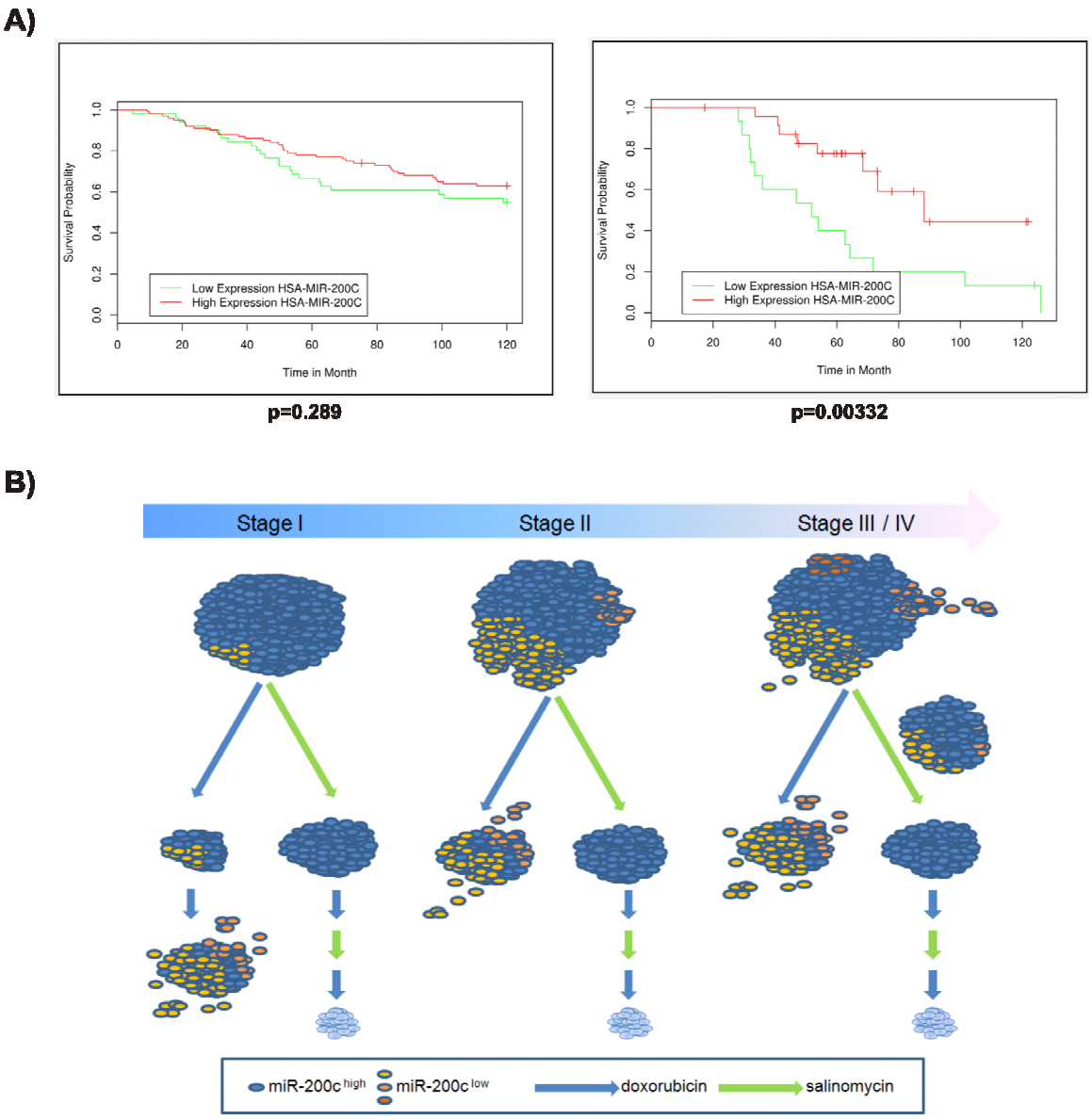

Figure 29. *Novel sequential treatment strategy with salinomycin and doxorubicin*

A) miR-200c-dependent survival probability. Analysis of data from two miRNA expression studies in early primary breast cancers (left panel) (148) and high-risk estrogen receptor-positive breast cancers (right panel) (149) was carried out using MIRUMIR. Patients were divided by the median into two groups either with high or low miR-200c expression. The resulting Kaplan-Meier survival curves are depicted in the graphs.
B) Sequential therapeutic approach for advanced tumors. Cancer stages are categorized in terms of their progression into localized miR-200c^{high} (stage I), early locally advanced miR-200c^{low} (stage II) and late locally advanced or metastatic miR-200c^{low} (stage III/IV) tumors. Salinomycin in addition to classical chemotherapy, for instance doxorubicin, may improve cancer therapy at all stages by targeting migratory and therapy-resistant mesenchymal cells with low miR-200c expression, resulting in MET and more differentiated tumors, which display higher miR-200c levels. These cells are less migratory and more susceptible to classical chemotherapy like doxorubicin treatment, which may result in a significant shrinkage or even an eradication of the existing tumor (respective combinatorial effects are shown on the right sides). In addition to the induction of MET, salinomycin can immediately inhibit the migration of spreading cancer cells in more advanced metastatic tumors (as indicated for tumors at stage III/IV). On the contrary, treatments limited to classical chemotherapeutic drugs will lead to clonal selection of aggressive cancer cells with low miR-200c expression, resulting in tumor progression, recurrence and metastases (as depicted on the left sides).

4.4 miR-143-controlled transgene expression

miRNA dysregulation often results in the development and progression of cancer. For instance, miR-143 is ubiquitously expressed in most human and murine tissues but down-regulated in many cancer types. This differential miRNA expression between healthy and cancerous tissue can be utilized for targeted cancer gene therapies. The concept of regulating transgene expression through miRNAs, which was initially described by Naldini and coworkers using viral vectors (82), should be now applied to non-viral vectors.

In this study, multiple copies of the miR-143 complementary target sequence were inserted into the 3'UTR of plasmid vectors encoding either for different reporter genes or for the therapeutic gene TNFα. All plasmids were shown to be precise sensors for the cellular levels of miR-143 both *in vitro* and *in vivo*. It was shown that the differential miR-143 expression between tumors and healthy tissues can be exploited for the de-targeting of healthy tissue. To utilize the endogenous miRNA machinery for the improved control of transgene expression at the posttranscriptional level is one step forward in decreasing side effects in cancer gene therapy. However, the ectopic expression of plasmids containing miRNA target sequences may affect the regulation of endogenous target genes by competition and saturation effects. In case of miR-143, this may lead to unfavorable side effects due to an up-regulation of several oncogenes. Nevertheless, combining different therapeutic strategies, such as specific targeting of the tumor, e.g. through certain ligands or tissue-specific promoters, and de-targeting, e.g. through miRNAs, may avoid these undesired side effects. Recently, a combination of targeted delivery of plasmids and radiation (157) or chemotherapeutic drugs (110) was applied to cancer gene therapy using peptide targeted non-viral gene carriers. The described de-targeting approach in combination with novel polymeric carriers (104) including specific targeting ligands (158) will further improve efficiency, specificity and safety of such approaches, paving the way towards preclinical development.

5. SUMMARY

The progression of tumors into advanced stages, which are characterized by an increased therapy resistance and a higher risk of metastasis formation, still represents the major threat for cancer patients. Despite of improved early detection methods and treatment options, the acquisition of chemoresistance to classical chemotherapeutic drugs and the switch from early local to late advanced and metastatic disease remain enormous challenges in the treatment of recurrent cancers. miRNAs have been previously demonstrated to be crucial regulators in oncogenesis modulating important processes like proliferation, migration, invasion and therapy susceptibility.

In this thesis, the molecular evolution assay, which mimics the pulsed chemotherapy of cancer patients in an *in vitro* cell culture assay, was established to analyze the underlying mechanisms of acquired chemoresistance in breast cancer cells. On the basis of the molecular evolution assay, an epithelial-mesenchymal transition (EMT)-like resistance mechanism was identified in which the loss of miR-200c was demonstrated to be responsible for the acquisition of doxorubicin resistance. By overexpressing miR-200c, doxorubicin-resistant breast cancer cells were sensitized to doxorubicin treatment due to the modulation of several miR-200c targets including TrkB, Bmi1 and K-ras. The respective targets were mechanistically linked to prominent cellular survival pathways, i.e. PI3K/AKT, p53 and RAS/MAPK pathway, deciphering a complex network of miR-200c-regulated acquired chemoresistance. Furthermore, the prominent proto-oncogene KRAS was for the first time reported to be a direct target of miR-200c. This interaction between miR-200c and KRAS was not only shown to be involved in resistance formation in breast cancer, but also to be relevant for tumorigenesis in general as miR-200c could interfere with mutated oncogenic KRAS resulting in reduced proliferation and disturbed cell cycle progression. Interestingly, the effect of miR-200c and siRNA against K-ras was comparable in cell lines harboring activated oncogenic KRAS, whereas only miR-200c displayed inhibitory effects on proliferation and cell cycle in KRAS wild-type cells. The negative regulation of cellular survival pathways and the interaction with the RAS pathway suggest a novel tumor suppressive role of miR-200c, making it a promising candidate also for cancer therapy. Thereby, miR-200c may directly

suppress tumor growth or sensitize cancer cells to additionally applied classical chemotherapy.

Moreover, the recently published cancer stem cell-specific drug salinomycin was evaluated for its therapeutic potential. Here, it was proven that salinomycin effectively inhibits cancer cell migration already at low doses. At higher doses, salinomycin was demonstrated to preferentially affect mesenchymal migratory cancer cells with low miR-200c expression, which were shown to be resistant to doxorubicin treatment. On the other hand, epithelial non-migratory cells with high miR-200c expression were rather resistant to salinomycin but susceptible to doxorubicin, revealing the differential activity of salinomycin and doxorubicin against mesenchymal and epithelial cancer cells. When applied in a long-term assay, salinomycin treatment induced mesenchymal-epithelial transition (MET) resulting in epithelial-like cancer cells with lower migratory capacity and higher susceptibility to doxorubicin. The switch from mesenchymal to epithelial cancer cells with elevated miR-200c levels upon salinomycin treatment was also verified *in vivo* using a syn- and transgenic mouse model. Furthermore, the metastatic tumor burden in a syngenic mouse model could be significantly reduced by salinomycin treatment. These findings led to the proposal of a sequential treatment regimen consisting of salinomycin and doxorubicin, in which salinomycin restrains the tumor in an epithelial, non-migratory and doxorubicin-sensitive state by targeting mesenchymal, migratory and commonly chemoresistant cancer cells. Thereby, miR-200c emerged as promising marker for cellular transitions upon treatment, therapy efficacy and the overall survival of breast cancer patients as determined by *in silico* analysis of miRNA expression profiles. With this novel treatment strategy the effects of ectopically overexpressed miR-200c could be mimicked by salinomycin treatment avoiding the difficulties of *in vivo* miRNA delivery. Thus, the outcome of patients suffering particularly from advanced or metastatic disease may be improved.

In addition, an alternative therapeutic approach was evaluated, utilizing the differential miRNA expression in healthy and cancerous tissue for tumor-specific non-viral gene therapy. miR-143 was validated as a suitable tumor suppressor miRNA displaying low and high expression levels in cancerous and non-malignant tissue, respectively. Five copies of the sequence complementary to miR-143 were inserted into the 3'UTR of plasmid vectors encoding either for different reporter genes or for

the therapeutic gene TNFα. All plasmids containing the miR-143 target sequences were shown to be precise sensors for miR-143 expression *in vitro*. In a xenograft mouse tumor model using miR-143^{low} cancer cells and a polymeric carrier for gene delivery, specific transgene expression was achieved in miR-143^{low} tumors by de-targeting miR-143^{high} non-cancerous tissues. This de-targeting approach in combination with novel carriers and specific targeting ligands may further improve the efficiency, the specificity and hence the safety of gene delivery systems, smoothing the path towards preclinical development.

6. APPENDIX

6.1 Abbreviations

ABC	Adenosine triphosphate (ATP) binding cassette
Ago	Argonaute
ALL	Acute lymphocytic leukemia
ATCC	American Type Culture Collection
BLI	Bioluminescence imaging
cDNA	Complementary DNA
CLL	Chronic lymphocytic leukemia
CMV	Cytomegalovirus
CSC	Cancer stem cells
Ct	Cycle of threshold
DAPI	4',6-diamidino-2-phenylindole
DAVID	Database for Annotation, Visualization and Integrated Discovery
DMSO	Dimethyl sulfoxide
DNA	Deoxyribonucleic acid
dxr	Doxorubicin
EDTA	Ethylenediamine tetraacetic acid
EF1α	Human elongation factor 1 alpha
ELISA	Enzyme linked immunosorbent assay
EMT	Epithelial-mesenchymal transition
FCS	Fetal calf serum
FDR	False discovery rate
Fluc	Firefly luciferase control plasmid
GTPase	Guanosine triphosphatase
hsa	Homo sapiens
HSV-1	Herpes simplex virus 1
IHC	Immunohistochemistry
IF	Immunofluorescence
KEGG	Kyoto Encyclopedia of Genes and Genomes
LNA	Locked nucleic acid

LPEI	Linear polyethylenimine
LSM	Laser scanning microscopy
MET	Mesenchymal-epithelial transition
miRNA	MicroRNA
mmu	Mus musculus
mRNA	MessengerRNA
MTT	3-(4,5-dimethylthiazol-2-yl)-2,5-diphenyltetrazolium bromide
NET	Buffer containing NaCl, EDTA and Tris-HCl
N/P	Nitrogen residues per phosphate of DNA
PBS	Phosphate buffered saline
polyA	Polyadenylation
PSMC	Porcine smooth muscle cells
RISC	RNA-induced silencing complex
Rluc	Renilla luciferase reporter plasmid
RNA	Ribonucleic acid
RNAi	RNA interference
ROUT	Robust regression and outlier removal
RT-PCR	Reverse transcription - polymerase chain reaction
sal	Salinomycin
SCEP	Synthetic CMV-EF1α hybrid promoter
SD	Standard deviation
SDS	Sodium dodecyl sulfate
SDS-PAGE	Sodium dodecyl sulfate - polyacrylamide gel
SEM	Standard error of the mean
siRNA	Small interfering RNA
SLP	Stem loop primer
SpC	Surfactant associated protein C promoter
TrisHCl	Tris(hydroxymethyl)aminomethane hydrochloride
UTR	Untranslated region
w:w	Weight to weight ratio
WB	Western blot

6.2 Genes and proteins

Akt	Protein kinase B (PKB)
Bad	Bcl-2-associated death promoter
BCL2	B-cell lymphoma 2
BIM	BCL2-like 11
BMI1	Polycomb ring finger oncogene
CDK4/6	Cyclin-dependent kinase 4/6
DGCR8	Di George syndrome critical region 8 (= Pasha in *D. melanogaster*)
DNMTs	DNA methyltransferases
E2F1	Transcription factor E2F1
EGFP	Enhanced green fluorescent protein
EGFR	Epidermal growth factor receptor
ERBB	Epidermal growth factor receptor family
EVI1	Ecotropic virus integration site 1 protein homolog
FAP-1	Protein tyrosine phosphatase, non-receptor type 13 (APO-1/CD95 (Fas)-associated phosphatase)
FHOD1	Formin homology (FH1/FH2) domain-containing protein 1
FN1	Fibronectin
GAPDH	Glyceraldehyde 3-phosphate dehydrogenase
HDAC4	Histone deacetylase 4
HER2	Human epidermal growth factor receptor 2
ICP4	Transcriptional regulator ICP4 (HSV)
JUN	Jun proto-oncogene
KRAS	Kirsten rat sarcoma viral oncogene homolog
lin-14	Protein lin-14 (*C. elegans*)
lin-4	MicroRNA lin-4 (*C. elegans*)
LucSH	Fusion gene of firefly luciferase and the Sh ble gene conferring Zeocin resistance
MAPK	Mitogen-activated protein kinases
MCL1	Myeloid cell leukemia sequence 1
MDM2	Mouse double minute 2 homolog oncogene, E3 ubiquitin protein ligase

MEKK1	Mitogen-activated protein kinase kinase kinase 1
MET	Met proto-oncogene, hepatocyte growth factor receptor
MSN	Moesin
MYC	V-myc avian myelocytomatosis viral oncogene homolog
NFκB	Protein complex, nuclear factor kappa-light-chain-enhancer of activated B cells
NRAS	Neuroblastoma RAS viral (v-ras) oncogene homolog
p16Ink4a	Cyclin-dependent kinase inhibitor 2A (CDKN2A), multiple tumor suppressor 1
p19Arf	Transcript with an alternate open reading frame from the CDKN2A gene
p53	Tumor protein p53
Pol II	RNA polymerase II
PDCD4	Programmed cell death 4 (neoplastic transformation inhibitor)
PI3K	Phosphatidylinositide 3-kinases
PKC	Protein kinase C
PLCγ	Phopholipase C, gamma (phosphatidylinositol-specific)
PPM1F	Protein phosphatase 1F
PTEN	Phosphatase and tensin homolog
RREB1	Ras-responsive element-binding protein 1
Shc	Src homology 2 domain containing transforming protein 1
SHIP1	Inositol polyphosphate-5-phosphatase containing a N-terminal SH2 domain
SIRT1	Sirtuin 1
Sos	Son of sevenless homologs, guanine nucleotide exchange factors
SRF	Serum response factor (c-fos serum response element-binding transcription factor)
SUZ12	SUZ12 polycomb repressive complex 2 subunit
TNFα	Tumor necrosis factor alpha
TRKB	Neurotrophic tyrosine kinase, receptor, type 2 (NTRK2)
TUBB3	Tubulin, beta 3 class III
Wnt	Wingless-type MMTV integration site family
WT1	Wilms tumor protein 1
ZEB1/2	Zinc finger E-box binding homeobox 1/2 (TCF8/SIP1)

7. PUBLICATIONS

7.1 Original articles

Oak PS, Kopp F, Thakur C, Ellwart JW, Rapp UR, Ullrich A, Wagner E, Knyazev P, Roidl A. *Combinatorial treatment of mammospheres with trastuzumab and salinomycin efficiently targets HER2-positive cancer cells and cancer stem cells.* Int J Cancer. 2012 Dec 15;131(12):2808-19. doi: 10.1002/ijc.27595. Epub 2012 May 21.

Kopp F, Oak PS, Wagner E, Roidl A. *miR-200c sensitizes breast cancer cells to doxorubicin treatment by decreasing TrkB and Bmi1 expression*. PLoS One. 2012;7(11):e50469. doi: 10.1371/journal.pone.0050469. Epub 2012 Nov 29.

Haase R, Magnusson T, Su B, Kopp F, Wagner E, Lipps H, Baiker A, Ogris M. *Generation of a tumor- and tissue-specific episomal non-viral vector system.* BMC Biotechnol. 2013 Jun 4;13(1):49. doi: 10.1186/1472-6750-13-49.

Kopp F, Schnoedt M, Haase R, Wagner E, Roidl A, Ogris M. *De-targeting by miR-143 decreases unwanted transgene expression in non-tumorigenic cells*. Gene Ther. 2013 Jun 27. doi: 10.1038/gt.2013.37. [Epub ahead of print]

Kopp F, Wagner E, Roidl A. *The proto-oncogene KRAS is targeted by miR-200c*. Submitted

Kopp F, Hermawan A, Oak PS, Herrmann A, Wagner E, Roidl A. *Salinomycin treatment reduces metastatic tumor burden by hampering cancer cell migration*. Submitted

Kopp F, Hermawan A, Oak PS, Ulaganathan VK, Herrmann A, Elnikhely N, Thakur T, Ataseven B, Rapp UR, Savai R, Wagner E, Roidl A. *Salinomycin treatment restrains cancer cells in an epithelial state by targeting mesenchymal miR-200c^{low} tumor cells*. Submitted

Kopp F, Hermawan A, Busse J, Herrmann A, Oak PS, Wagner E, Roidl A. *Sequential treatment with doxorubicin and salinomycin as novel treatment strategy in cancer*. In preparation

7.2 Posters

Oak PS*, Kopp F, Ellwart JW, Ullrich A, Wagner E, Knyazev P, Roidl A. *Salinomycin as an effective drug in combinatorial treatment of breast carcinoma*. AACR Special Conference, Advances in Breast Cancer Research: Genetics, Biology, and Clinical Applications, San Francisco, CA, USA (October 2011).

Kopp F*, Schnoedt M, Haase R, Wagner E, Ogris M, Roidl A. *miR-143-dependent transgene expression for cancer gene therapy*. German Society for Gene Therapy, Annual Meeting 2012, Frankfurt, Germany (March 2012).

Kopp F*, Wagner E, Roidl A. *miR-200c regulates cell cycle, proliferation and migration in cancer cells by targeting the proto-oncogene KRAS*. Keystone Symposia, Noncoding RNAs in Development and Cancer, Vancouver, BC, Canada (January 2013).

* Presenting author

.

8. REFERENCES

1. Bartel, D.P., *MicroRNAs: genomics, biogenesis, mechanism, and function.* Cell, 2004. **116**(2): p. 281-97.
2. Bartel, D.P., *MicroRNAs: target recognition and regulatory functions.* Cell, 2009. **136**(2): p. 215-33.
3. Inui, M., G. Martello, and S. Piccolo, *MicroRNA control of signal transduction.* Nat Rev Mol Cell Biol, 2010. **11**(4): p. 252-63.
4. Huntzinger, E. and E. Izaurralde, *Gene silencing by microRNAs: contributions of translational repression and mRNA decay.* Nat Rev Genet, 2011. **12**(2): p. 99-110.
5. Garzon, R., G. Marcucci, and C.M. Croce, *Targeting microRNAs in cancer: rationale, strategies and challenges.* Nat Rev Drug Discov, 2010. **9**(10): p. 775-89.
6. Iorio, M.V. and C.M. Croce, *MicroRNA dysregulation in cancer: diagnostics, monitoring and therapeutics. A comprehensive review.* EMBO Mol Med, 2012. **4**(3): p. 143-59.
7. Croce, C.M., *Causes and consequences of microRNA dysregulation in cancer.* Nat Rev Genet, 2009. **10**(10): p. 704-14.
8. Esquela-Kerscher, A. and F.J. Slack, *Oncomirs - microRNAs with a role in cancer.* Nat Rev Cancer, 2006. **6**(4): p. 259-69.
9. *American Cancer Society, Cancer Facts & Figures*. 2012; Available from: http://www.cancer.org/acs/groups/content/@epidemiologysurveilance/documents/document/acspc-031941.pdf.
10. Gonzalez-Angulo, A.M., F. Morales-Vasquez, and G.N. Hortobagyi, *Overview of resistance to systemic therapy in patients with breast cancer.* Adv Exp Med Biol, 2007. **608**: p. 1-22.
11. O'Driscoll, L. and M. Clynes, *Biomarkers and multiple drug resistance in breast cancer.* Curr Cancer Drug Targets, 2006. **6**(5): p. 365-84.
12. Coley, H.M., *Mechanisms and strategies to overcome chemotherapy resistance in metastatic breast cancer.* Cancer Treat Rev, 2008. **34**(4): p. 378-90.

13. Raguz, S. and E. Yague, *Resistance to chemotherapy: new treatments and novel insights into an old problem.* Br J Cancer, 2008. **99**(3): p. 387-91.
14. Blower, P.E., J.H. Chung, J.S. Verducci, S. Lin*, et al.*, *MicroRNAs modulate the chemosensitivity of tumor cells.* Mol Cancer Ther, 2008. **7**(1): p. 1-9.
15. Kutanzi, K.R., O.V. Yurchenko, F.A. Beland, V.F. Checkhun*, et al.*, *MicroRNA-mediated drug resistance in breast cancer.* Clin Epigenetics, 2011. **2**(2): p. 171-185.
16. Sarkar, F.H., Y. Li, Z. Wang, D. Kong*, et al.*, *Implication of microRNAs in drug resistance for designing novel cancer therapy.* Drug Resist Updat, 2010. **13**(3): p. 57-66.
17. Bao, L., S. Hazari, S. Mehra, D. Kaushal*, et al.*, *Increased expression of P-glycoprotein and doxorubicin chemoresistance of metastatic breast cancer is regulated by miR-298.* Am J Pathol, 2012. **180**(6): p. 2490-503.
18. Kovalchuk, O., J. Filkowski, J. Meservy, Y. Ilnytskyy*, et al.*, *Involvement of microRNA-451 in resistance of the MCF-7 breast cancer cells to chemotherapeutic drug doxorubicin.* Mol Cancer Ther, 2008. **7**(7): p. 2152-9.
19. Gregory, P.A., A.G. Bert, E.L. Paterson, S.C. Barry*, et al.*, *The miR-200 family and miR-205 regulate epithelial to mesenchymal transition by targeting ZEB1 and SIP1.* Nat Cell Biol, 2008. **10**(5): p. 593-601.
20. Park, S.M., A.B. Gaur, E. Lengyel, and M.E. Peter, *The miR-200 family determines the epithelial phenotype of cancer cells by targeting the E-cadherin repressors ZEB1 and ZEB2.* Genes Dev, 2008. **22**(7): p. 894-907.
21. Hurteau, G.J., J.A. Carlson, S.D. Spivack, and G.J. Brock, *Overexpression of the microRNA hsa-miR-200c leads to reduced expression of transcription factor 8 and increased expression of E-cadherin.* Cancer Res, 2007. **67**(17): p. 7972-6.
22. Cochrane, D.R., N.S. Spoelstra, E.N. Howe, S.K. Nordeen*, et al.*, *MicroRNA-200c mitigates invasiveness and restores sensitivity to microtubule-targeting chemotherapeutic agents.* Mol Cancer Ther, 2009. **8**(5): p. 1055-66.
23. Hurteau, G.J., J.A. Carlson, E. Roos, and G.J. Brock, *Stable expression of miR-200c alone is sufficient to regulate TCF8 (ZEB1) and restore E-cadherin expression.* Cell Cycle, 2009. **8**(13): p. 2064-9.

24. Korpal, M., E.S. Lee, G. Hu, and Y. Kang, *The miR-200 family inhibits epithelial-mesenchymal transition and cancer cell migration by direct targeting of E-cadherin transcriptional repressors ZEB1 and ZEB2.* J Biol Chem, 2008. **283**(22): p. 14910-4.
25. Burk, U., J. Schubert, U. Wellner, O. Schmalhofer*, et al.*, *A reciprocal repression between ZEB1 and members of the miR-200 family promotes EMT and invasion in cancer cells.* EMBO Rep, 2008. **9**(6): p. 582-9.
26. Gibbons, D.L., W. Lin, C.J. Creighton, Z.H. Rizvi*, et al.*, *Contextual extracellular cues promote tumor cell EMT and metastasis by regulating miR-200 family expression.* Genes Dev, 2009. **23**(18): p. 2140-51.
27. Howe, E.N., D.R. Cochrane, and J.K. Richer, *Targets of miR-200c mediate suppression of cell motility and anoikis resistance.* Breast Cancer Res, 2011. **13**(2): p. R45.
28. Jurmeister, S., M. Baumann, A. Balwierz, I. Keklikoglou*, et al.*, *MicroRNA-200c represses migration and invasion of breast cancer cells by targeting actin-regulatory proteins FHOD1 and PPM1F.* Mol Cell Biol, 2012. **32**(3): p. 633-51.
29. Olson, P., J. Lu, H. Zhang, A. Shai*, et al.*, *MicroRNA dynamics in the stages of tumorigenesis correlate with hallmark capabilities of cancer.* Genes Dev, 2009. **23**(18): p. 2152-65.
30. Iliopoulos, D., M. Lindahl-Allen, C. Polytarchou, H.A. Hirsch*, et al.*, *Loss of miR-200 inhibition of Suz12 leads to polycomb-mediated repression required for the formation and maintenance of cancer stem cells.* Mol Cell, 2010. **39**(5): p. 761-72.
31. Shimono, Y., M. Zabala, R.W. Cho, N. Lobo*, et al.*, *Downregulation of miRNA-200c links breast cancer stem cells with normal stem cells.* Cell, 2009. **138**(3): p. 592-603.
32. Cochrane, D.R., E.N. Howe, N.S. Spoelstra, and J.K. Richer, *Loss of miR-200c: A Marker of Aggressiveness and Chemoresistance in Female Reproductive Cancers.* J Oncol, 2010. **2010**: p. 821717.
33. Pogribny, I.P., J.N. Filkowski, V.P. Tryndyak, A. Golubov*, et al.*, *Alterations of microRNAs and their targets are associated with acquired resistance of MCF-7 breast cancer cells to cisplatin.* Int J Cancer, 2010. **127**(8): p. 1785-94.
34. Campbell, P.M. and C.J. Der, *Oncogenic Ras and its role in tumor cell invasion and metastasis.* Semin Cancer Biol, 2004. **14**(2): p. 105-14.

35. Friday, B.B. and A.A. Adjei, *K-ras as a target for cancer therapy.* Biochim Biophys Acta, 2005. **1756**(2): p. 127-44.
36. Califano, R., L. Landi, and F. Cappuzzo, *Prognostic and predictive value of K-RAS mutations in non-small cell lung cancer.* Drugs, 2012. **72 Suppl 1**: p. 28-36.
37. Vakiani, E. and D.B. Solit, *KRAS and BRAF: drug targets and predictive biomarkers.* J Pathol, 2011. **223**(2): p. 219-29.
38. Wheeler, D.L., E.F. Dunn, and P.M. Harari, *Understanding resistance to EGFR inhibitors-impact on future treatment strategies.* Nat Rev Clin Oncol, 2010. **7**(9): p. 493-507.
39. Riely, G.J., J. Marks, and W. Pao, *KRAS mutations in non-small cell lung cancer.* Proc Am Thorac Soc, 2009. **6**(2): p. 201-5.
40. Calin, G.A. and C.M. Croce, *MicroRNA signatures in human cancers.* Nat Rev Cancer, 2006. **6**(11): p. 857-66.
41. Kent, O.A. and J.T. Mendell, *A small piece in the cancer puzzle: microRNAs as tumor suppressors and oncogenes.* Oncogene, 2006. **25**(46): p. 6188-96.
42. Johnson, S.M., H. Grosshans, J. Shingara, M. Byrom*, et al.*, *RAS is regulated by the let-7 microRNA family.* Cell, 2005. **120**(5): p. 635-47.
43. Esquela-Kerscher, A., P. Trang, J.F. Wiggins, L. Patrawala*, et al.*, *The let-7 microRNA reduces tumor growth in mouse models of lung cancer.* Cell Cycle, 2008. **7**(6): p. 759-64.
44. Johnson, C.D., A. Esquela-Kerscher, G. Stefani, M. Byrom*, et al.*, *The let-7 microRNA represses cell proliferation pathways in human cells.* Cancer Res, 2007. **67**(16): p. 7713-22.
45. Kumar, M.S., S.J. Erkeland, R.E. Pester, C.Y. Chen*, et al.*, *Suppression of non-small cell lung tumor development by the let-7 microRNA family.* Proc Natl Acad Sci U S A, 2008. **105**(10): p. 3903-8.
46. Chen, X., X. Guo, H. Zhang, Y. Xiang*, et al.*, *Role of miR-143 targeting KRAS in colorectal tumorigenesis.* Oncogene, 2009. **28**(10): p. 1385-92.
47. Xu, B., X. Niu, X. Zhang, J. Tao*, et al.*, *miR-143 decreases prostate cancer cells proliferation and migration and enhances their sensitivity to docetaxel through suppression of KRAS.* Mol Cell Biochem, 2011. **350**(1-2): p. 207-13.

48. To, M.D., R.D. Rosario, P.M. Westcott, K.L. Banta*, et al.*, *Interactions between wild-type and mutant Ras genes in lung and skin carcinogenesis.* Oncogene, 2012.
49. Tanic, M., K. Yanowsky, C. Rodriguez-Antona, R. Andres*, et al.*, *Deregulated miRNAs in hereditary breast cancer revealed a role for miR-30c in regulating KRAS oncogene.* PLoS One, 2012. **7**(6): p. e38847.
50. Howe, E.N., D.R. Cochrane, and J.K. Richer, *The miR-200 and miR-221/222 microRNA families: opposing effects on epithelial identity.* J Mammary Gland Biol Neoplasia, 2012. **17**(1): p. 65-77.
51. Adam, L., M. Zhong, W. Choi, W. Qi*, et al.*, *miR-200 expression regulates epithelial-to-mesenchymal transition in bladder cancer cells and reverses resistance to epidermal growth factor receptor therapy.* Clin Cancer Res, 2009. **15**(16): p. 5060-72.
52. Bryant, J.L., J. Britson, J.M. Balko, M. Willian*, et al.*, *A microRNA gene expression signature predicts response to erlotinib in epithelial cancer cell lines and targets EMT.* Br J Cancer, 2012. **106**(1): p. 148-56.
53. Polyak, K. and R.A. Weinberg, *Transitions between epithelial and mesenchymal states: acquisition of malignant and stem cell traits.* Nat Rev Cancer, 2009. **9**(4): p. 265-73.
54. Dykxhoorn, D.M., Y. Wu, H. Xie, F. Yu*, et al.*, *miR-200 enhances mouse breast cancer cell colonization to form distant metastases.* PLoS One, 2009. **4**(9): p. e7181.
55. Hur, K., Y. Toiyama, M. Takahashi, F. Balaguer*, et al.*, *MicroRNA-200c modulates epithelial-to-mesenchymal transition (EMT) in human colorectal cancer metastasis.* Gut, 2012.
56. Korpal, M., B.J. Ell, F.M. Buffa, T. Ibrahim*, et al.*, *Direct targeting of Sec23a by miR-200s influences cancer cell secretome and promotes metastatic colonization.* Nat Med, 2011. **17**(9): p. 1101-8.
57. Mani, S.A., W. Guo, M.J. Liao, E.N. Eaton*, et al.*, *The epithelial-mesenchymal transition generates cells with properties of stem cells.* Cell, 2008. **133**(4): p. 704-15.
58. Gupta, P.B., T.T. Onder, G. Jiang, K. Tao*, et al.*, *Identification of selective inhibitors of cancer stem cells by high-throughput screening.* Cell, 2009. **138**(4): p. 645-59.

59. Naujokat, C. and R. Steinhart, *Salinomycin as a drug for targeting human cancer stem cells.* J Biomed Biotechnol, 2012. **2012**: p. 950658.
60. Jangamreddy, J.R., S. Ghavami, J. Grabarek, G. Kratz*, et al.*, *Salinomycin induces activation of autophagy, mitophagy and affects mitochondrial polarity: Differences between primary and cancer cells.* Biochim Biophys Acta, 2013.
61. Verdoodt, B., M. Vogt, I. Schmitz, S.T. Liffers*, et al.*, *Salinomycin induces autophagy in colon and breast cancer cells with concomitant generation of reactive oxygen species.* PLoS One, 2012. **7**(9): p. e44132.
62. Yue, W., A. Hamai, G. Tonelli, C. Bauvy*, et al.*, *Inhibition of the autophagic flux by salinomycin in breast cancer stem-like/progenitor cells interferes with their maintenance.* Autophagy, 2013. **9**(5): p. 714-29.
63. Dong, T.T., H.M. Zhou, L.L. Wang, B. Feng*, et al.*, *Salinomycin selectively targets 'CD133+' cell subpopulations and decreases malignant traits in colorectal cancer lines.* Ann Surg Oncol, 2011. **18**(6): p. 1797-804.
64. Ketola, K., M. Hilvo, T. Hyotylainen, A. Vuoristo*, et al.*, *Salinomycin inhibits prostate cancer growth and migration via induction of oxidative stress.* Br J Cancer, 2012. **106**(1): p. 99-106.
65. Friedman, R.C., K.K. Farh, C.B. Burge, and D.P. Bartel, *Most mammalian mRNAs are conserved targets of microRNAs.* Genome Res, 2009. **19**(1): p. 92-105.
66. Kahlert, C., F. Klupp, K. Brand, F. Lasitschka*, et al.*, *Invasion front-specific expression and prognostic significance of microRNA in colorectal liver metastases.* Cancer Sci, 2011. **102**(10): p. 1799-807.
67. Pichler, M., E. Winter, M. Stotz, K. Eberhard*, et al.*, *Down-regulation of KRAS-interacting miRNA-143 predicts poor prognosis but not response to EGFR-targeted agents in colorectal cancer.* Br J Cancer, 2012. **106**(11): p. 1826-32.
68. Takagi, T., A. Iio, Y. Nakagawa, T. Naoe*, et al.*, *Decreased expression of microRNA-143 and -145 in human gastric cancers.* Oncology, 2009. **77**(1): p. 12-21.
69. Kent, O.A., K. Fox-Talbot, and M.K. Halushka, *RREB1 repressed miR-143/145 modulates KRAS signaling through downregulation of multiple targets.* Oncogene, 2012.

70. Borralho, P.M., B.T. Kren, R.E. Castro, I.B. da Silva*, et al.*, *MicroRNA-143 reduces viability and increases sensitivity to 5-fluorouracil in HCT116 human colorectal cancer cells.* FEBS J, 2009. **276**(22): p. 6689-700.
71. Kulda, V., M. Pesta, O. Topolcan, V. Liska*, et al.*, *Relevance of miR-21 and miR-143 expression in tissue samples of colorectal carcinoma and its liver metastases.* Cancer Genet Cytogenet, 2010. **200**(2): p. 154-60.
72. Zhang, Y., Z. Wang, M. Chen, L. Peng*, et al.*, *MicroRNA-143 targets MACC1 to inhibit cell invasion and migration in colorectal cancer.* Mol Cancer, 2012. **11**: p. 23.
73. Peng, X., W. Guo, T. Liu, X. Wang*, et al.*, *Identification of miRs-143 and -145 that is associated with bone metastasis of prostate cancer and involved in the regulation of EMT.* Plos One, 2011. **6**(5): p. e20341.
74. Borralho, P.M., A.E. Simoes, S.E. Gomes, R.T. Lima*, et al.*, *miR-143 overexpression impairs growth of human colon carcinoma xenografts in mice with induction of apoptosis and inhibition of proliferation.* Plos One, 2011. **6**(8): p. e23787.
75. Pramanik, D., N.R. Campbell, C. Karikari, R. Chivukula*, et al.*, *Restitution of tumor suppressor microRNAs using a systemic nanovector inhibits pancreatic cancer growth in mice.* Mol Cancer Ther, 2011. **10**(8): p. 1470-80.
76. Lee, C.Y., P.S. Rennie, and W.W. Jia, *MicroRNA regulation of oncolytic herpes simplex virus-1 for selective killing of prostate cancer cells.* Clin Cancer Res, 2009. **15**(16): p. 5126-35.
77. Cawood, R., H.H. Chen, F. Carroll, M. Bazan-Peregrino*, et al.*, *Use of tissue-specific microRNA to control pathology of wild-type adenovirus without attenuation of its ability to kill cancer cells.* PLoS Pathog, 2009. **5**(5): p. e1000440.
78. Edge, R.E., T.J. Falls, C.W. Brown, B.D. Lichty*, et al.*, *A let-7 MicroRNA-sensitive vesicular stomatitis virus demonstrates tumor-specific replication.* Mol Ther, 2008. **16**(8): p. 1437-43.
79. Kelly, E.J., R. Nace, G.N. Barber, and S.J. Russell, *Attenuation of vesicular stomatitis virus encephalitis through microRNA targeting.* J Virol, 2010. **84**(3): p. 1550-62.

80. Perez, J.T., A.M. Pham, M.H. Lorini, M.A. Chua*, et al.*, *MicroRNA-mediated species-specific attenuation of influenza A virus.* Nat Biotechnol, 2009. **27**(6): p. 572-6.

81. Ylosmaki, E., T. Hakkarainen, A. Hemminki, T. Visakorpi*, et al.*, *Generation of a conditionally replicating adenovirus based on targeted destruction of E1A mRNA by a cell type-specific MicroRNA.* J Virol, 2008. **82**(22): p. 11009-15.

82. Brown, B.D., M.A. Venneri, A. Zingale, L. Sergi Sergi*, et al.*, *Endogenous microRNA regulation suppresses transgene expression in hematopoietic lineages and enables stable gene transfer.* Nat Med, 2006. **12**(5): p. 585-91.

83. Kamrud, K.I., V.M. Coffield, G. Owens, C. Goodman*, et al.*, *In vitro and in vivo characterization of microRNA-targeted alphavirus replicon and helper RNAs.* J Virol, 2010. **84**(15): p. 7713-25.

84. Lee, T.C., Y.L. Lin, J.T. Liao, C.M. Su*, et al.*, *Utilizing liver-specific microRNA-122 to modulate replication of dengue virus replicon.* Biochem Biophys Res Commun, 2010. **396**(3): p. 596-601.

85. Suzuki, T., F. Sakurai, S. Nakamura, E. Kouyama*, et al.*, *miR-122a-regulated expression of a suicide gene prevents hepatotoxicity without altering antitumor effects in suicide gene therapy.* Mol Ther, 2008. **16**(10): p. 1719-26.

86. Wagner, E., *Polymers for siRNA delivery: inspired by viruses to be targeted, dynamic, and precise.* Acc Chem Res, 2012. **45**(7): p. 1005-13.

87. Chen, C., D.A. Ridzon, A.J. Broomer, Z. Zhou*, et al.*, *Real-time quantification of microRNAs by stem-loop RT-PCR.* Nucleic Acids Res, 2005. **33**(20): p. e179.

88. Tang, F., P. Hajkova, S.C. Barton, K. Lao*, et al.*, *MicroRNA expression profiling of single whole embryonic stem cells.* Nucleic Acids Res, 2006. **34**(2): p. e9.

89. Varkonyi-Gasic, E., R. Wu, M. Wood, E.F. Walton*, et al.*, *Protocol: a highly sensitive RT-PCR method for detection and quantification of microRNAs.* Plant Methods, 2007. **3**: p. 12.

90. Peltier, H.J. and G.J. Latham, *Normalization of microRNA expression levels in quantitative RT-PCR assays: identification of suitable reference RNA targets in normal and cancerous human solid tissues.* RNA, 2008. **14**(5): p. 844-52.

91. Rasband, W.S. *ImageJ, U.S. National Institutes of Health, Bethesda, Maryland, USA*. 1997 - 2008; Available from: http://rsb.info.nih.gov/ij/.

92. Philipp, A., X. Zhao, P. Tarcha, E. Wagner*, et al.*, *Hydrophobically modified oligoethylenimines as highly efficient transfection agents for siRNA delivery.* Bioconjug Chem, 2009. **20**(11): p. 2055-61.

93. Kopp, F., P.S. Oak, E. Wagner, and A. Roidl, *miR-200c sensitizes breast cancer cells to doxorubicin treatment by decreasing TrkB and Bmi1 expression.* PLoS One, 2012. **7**(11): p. e50469.

94. Chin, L.J., E. Ratner, S. Leng, R. Zhai*, et al.*, *A SNP in a let-7 microRNA complementary site in the KRAS 3' untranslated region increases non-small cell lung cancer risk.* Cancer Res, 2008. **68**(20): p. 8535-40.

95. Lewis, B.P., I.H. Shih, M.W. Jones-Rhoades, D.P. Bartel*, et al.*, *Prediction of mammalian microRNA targets.* Cell, 2003. **115**(7): p. 787-98.

96. John, B., A.J. Enright, A. Aravin, T. Tuschl*, et al.*, *Human MicroRNA targets.* PLoS Biol, 2004. **2**(11): p. e363.

97. Maragkakis, M., P. Alexiou, G.L. Papadopoulos, M. Reczko*, et al.*, *Accurate microRNA target prediction correlates with protein repression levels.* BMC Bioinformatics, 2009. **10**: p. 295.

98. Maragkakis, M., M. Reczko, V.A. Simossis, P. Alexiou*, et al.*, *DIANA-microT web server: elucidating microRNA functions through target prediction.* Nucleic Acids Res, 2009. **37**(Web Server issue): p. W273-6.

99. Huang da, W., B.T. Sherman, and R.A. Lempicki, *Systematic and integrative analysis of large gene lists using DAVID bioinformatics resources.* Nat Protoc, 2009. **4**(1): p. 44-57.

100. Huang da, W., B.T. Sherman, and R.A. Lempicki, *Bioinformatics enrichment tools: paths toward the comprehensive functional analysis of large gene lists.* Nucleic Acids Res, 2009. **37**(1): p. 1-13.

101. Ehrhardt, A., T. Bartels, R. Klocke, D. Paul*, et al.*, *Increased susceptibility to the tobacco carcinogen 4-(methylnitrosamino)-1-(3-pyridyl)-1-butanone in transgenic mice overexpressing c-myc and epidermal growth factor in alveolar type II cells.* J Cancer Res Clin Oncol, 2003. **129**(2): p. 71-5.

102. Rapp, U.R., C. Korn, F. Ceteci, C. Karreman*, et al.*, *MYC is a metastasis gene for non-small-cell lung cancer.* PLoS One, 2009. **4**(6): p. e6029.

103. Wiedmann, R.M., K. von Schwarzenberg, A. Palamidessi, L. Schreiner*, et al.*, *The V-ATPase-inhibitor archazolid abrogates tumor metastasis via inhibition of*

endocytic activation of the Rho-GTPase Rac1. Cancer Res, 2012. **72**(22): p. 5976-87.

104. Schaffert, D., C. Troiber, E.E. Salcher, T. Frohlich*, et al.*, *Solid-phase synthesis of sequence-defined T-, i-, and U-shape polymers for pDNA and siRNA delivery.* Angew Chem Int Ed Engl, 2011. **50**(38): p. 8986-9.
105. Antonov, A.V., R.A. Knight, G. Melino, N.A. Barlev*, et al.*, *MIRUMIR: an online tool to test microRNAs as biomarkers to predict survival in cancer using multiple clinical data sets.* Cell Death Differ, 2013. **20**(2): p. 367.
106. Haase, R., O. Argyros, S.P. Wong, R.P. Harbottle*, et al.*, *pEPito: a significantly improved non-viral episomal expression vector for mammalian cells.* BMC Biotechnol, 2010. **10**: p. 20.
107. Navarro, G., G. Maiwald, R. Haase, A.L. Rogach*, et al.*, *Low generation PAMAM dendrimer and CpG free plasmids allow targeted and extended transgene expression in tumors after systemic delivery.* J Control Release, 2010. **146**(1): p. 99-105.
108. Magnusson, T., R. Haase, M. Schleef, E. Wagner*, et al.*, *Sustained, high transgene expression in liver with plasmid vectors using optimized promoter-enhancer combinations.* J Gene Med, 2011. **13**(7-8): p. 382-91.
109. Russ, V., H. Elfberg, C. Thoma, J. Kloeckner*, et al.*, *Novel degradable oligoethylenimine acrylate ester-based pseudodendrimers for in vitro and in vivo gene transfer.* Gene Ther, 2008. **15**(1): p. 18-29.
110. Su, B., A. Cengizeroglu, K. Farkasova, J.R. Viola*, et al.*, *Systemic TNFalpha gene therapy synergizes with liposomal doxorubicine in the treatment of metastatic cancer.* Mol Ther, 2013. **21**(2): p. 300-8.
111. Salcher, E.E., P. Kos, T. Frohlich, N. Badgujar*, et al.*, *Sequence-defined four-arm oligo(ethanamino)amides for pDNA and siRNA delivery: Impact of building blocks on efficacy.* J Control Release, 2012. **164**(3): p. 380-6.
112. Aigner, K., B. Dampier, L. Descovich, M. Mikula*, et al.*, *The transcription factor ZEB1 (deltaEF1) promotes tumour cell dedifferentiation by repressing master regulators of epithelial polarity.* Oncogene, 2007. **26**(49): p. 6979-88.
113. Bracken, C.P., P.A. Gregory, N. Kolesnikoff, A.G. Bert*, et al.*, *A double-negative feedback loop between ZEB1-SIP1 and the microRNA-200 family regulates epithelial-mesenchymal transition.* Cancer Res, 2008. **68**(19): p. 7846-54.

114. Kokkinos, M.I., R. Wafai, M.K. Wong, D.F. Newgreen*, et al.*, *Vimentin and epithelial-mesenchymal transition in human breast cancer--observations in vitro and in vivo.* Cells Tissues Organs, 2007. **185**(1-3): p. 191-203.

115. Segal, R.A., *Selectivity in neurotrophin signaling: theme and variations.* Annu Rev Neurosci, 2003. **26**: p. 299-330.

116. Crea, F., M.A. Duhagon Serrat, E.M. Hurt, S.B. Thomas*, et al.*, *BMI1 silencing enhances docetaxel activity and impairs antioxidant response in prostate cancer.* Int J Cancer, 2011. **128**(8): p. 1946-54.

117. Wu, Z., L. Min, D. Chen, D. Hao*, et al.*, *Overexpression of BMI-1 promotes cell growth and resistance to cisplatin treatment in osteosarcoma.* PLoS One, 2011. **6**(2): p. e14648.

118. Park, I.K., S.J. Morrison, and M.F. Clarke, *Bmi1, stem cells, and senescence regulation.* J Clin Invest, 2004. **113**(2): p. 175-9.

119. Tryndyak, V.P., F.A. Beland, and I.P. Pogribny, *E-cadherin transcriptional down-regulation by epigenetic and microRNA-200 family alterations is related to mesenchymal and drug-resistant phenotypes in human breast cancer cells.* Int J Cancer, 2010. **126**(11): p. 2575-83.

120. Lim, L.P., N.C. Lau, P. Garrett-Engele, A. Grimson*, et al.*, *Microarray analysis shows that some microRNAs downregulate large numbers of target mRNAs.* Nature, 2005. **433**(7027): p. 769-73.

121. Hollestelle, A., F. Elstrodt, J.H. Nagel, W.W. Kallemeijn*, et al.*, *Phosphatidylinositol-3-OH kinase or RAS pathway mutations in human breast cancer cell lines.* Mol Cancer Res, 2007. **5**(2): p. 195-201.

122. Kozma, S.C., M.E. Bogaard, K. Buser, S.M. Saurer*, et al.*, *The human c-Kirsten ras gene is activated by a novel mutation in codon 13 in the breast carcinoma cell line MDA-MB231.* Nucleic Acids Res, 1987. **15**(15): p. 5963-71.

123. Sunaga, N., D.S. Shames, L. Girard, M. Peyton*, et al.*, *Knockdown of oncogenic KRAS in non-small cell lung cancers suppresses tumor growth and sensitizes tumor cells to targeted therapy.* Mol Cancer Ther, 2011. **10**(2): p. 336-46.

124. Tuveson, D.A., A.T. Shaw, N.A. Willis, D.P. Silver*, et al.*, *Endogenous oncogenic K-ras(G12D) stimulates proliferation and widespread neoplastic and developmental defects.* Cancer Cell, 2004. **5**(4): p. 375-87.

125. Wang, X.Q., H. Li, V. Van Putten, R.A. Winn*, et al.*, *Oncogenic K-Ras regulates proliferation and cell junctions in lung epithelial cells through induction of cyclooxygenase-2 and activation of metalloproteinase-9.* Mol Biol Cell, 2009. **20**(3): p. 791-800.

126. Agbunag, C. and D. Bar-Sagi, *Oncogenic K-ras drives cell cycle progression and phenotypic conversion of primary pancreatic duct epithelial cells.* Cancer Res, 2004. **64**(16): p. 5659-63.

127. Fan, J. and J.R. Bertino, *K-ras modulates the cell cycle via both positive and negative regulatory pathways.* Oncogene, 1997. **14**(21): p. 2595-607.

128. Shimizu, K., D. Birnbaum, M.A. Ruley, O. Fasano*, et al.*, *Structure of the Ki-ras gene of the human lung carcinoma cell line Calu-1.* Nature, 1983. **304**(5926): p. 497-500.

129. Valenzuela, D.M. and J. Groffen, *Four human carcinoma cell lines with novel mutations in position 12 of c-K-ras oncogene.* Nucleic Acids Res, 1986. **14**(2): p. 843-52.

130. Korpal, M. and Y. Kang, *The emerging role of miR-200 family of microRNAs in epithelial-mesenchymal transition and cancer metastasis.* RNA Biol, 2008. **5**(3): p. 115-9.

131. Smrekar, B., L. Wightman, M.F. Wolschek, C. Lichtenberger*, et al.*, *Tissue-dependent factors affect gene delivery to tumors in vivo.* Gene Ther, 2003. **10**(13): p. 1079-88.

132. Oak, P.S., F. Kopp, C. Thakur, J.W. Ellwart*, et al.*, *Combinatorial treatment of mammospheres with trastuzumab and salinomycin efficiently targets HER2-positive cancer cells and cancer stem cells.* Int J Cancer, 2012.

133. Fojo, T. and H.M. Coley, *The role of efflux pumps in drug-resistant metastatic breast cancer: new insights and treatment strategies.* Clin Breast Cancer, 2007. **7**(10): p. 749-56.

134. Martin, M., *Docetaxel, doxorubicin and cyclophosphamide (the TAC regimen): an effective adjuvant treatment for operable breast cancer.* Womens Health (Lond Engl), 2006. **2**(4): p. 527-37.

135. Mittmann, N., S. Verma, M. Koo, K. Alloul*, et al.*, *Cost effectiveness of TAC versus FAC in adjuvant treatment of node-positive breast cancer.* Curr Oncol, 2010. **17**(1): p. 7-16.

136. Iorio, M.V. and C.M. Croce, *Causes and Consequences of MicroRNA Dysregulation.* Cancer J, 2012. **18**(3): p. 215-22.
137. Altomare, D.A. and J.R. Testa, *Perturbations of the AKT signaling pathway in human cancer.* Oncogene, 2005. **24**(50): p. 7455-64.
138. Kim, D. and J. Chung, *Akt: versatile mediator of cell survival and beyond.* J Biochem Mol Biol, 2002. **35**(1): p. 106-15.
139. Cahill, D.P., K.W. Kinzler, B. Vogelstein, and C. Lengauer, *Genetic instability and darwinian selection in tumours.* Trends Cell Biol, 1999. **9**(12): p. M57-60.
140. Gil, J., D. Bernard, and G. Peters, *Role of polycomb group proteins in stem cell self-renewal and cancer.* DNA Cell Biol, 2005. **24**(2): p. 117-25.
141. Rajasekhar, V.K. and M. Begemann, *Concise review: roles of polycomb group proteins in development and disease: a stem cell perspective.* Stem Cells, 2007. **25**(10): p. 2498-510.
142. Sparmann, A. and M. van Lohuizen, *Polycomb silencers control cell fate, development and cancer.* Nat Rev Cancer, 2006. **6**(11): p. 846-56.
143. She, Q.B., S. Chandarlapaty, Q. Ye, J. Lobo*, et al.*, *Breast tumor cells with PI3K mutation or HER2 amplification are selectively addicted to Akt signaling.* PLoS One, 2008. **3**(8): p. e3065.
144. Uhlmann, S., J.D. Zhang, A. Schwager, H. Mannsperger*, et al.*, *miR-200bc/429 cluster targets PLCgamma1 and differentially regulates proliferation and EGF-driven invasion than miR-200a/141 in breast cancer.* Oncogene, 2010. **29**(30): p. 4297-306.
145. Marusyk, A., V. Almendro, and K. Polyak, *Intra-tumour heterogeneity: a looking glass for cancer?* Nat Rev Cancer, 2012. **12**(5): p. 323-34.
146. Saunders, N.A., F. Simpson, E.W. Thompson, M.M. Hill*, et al.*, *Role of intratumoural heterogeneity in cancer drug resistance: molecular and clinical perspectives.* EMBO Mol Med, 2012. **4**(8): p. 675-84.
147. Li, T., L. Su, N. Zhong, X. Hao*, et al.*, *Salinomycin induces cell death with autophagy through activation of endoplasmic reticulum stress in human cancer cells.* Autophagy, 2013. **9**(7).
148. Buffa, F.M., C. Camps, L. Winchester, C.E. Snell*, et al.*, *microRNA-associated progression pathways and potential therapeutic targets identified by integrated mRNA and microRNA expression profiling in breast cancer.* Cancer Res, 2011. **71**(17): p. 5635-45.

149. Lyng, M.B., A.V. Laenkholm, R. Sokilde, K.H. Gravgaard*, et al.*, *Global microRNA expression profiling of high-risk ER+ breast cancers from patients receiving adjuvant tamoxifen mono-therapy: a DBCG study.* PLoS One, 2012. **7**(5): p. e36170.

150. Chang, C.J., C.H. Chao, W. Xia, J.Y. Yang*, et al.*, *p53 regulates epithelial-mesenchymal transition and stem cell properties through modulating miRNAs.* Nat Cell Biol, 2011. **13**(3): p. 317-23.

151. Carlson, R.W., D.C. Allred, B.O. Anderson, H.J. Burstein*, et al.*, *Breast cancer. Clinical practice guidelines in oncology.* J Natl Compr Canc Netw, 2009. **7**(2): p. 122-92.

152. Ceppi, P., G. Mudduluru, R. Kumarswamy, I. Rapa*, et al.*, *Loss of miR-200c expression induces an aggressive, invasive, and chemoresistant phenotype in non-small cell lung cancer.* Mol Cancer Res, 2010. **8**(9): p. 1207-16.

153. Kajiyama, H., K. Shibata, M. Terauchi, M. Yamashita*, et al.*, *Chemoresistance to paclitaxel induces epithelial-mesenchymal transition and enhances metastatic potential for epithelial ovarian carcinoma cells.* Int J Oncol, 2007. **31**(2): p. 277-83.

154. Liu, S., M.T. Tetzlaff, R. Cui, and X. Xu, *miR-200c inhibits melanoma progression and drug resistance through down-regulation of BMI-1.* Am J Pathol, 2012. **181**(5): p. 1823-35.

155. Kim, J.H., M. Chae, W.K. Kim, Y.J. Kim*, et al.*, *Salinomycin sensitizes cancer cells to the effects of doxorubicin and etoposide treatment by increasing DNA damage and reducing p21 protein.* Br J Pharmacol, 2011. **162**(3): p. 773-84.

156. Kim, J.H., H.I. Yoo, H.S. Kang, J. Ro*, et al.*, *Salinomycin sensitizes antimitotic drugs-treated cancer cells by increasing apoptosis via the prevention of G2 arrest.* Biochem Biophys Res Commun, 2012. **418**(1): p. 98-103.

157. Klutz, K., D. Schaffert, M.J. Willhauck, G.K. Grunwald*, et al.*, *Epidermal Growth Factor Receptor-targeted (131)I-therapy of Liver Cancer Following Systemic Delivery of the Sodium Iodide Symporter Gene.* Mol Ther, 2011. **19**(4): p. 676-85.

158. Ogris, M. and E. Wagner, *To be targeted: is the magic bullet concept a viable option for synthetic nucleic acid therapeutics?* Hum Gene Ther, 2011. **22**(7): p. 799-807.

9. ACKNOWLEDGEMENTS

At the end of a PhD thesis it is a pleasure to be able to look back in satisfaction at each experience you have made, and of course there are many people you would like to express your gratitude to.

First of all, I would like to thank Prof. Dr. Ernst Wagner for giving me the opportunity to conduct my PhD thesis in his working group. I am really grateful for his guidance, trust and helpful advice, making this study successful.

Furthermore, I would like to thank my supervisor Dr. Andreas Roidl for teaching me the “first steps” in the world of science. I also appreciate his personal guidance, the many fruitful discussions we had and the numerous great events outside the lab. Likewise, I want to thank the whole “Roidl group” Adam Hermawan, Dr. Prajakta Oak and Dr. Rebekka Kubisch for myriad discussions in our Friday seminars.

Over the last four years, I also have to express my gratitude to many co-workers and collaboration partners for their valuable contributions in terms of providing help, advice, materials and data. In particular, I want to thank Dr. Prajakta Oak, Adam Hermawan, Prof. Dr. Manfred Ogris, Maria Schnoedt, Dr. Rudolf Haase, Dr. Raphaela Klaeger, Dr. Laura Schreiner, Annika Herrmann, Dr. Rebekka Kubisch, Petra Kos, Dr. Daniel Edinger, Ann-Katrin Sommer, Prof. Dr. Ulf Rapp, Dr. Chitra Thakur, Dr. Vijay Ulaganathan, Nefertiti Elnikhely, Dr. Beyhan Ataseven, Prof. Dr. Axel Ullrich and Dr. Pjotr Knyazev, whose contributions allowed me to complete my projects and write my publications.

Many thanks go to Wolfgang Rödl and Dr. Martina Rüffer who kept everything running smoothly in the lab. Thanks also to Miriam, Anna, Ursula, Markus and Olga who steadily fulfilled their duties in the lab.

Moreover, I would particularly thank all the former members of our group, especially Thomas, Christian D., Rebekka, Raphaela, Laura and Alex for a great time and the best working atmosphere I can imagine. On this occasion, I want to express my special thanks to Daniel who has not only been the best colleague during the last four years, but also one of my best friends for the last ten years.

Last but not least, I want to thank my friends, my girlfriend Petra for her great support in and outside the lab and my family for always standing by my side.